UNIVERSITAT POLITÈCNICA DE CATALUNYA
BARCELONATECH
Escola d'Enginyeria de Barcelona Est

TREBALL FI DE MÀSTER

Màster Universitari en Enginyeria Química

ANALYSIS OF VENTILATION EFFECT ON FIRES OCCURRED IN INDUSTRIAL WAREHOUSES USING FDS SIMULATION TOOL

Memòria i Annexos

Autor: Juan Carlos Bueno Arcos

Director: Eulàlia Planas Cuchi

Co-Director: Oriol Rios Rubiras

Convocatòria: Maig 2018

Resum

El projecte descriu, en un apartat d'antecedents, la motivació del treball, què s'entén per incendi confinat i els principals models matemàtics proposats per la literatura per tal de modelar-los, dels quals es desprenen els paràmetres a variar per modificar les característiques d'aquest tipus d'incendis, i s'ha dedicat un capítol sencer a la descripció dels principals models matemàtics que el simulador *Fire Dynamics Simulator* (FDS) fa servir per realitzar els seus càlculs.

Com a estat de l'art, es situa breument el marc legal vigent actualment, a nivell de requeriments estructurals per a materials que es puguin veure exposats al foc, focalitzant en el contingut del Reglament de Seguretat Contra Incendis en Establiments Industrials i s'ha dedicat un capítol a descriure l'estudi realitzat pels bombers de la Generalitat, indicant les característiques de l'escenari estudiat i, breument, els resultats de l'estudi.

Posteriorment, es descriu l'escenari implementat a FDS i quins han estat els resultats estudiats, d'entre tot el ventall d'*outputs* que proporciona el simulador i s'han realitzat els estudis previs adients (mallat i verificar que es compleix la conservació de la massa).

A mode preliminar, per a conèixer l'efecte general que pot tenir la ventilació sobre els resultats finals observats, s'han efectuat estudis centrats en l'efecte en els resultats de la variació de la mida, la distribució i la ubicació dels exutoris, elements fàcilment modificables en instal·lacions reals.

Finalment, s'efectuen algunes simulacions amb FDS dels casos analitzats pels bombers amb OZone, tot comparant-los i exposant les conclusions finals.

Resumen

El proyecto describe, en un apartado de antecedentes, la motivación del trabajo, qué se entiende por incendio confinado y los principales modelos matemáticos propuestos por la literatura para modelarlos, de los cuales se desprenden los parámetros a variar para modificar las características de este tipo de incendios, y se ha dedicado un capítulo entero a la descripción de los principales modelos matemáticos que el simulador Ferio DynamicsSimulator (FDS) usa para realizar sus cálculos.

Como estado del arte, se sitúa brevemente el marco legal vigente actualmente a nivel de requerimientos estructurales para materiales que se puedan ver expuestos al fuego, focalizando en el contenido del Reglamento de Seguridad Contra Incendios en Establecimientos Industriales y se ha dedicado un capítulo a describir el estudio realizado por los bomberos de la Generalitat, indicando las características del escenario estudiado y, brevemente, los resultados del estudio. Posteriormente, se describe el escenario implementado a FDS y cuales han sido los resultados estudiados, de entre todo el abanico de *outputs* que proporciona el simulador, además de realizarse los estudios previos necesarios (mallado y verificación de la conservación de la masa).

A modo preliminar, para conocer el efecto general que puede tener la ventilación sobre los resultados finales observados, se han efectuado estudios centrados en el efecto en los resultados de la variación del tamaño, la distribución y la ubicación de los exutorios, elementos fácilmente modificables en instalaciones reales.

Finalmente, se efectúan algunas simulaciones con FDS de los casos analizados por los bomberos con OZone, comparándolos y exponiendo las conclusiones finales.

Abstract

The project is introduced with a background section, in which the definition of fire basic concepts and compartment fire are exposed, and after these, main mathematical models proposed by literature in order to model them are described, from which are detached the set of parameters to vary in order to modify the features of these kind of fires, and whole chapter has been dedicated to describing the main mathematical models implemented in Fire Dynamics Simulator (FDS) in order to perform its calculations.

Once technical background is clear, this project has been ubicated within the applicable legal framework in force at the date this project was handed, concerning requirements of materials constituting structures that might be exposed to fire, focusing on the content of the Spanish Regulation of Fire Safety in Industrial Establishments, and, a whole chapter has been dedicated to describe the study performed by Generalitat de Catalunya Fire Service, indicating the features of simulated scenario and, briefly, its results.

It has been explained, by first, how experimental scenario has been implemented in FDS and which have been those variables selected in order to be provided within the wide range of possible output values that FDS offers. Previous simple studies have been carried out, such as setting the most suitable mesh size or proving that mass is conserved according to input data provided to simulator.

In order to know which is the possible effect that ventilation variations could have on final observed results, the effect of size, distribution and ubication of ventilation gaps has been studied.

Finally, some of the simulations originally performed by Generalitat de Catalunya Fire Service with OZone have been reproduced with FDS, followed by the corresponding comparison and exposing final results.

Index of contents

Preface

At the end of the XVIII century, Industrial Revolution provoked several changes on working methods and on demography of the new industrial areas that grew up next to sources of raw materials or important centers of trade. These new industrial zones experienced an exponential growth on land demands, that up to then where practically only used for agriculture, and therefore, since then, the use of industrial terrain has been optimized due to high price and low availability; so that nowadays, the construction of townhouse buildings that share structure with the neighbors is a common fact.

Moreover, the Industrial Revolution was accompanied by the birth of modern days chemistry, the invention of the vapor machine and the discovery of electric current, that allowed a fast improvement of confection and overall fabrication techniques. However, these new technologies also brought to industry new risk related to the manipulation and storage of certain substances such as fuels or dyes, able to ignite easily and provoke scenarios such as toxic leaks, explosions, or devastating fires that might spread fast around the whole industrial area.

Additionally to the obvious potential damage that explosions may cause to structures, fires, which are able to expand rapidly along all the surface occupied by flammable materials as textiles, fuels, chemicals, plastics, electronic devices or even, constructive materials, can cause serious damages to structures, as these tend to lose their mechanical properties when their temperature is highly increased. Often, these structural damages also affect neighboring buildings, usually very nearby in towns and industrial parks and that possibly share a part of the structure with the building where the fire started.

First experiences led to the development of both new structural elements to alleviate the potential damages between nearby and contiguous constructions, safeguards, extinguishing agents, safety protocols and a legal framework that aimed to define the proper conditions to avoid undesired events to happen. This environment lead to the foundation of entities, such as the US National Fire Protection Agency in 1896, that contributed to the normalization of protective measures and safety practices, defined in their National Fire Codes, elaborated by experts of fire protection, but also agreed with interested parts such as manufacturers, firefighters, syndicates, and administration, among many others, which are usually used for national fire regulations in some countries.

Precisely, the work and publications of the entities founded with the aim of normalizing good practices on fire protection, have inspired the fire protection normative of forced compliance applicable in many countries.

The present project focuses on normative applicable in Catalonia, where lack of space due to the high population density of the zone and the intense economic activity have been causes for the constructors to build spaces with different ownership that often are stuck to the next building or, even, different floors or compartments of the same have different ownership. These type of establishments are those that need to fulfill the most strict requirements in order to be legalized, that sometimes are translated into higher expenses and waste of space; however, in the case of horizontal buildings, applicable normative, in virtude of ITC SP 119 contemplates the possibility to grant the dealing of these establishments as constructions that are completely isolated of their buildings if, according to technical methods, no affectation to neighboring structures is proven. This specific case has been the main motivation of this project.

1. Introduction

1.1 Objective

One of the firsts steps to follow for setting up a new activity in each building should be its legalization regarding criteria of fire resistance. The Spanish regulation (*Reglamento de Seguridad Contra Incendios en Establecimientos Industriales*, RSCIEI, whose last update was approved with RD 2267/04 on 3rd December of 2004) stablishes a criterion for the election of affected building features to determine fire load, so that isolated buildings are allowed to store a larger amount of flammable material since the possible consequences in case of real fire would lead to less severe consequences. However, most of buildings in industrial parks are wall to wall (A type) which might lead to the failure of the bearing structure of these neighbors due to a fire declared in a certain industrial establishment.

Since structural resistance against fire is the most critical aspect regarding effect on neighbors, regulation allows to deal the building (if has no neighbors at upper or lower levels) as a B type building, which is much less restrictive regarding to technical requirements. The main objective of this project is to validate the results obtained by the Generalitat de Catalunya Fire Service regarding the analysis of possible effect on fire development of adding five ventilation gaps to a certain compartment, which could be considered either A or B type (depending on whether fire could provoke or not structure collapse). The effect on fire duration and reached peaks of temperature will determine suitability of structure against different hypothetical fire scenarios, which could be used as a technical justification in order to decide if the establishment can be dealt as B type or not.

Additionally, secondary objectives have been proposed for this project, such as building a proper model in FDS in order to simulate desired compartment fire scenario; determining how variations on ventilation could cause effect on simulation results in the case of a generic compartment fire and judging the validity of FDS simulation results after comparison with expected results.

1.2 Scope

Due to lack of time, computational resources and drawbacks, such as multiple blackouts and loss of progress in running simulations, the scope of the project has been adapted to just low and medium intrinsic risk level cases, in which a single scenario (already proposed by Illa in his final degree project [1]) was contemplated. Study of ventilation effect was reduced to variation on ventilation gaps: size, spatial disposition and position, which could help to study the possible effect of ventilation on the heat release rate and wall temperatures in compartment fires.

An interesting option, the definition of a proper pyrolysis-based ignition criterion for granting a free burning fire, could not be set due to lack of time and reiterate obtaining of not pleasing results. This is why the simulations were restricted to predefined fires following a realistic fire growth curve-based ignition strategy, which had been previously developed by Illa in his final degree project.

Limited computational capacity also impeded to finish simulations that were thought to be used in order to validate results obtained previously by Generalitat de Catalunya Fire Service with OZone, so that 3 and 4 intrinsic level simulations could not be finished (and therefore, fire duration had to be estimated according to fuel load and observed steady-state burning rate) and 5 intrinsic risk level simulations could not be even launched, as these last would have needed the use of at least 8 computational cores during more than two months.

1.3 Aim

The aim of this project is to provide results that help, in a future, to the development of a guide or manual that helps the users to give technical justification for allowing the legalization of horizontal industrial establishments of A type following the requirements set for B type establishments, much less restrictive.

In addition, this project provides simulation results of how changes on ventilation gaps cause effect on reached temperatures, fire duration, and, therefore, helps to judge if a certain structure could resist or not different kinds of fire scenarios.

2. Preliminary concepts

2.1. First approach on fire science

Oxford Dictionary for advanced learners [2] defines fire as:

"Set of flames, light, heat and often smoke that are produced when something burns, that is, when a combustion reaction takes place".

A flame could be defined as a gas phase chemical reaction producing very high temperatures and a fire, as a turbulent ensemble of flames [3]. This chemical reaction, called combustion, is a drastic oxidation, which requires a substance to be ignited (combustible), a heavy oxidizing substance (oxygen) and a source of energy that permits to beat the barrier of activation energy and so, start the reaction, which can be external (for example, a spark) in the case of piloted ignition or thanks to temperature in the case of auto ignition.

Only substances susceptible to be oxidized will burn; so basically, organic molecules and few inorganic molecules can experience a combustion reaction. Combustion is not always complete and, as any chemical reaction, depends on the concentration of reactants:

- If limiting reactant is the fuel, combustion tends to be complete if there is no external interference, such as cooling or choking. In complete combustions, products are those compounds whose atoms show their maximum possible oxidation number. Most common species, present on most of combustions are carbon dioxide (present on combustions of all carbon-containing molecules), steam (present on combustions of all hydrogen-containing molecules); however, nitrous and sulfur oxides, hydrogen halides or others are also present in some combustions of materials containing nitrogen, sulfur, halogens, phosphor, boron, silicon, metals…

- If limiting reactant is oxygen or the oxidizer, combustion will show the maximum yield of for the most spontaneous oxidations, but whole combustion reaction mechanism will not be completed. This will lead to an incomplete combustion, which will yield to substances whose atoms are not on their maximum oxidation number. Common products found in incomplete combustions are carbon (in the form of soot or char) and carbon monoxide, present in all combustions involving carbon compunds; but also, in some cases, other species such as toxic cyanic acid will be generated.

Molecules like water or carbon dioxide are on their maximum oxidation number and therefore, will not burn.

These substances that cannot produce fire are known as *inert* or *non-combustibles*, while those that can experience combustion are called *combustibles*. However, not all combustible substances are burnt with the same ease; substances (i.e. gasoline) that can be ignited at ambient conditions with a small energetic spur are known as *flammable*, while combustible substances (i.e. diesel) that cannot burn in these conditions but could be ignited if reached by a fire are known as *non-flammable*. In addition, there are substances that can be ignited with a simple contact with air, with no need of energetic initiator, which are known as *pyrophoric*.

When combustible substances are exposed to heat and oxygen, these experience different phenomena according to their aggregation state:

- Gaseous substance in presence of air will burn directly, but only if the fuel concentration in air is between its lower and upper flammability limits. Since combustion is a chemical reaction, it needs certain stoichiometric ratios, so that mixtures below LFL are too fuel lean to produce combustion and mixtures over UFL are too fuel rich to produce combustion.

- Liquids, unlike gases, are not able to burn directly since combustion is a gas-state reaction; then, exposed to heat, these will have to vaporize defeating the barrier given by the latent heat of vaporization. Notice that flammable liquids are those whose concentration of flammable gases, according to vapor-liquid equilibria, at ambient temperature is between both LFL and UFL.

- Solids will experience first a drying, where possible humidity absorbed is removed. After this, a decomposition reaction occurs (pyrolysis), when complex molecules will decompose into simpler ones, capable to vaporize and burn. Pyrolysis occurs at slightly high temperatures (generally from 80 to 200 ˚C [4]) and unlike combustion, does not require the presence of oxygen.

2.2. Compartment fires

This project focuses on confined fires, occurred within an enclosure, partially isolated from environment. These can be better understand dividing the progress of a fire within a compartment with no air entrance into three stages [5].

- The first stage corresponds to a fast growth of fire temperature few seconds after its initiation due to the high exothermic behavior of the combustion reaction, as oxygen concentration is still high and therefore, a large amount of limiting reactant exists. Flame region temperatures can rise to 1600 ˚C and compartment temperature can experience a sensible increase from its initial value.

- During the next phase free combustion occurs as there is a continuous feedback of reactive helped by the natural movement of hot gases to the top of the compartment due to their lower density, which are ignited there because of the high temperatures that might reach values over 700 ˚C. Cold air, denser than hot gases, is forced to stay at the bottom of the compartment, whereas smoke tends to be accumulated at the top of the compartment, due to the effect of density-differences induced buoyancy, constituting the known as *smoke layer*, the height of which is an important control parameter in order to design emergency plans (humans cannot tolerate its temperatures), and, is increasing constantly until the oxygen originally present within the enclosure is consumed to the point of not being able to keep the combustion active, leading to a latent phase.

- The final phase consists on a latent combustion as there is no enough oxygen to feed the fire. However, the heat generated in the previous stage is kept and the fuel pyrolysis will persist. At this point, if oxygen is provided, combustion of hot unburnt pyrolysis gases will restart, leading to different scenarios [5]:

    - If oxygen entrance is produced within a small amount of time after the initiation of the latent phase, pyrolysis gases over their autoignition point will be only accumulated at the top of the building (smoke layer), so that only the zone adjacent to the roof will burn leading to the phenomena known as a *rollover*.

    - If pyrolysis gases are present along the whole compartment and are all over their autoignition point, a sudden oxygen entrance could also provoke a generalized combustion in the whole compartment volume, known as *flashover*. Under this condition, no humans are able to resist room conditions, even with special fire and radiation protection clothing, so that the most prudent action is to wait until the fire is over due to fuel extinction.

    - In the worst possible case, hot pyrolysis products will be over their autoignition temperature and within the optimal concentration, so that a sudden entrance of

oxygen will provoke a violent explosion known as *backdraft,* as result of a fast volume growth.

If proper smoke and temperature evacuation systems are not set, sudden air entrance is not difficult, since glasses break easily due to thermal shock.

An important feature of these fires, in addition to their fuel-lean condition is that, compartment pressure will increase with the elapse of the reaction. This is due to the facts that:

- Initial solid or liquid fuels stored at the compartment will be converted into gaseous products, so, according to perfect gases law, as the amount of gas moles is larger, the compartment pressure is also higher.

- Gaseous products are constantly increasing their temperature due to the elapse of the exothermic reaction. As compartment volume stays constant and temperature rises, due to ideal gases law, pressure is also increased.

This increment of pressure is especially remarkable at the top of the building. A possible advantage of this phenomena is that evacuation of smoke can be easily achieved at the cowling of the construction: if from the initial phase of the fire, a proper extraction system is set, smokes will be evacuating (since their higher temperature will drive them to the cowling and there, their higher pressure will push them out of the building). This strategy may save drawbacks, such as corrosion or damage after properties loss by temperature of structures due to combustion gases; will grant the possibility of the people present at the building to escape safely and will prevent the flashover and backdraft phenomena. Anyway, the devices used for this aim are described at section 4.5.

2.3. Characteristic parameters of fires

This section describes the main parameters of interest that might affect the fire behaviour, the consequences of fire or be of interest when designing fire protection equipment. However, very important parameters in generic fires such as vortex shedding are not discussed here due to neglectable influence in the objective of this project.

2.3.1. Heat release rate (HRR) and fire growth

The heat power produced by combustion of a substance is given by the product between heat of combustion of the fuel and the mass loss rate (fuel mass consumed by the reaction per unit time):

$$\frac{\dot{Q}}{A} = \dot{q}'' = \dot{m}'' \Delta H_c \tag{2.1}$$

This parameter is very important for the determination of the magnitude of the fire, as well as the fire growth. In the particular case of compartment fires, assuming flame spread as constant, the fire growth is parabolical, so that HRR vs time curve is given by the known as t-square fire growth parabola (equation (2.2).

$$\dot{Q} = \alpha(t)^2 \tag{2.2}$$

Where:

- $\dot{Q}$ is the heat release rate, expressed in kW.
- α is a parameter that indicates the fire growth velocity, expressed in $kW \cdot s^{-2}$.
- t is the time elapsed since the initiation of the fire, expressed in seconds.

2.3.2. Heat of combustion

Heat of combustion depends basically on the nature of the fuel. These values can be frequently found in bibliography or experimentally measured experimentally through calorimeters, although sometimes, especially in the case of new synthetical chemicals, lack of bibliographic records and the impossibility to carry out experiments due to the high price of small samples (for example, in the case of active pharmaceutical ingredients), make theoretical estimation of this parameter compulsory in order to predict HRR.

Some methods used to predict heat of reaction are the usage of specific software (in ex. Chetah, by ASTM) or the manual calculation of heat of reaction at a given temperature (in Kelvin) as the difference of the heat of formation of products and reactants at 25 ˚C (298 K) and 1 atm:

$$\Delta H_C(T) = \sum_{i=1}^{N} \Delta H_{f\ 298K\ i,Product} - \sum_{i=1}^{N} \Delta H_{f\ 298K\ i,Reactant} \quad (2.3)$$

In this case, heats of formation can be easily predicted from chemical structure through computational tools implementing group contribution methods (such as Joback method) or QSPR (Quantitative Structure Activity Relationship) methods; in addition, these last ones often provide a direct estimation of the heat of combustion.

In addition to methods exposed previously, Huggett suggested an alternative method to predict heat of combustion from air or oxygen consumption, as heat produced per unit mass of air consumed is -2,97 kJ/g and heat produced per unit oxygen consumed is 12,77 kJ/g [6]. This method has proven to provide very reliable results.

2.3.3. Mass loss rate

As any chemical reaction, a combustion constantly consumes the fuel (reactant), which disappears to form gaseous combustion products that may vary according to the chemical formula of the fuel and the combustion efficiency, but in most of cases, are carbon dioxide and gaseous water for complete combustions, leading to the formation of carbon monoxides and solid carbon if combustion is not complete. The buoyancy of hot gases to upper regions of the room (in the case of compartment fires) or up to atmosphere (in open air fires) remove continuously the products of the reaction media yielding to a continuous depletion of fuel as equilibrium is not attained if there are no products.

The combustible mass loss rate depends on the heat transferred from the flame back to the fuel and by the hot product gases (convective feedback), on the heat loses by conduction and radiation and in the heat required to bring the fuel to gaseous state, as expressed in the following equation:

$$\dot{m}'' = \frac{\dot{q}''_{C,F} + \dot{q}''_{C,G} - \dot{q}''_{W} - \dot{q}''_{R}}{L_g} \quad (2.4)$$

In the case of materials whose combustion generates char (solid carbon), the heat of gasification may vary, as the solid soot traces suspended in air may absorb part of the heat provided from flames and solid gases.

In the case of liquid fuels, heat of gasification is actually the heat of vaporization, which can be estimated from chemical structure through group contribution or QSPR methods.

2.3.4. Adiabatic temperature and heat loses

Adiabatic flame temperature can be understood as the temperature that reaches a flame that cannot gain or lose energy to environment, which is heated up due to exclusively the effect of exothermic reaction.

This concept can also be applied in the case of a surface heated up by the effect of a fire. FDS allows to collect this parameter, and thus, their advantages will be considered.

The adiabatic surface temperature is, then the maximum temperature that it would reach if loses to environment due to radiation and convection did not exist. Therefore, the knowledge of this value allows to measure the effect of heat dissipation of a certain body, according to the balance

$$\dot{q}_R'' + \dot{q}_C'' = \sigma\varepsilon({T_{AST}}^4 - {T_S}^4) + h(T_{AST} - T_S) \quad (2.5)$$

Where:

- $\dot{q}_R''$ is the heat flux lost by radiation, given in kW·m^{-2}.
- $\dot{q}_C''$ is the heat flux lost by convection, given in kW·m^{-2}.
- σ is the Stefan-Boltzmann constant, equal to 5,67·10-8 W·m^{-2}·K^{-4}.
- ε is the emissivity factor of the surface, non-dimensional.
- h is the convective heat transfer coefficient, given in W·m^{-2}·K.
- T_{AST} is the adiabatic surface temperature, expressed in K.
- T_S is the surface real temperature, expressed in K.

Emissivity (ε) is a factor compressed between 0 (white body) and 1 (black body), it is different for different materials. Average emissivity of a flame can be expressed as the difference of the sum of all constituents' partial emissivity and a corrector factor for the overlapping of CO_2 and H_2O bands, which unlike flame gases, do not have a continuous spectrum from visible light to infrared.

2.3.5. Fire geometry

As well as in the case of ventilated fires, fire geometry is also an interesting issue in the case of compartment fires, sometimes being translated into legal requirements when manufacturing or storage activity within an enclosure must be legalized. Unlike in the case of pool fires, compartment fires usually do not have a regular shape, and therefore the determination of their perimeter may be tough. Perimeter of a square-shaped burner fire can be determined according to its mathematical definition, see equation (2.6).

$$\pi\frac{D^2}{4} = \left(\frac{P}{4}\right)^2 \quad (2.6)$$

Where:

- P is the fire perimeter, expressed in meters.
- D is the fire theoretical diameter, expressed in meters.

In order to calculate the theoretical fire diameter, it is possible to use Heskestad equation (2.7) [7]. Although this empirical correlation was built with data coming from free burning pool fires, some authors found this reliable in compartment fires [8].

$$L = -1{,}02D + 0{,}23\dot{Q}^{2/5} \quad (2.7)$$

Where:

- L is the flame length, expressed in meters.
- $\dot{Q}$ is the fire heat release rate, expressed in kW.

Flame length is directly related to heat release rate, according to relationships proposed by some authors. For example, expression suggested by Alpert and Ward (2.8) [9] provides flame length with HRR as only input.

$$L = 0{,}174\left(k\dot{Q}\right)^{2/5} \quad (2.8)$$

Where k is a parameter whose value depends on the disposition of the fuel along the room (1 if the burner is placed at the center of the room; 2 if it is placed against the wall and 4 if it is placed at a corner).

Combining equations from (2.6) to (2.8) and setting k=1, a fast expression for the determination of the perimeter of square contoured irregular burners according to HRR has been found.

$$P = 0{,}195\dot{Q}^{\frac{2}{5}} \tag{2.9}$$

2.4. Ventilation dynamics in compartment fires

2.4.1. Constant pressure difference over the openings cross section

The simplest case, in order to illustrate how ventilation dynamics work, could be an enclosure with two openings, placed in both upper and lower bottoms of the building, as Figure 2.1 shows.

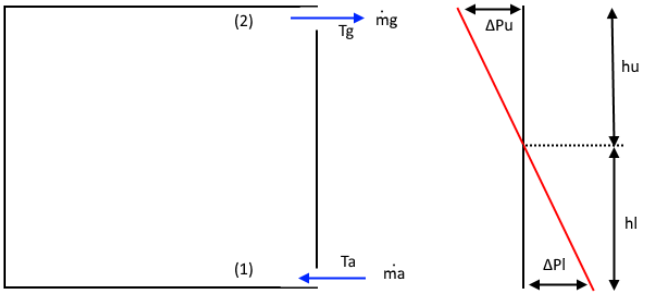

Figure 2.1 Air entrance mechanism in the case of a compartment with openings at lower (1) and upper (2) zone. Source: Prepared by the author according to information available at reference [5].

- Lower zone. Pressure differential between ambient and room interior is positive in the first case: ambient pressure is constant (101325 Pa), while initial pressure within the compartment was lower at the bottom as natural buoyancy movement brought gases up, generating a certain vacuum at the ground level. The natural tendency of air outside will be to compensate this pressure loss, entering the compartment through the gap.

- Upper zone. Pressure differential between ambient and room interior is negative in the latter case: ambient pressure stays constant, while initial pressure within the compartment was higher, due to buoyancy-induced accumulation of air at high temperature. The natural tendency of air outside will be to compensate this pressure gain, evacuating the compartment through the gap.

Pressure differential varies from ΔP_u to ΔP_l, so that there is a point with differential equal to zero. This point, which marks the border between lower and upper regions is known as neutral plane and sets the pressure reference height, so that variations from this value induce the entrance or expulsion of air. After applying the general Bernouilli equation, these two phenomena could be quantified according to equations (2.10) and (2.11) respectively [5].

$$\dot{m}_g = C_d A_u \rho_g \sqrt{\frac{2\, h_u(\rho_a - \rho_g)g}{\rho_g}} \tag{2.10}$$

$$\dot{m}_a = C_d A_l \rho_g \sqrt{\frac{2\, h_l(\rho_a - \rho_g)g}{\rho_a}} \tag{2.11}$$

Where:

- $\dot{m}_g$ and $\dot{m}_a$ are, respectively, hot gases evacuation and fresh air entrainment mass fluxes.

- A_u and A_l are, respectively, cross sectional areas of ventilations at upper and lower zones.
- h_u and h_l are, respectively, distances from the ceiling and from the ground to the neutral plane.
- ρ_g and ρ_a are, respectively, the densities of hot gases and fresh air.
- g is the acceleration of gravity.
- C_d are discharge coefficients, depending on the size and shape of the gaps and account for edge effects [5].

Neutral plain height can be calculated setting as condition that the air entrance flow is equal to the hot gases evacuation flow. The relative position of this plane depends on the square of the relation of ventilation areas and on the relation of temperatures inside and outside of the compartment. However, the effect of outside temperature on ventilation is out of the scope of this project.

2.4.2. Different ventilation stages within a room with a side vent

Fires occurred within compartments provided with a large opening (for example, doors or large windows), in which pressure difference and velocity vary over the cross section of the opening, evolve following four different stages [5], schematized at Figure 2.2.

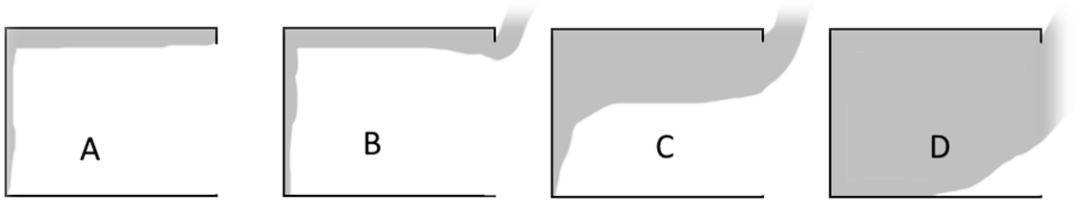

Figure 2.2 Classical ventilation stages for compartments provided with side vent Source: Prepared by the author according to information available at reference [5].

A) Corresponds to the initial stage, in which smoke is not leaving the compartment through the opening yet. Pressure inside is larger than outside.
B) Corresponds to the instant in which smoke is beginning to vent through the opening, but pressure inside is still higher than outside along whole compartment height, so that neutral plane is not formed.
C) Corresponds to the stratified case, which lasts during the most of steady state. This stage is further analyzed below.
D) Corresponds to a well-mixed case, in which hot layer extends to the floor, usually after a flashover.

The stratified (C) and well-mixed cases (D) represent the classical steady state scenarios during the development of a compartment fire

When smoke layer is close to floor enough (C), air at low regions is heated up and therefore, displaced to upper regions due to buoyancy, creating a certain vacuum at this region, which provokes the formation of a neutral plane (see Figure 2.3). Air speed is not constant along the opening and equations proposed previously cannot be directly applied, which implies the resolution of an integral in which axial coordinate z is the variable.

After proper mathematical operations, equations (2.12) and *(2.13)* are finally obtained [5].

$$\dot{m}_g = \frac{2}{3} C_d W \rho_a \sqrt{2g \frac{T_a}{T_g}\left(1 - \frac{T_a}{T_g}\right)(H_o - H_N)^3} \qquad (2.12)$$

$$\dot{m}_g = \frac{2}{3} C_d W \rho_a (H_N + 0{,}5 H_D) \sqrt{2g\left(1 - \frac{T_a}{T_g}\right)(H_N - H_D)} \tag{2.13}$$

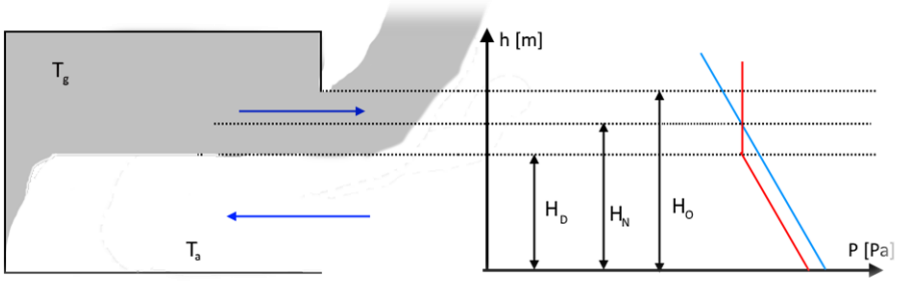

Figure 2.3 Air entrance mechanism in a stratified case. Red/blue line represents pressure inside/ outside. Source: Prepared by the author according to information available at reference [5].

Regarding to well mixed case (D), smoke layer height no longer exists, but neutral plane remains. Integrating over vents height, air entrance mass flow turns out to be given by equation (*2.14*) [5].

$$\dot{m}_a = \frac{2}{3} C_d A \sqrt{H_o} \sqrt{2g\rho_a} \sqrt{\frac{\left(\rho_a - \rho_g\right)\rho_a}{\left[1 + \left(\frac{\rho_a}{\rho_g}\right)^{1/3}\right]^3}} \tag{2.14}$$

In previous equations, all elements symbolize the same as in (2.11) and:

- H_o stands for the opening total height, given in m.
- H_D stands for the distance from floor to the smoke layer, in m.
- H_N stands for the distance from floor to the neutral plane, in m.
- W stands for the opening width, in m.
- T_a and T_g are temperatures of fresh air and smoke layer, respectively, given in K.

2.4.3. Ventilation through a ceiling vent

Often, compartments, as happens in the scenario simulated in this project, count on vents placed at ceiling (see Figure 2.4), which seize buoyancy effect to evacuate hot gases out of the room. In this case, pressure difference, as well as velocity, is constant along vents, although values at top and bottom are not equal. Considering that mass flows in and out are equal, evacuated mass flow is found to be given by equation *(2.15)*.

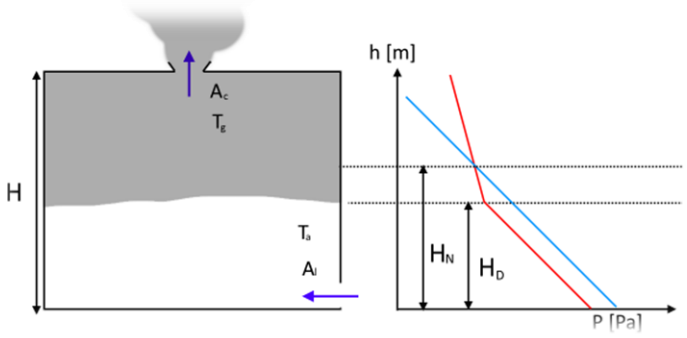

Figure 2.4 Air entrance mechanism in a ceiling vent. Red/blue line represents pressure inside/ outside. Source: Prepared by the author according to information available at reference [5].

$$\dot{m}_g = C_d A_c \rho_a \sqrt{\frac{2gT_a(T_g - T_a)(H - H_D)}{T_g\left(T_g + \frac{A_c^2}{A_l^2}T_a\right)}} \tag{2.15}$$

Where all symbols have the same meaning as in previous equations. In this case, A_c and A_l stand for the areas of mass flow evacuation and entrance, respectively.

2.4.4. Smoke layer

Accumulation of smoke at the region adjacent to the ceiling of the compartment and its constant growth is one of the most important aspects in order to be contemplated in the design of the evacuation plans and the installation of safeguards. Smokes, which are found at very high temperatures might contain, moreover, toxic and corrosive chemical species that could cause a drastic adverse effect on the health of people present at the building during the evacuation and, besides, a significant damage for structures due to temperatures and corrosion.

Some authors [8] have proposed different approaches for the estimation of smoke layer height, which are summarized at Table 2.1 and Table 2.2. All parameters have the same meaning as in previous equations, while L stands for flame length.

Table 2.1 Different correlations for the prediction of smoke layer height for steady state compartment fires

Author	Year	Formula
McCaffrey	1983	$H_D = \left(0{,}111\rho_g^{-1}A^{-1}\dot{Q}^{0{,}242}t + H^{-0{,}895}\right)^{-1{,}1173}$
Zukoski	1981	$H_D = \left(0{,}0507\rho_g^{-1}A^{-1}\dot{Q}^{0{,}242}t + H^{-2/3}\right)^{-3/2} + 0{,}0468\dot{Q}^{2/5} - 0{,}4902L$
Thomas	1963	$H_D = \left[\rho_g^{-1}A^{-1}t\left(0{,}0754\dot{Q}^{2/5} - 0{,}3267L\right) + H^{-1/2}\right]^{-2{,}0}$
NFPA	2005	$H_D = \left[1{,}11 - 0{,}28\ln\left(A^{-1}H^{2/3}\dot{Q}^{1/3}t\right)\right]H$

Table 2.2 Different correlations for the prediction of smoke layer height for unsteady state compartment fires

Author	Year	Formula
McCaffrey	1983	$H_D = \left(0{,}07479\rho_g^{-1}A^{-1}\alpha^{0{,}242}t^{1{,}484} + H^{-0{,}895}\right)^{-1{,}1173}$
Zukoski	1981	$H_D = \left(0{,}0304\rho_g^{-1}A^{-1}\alpha^{1/3}t^{5/3} + H^{-2/3}\right)^{-3/2} + 0{,}0468\dot{Q}^{2/5} - 0{,}4902L$
Thomas	1963	$H_D = \left[\rho_g^{-1}A^{-1}t\left(0{,}0417\alpha^{2/5}t^{4/5} - 0{,}3267L\right) + H^{-1/2}\right]^{-2{,}0}$
NFPA	2005	$H_D = \left[0{,}91\left(A^{-3/5}H^{2/5}\tau^{-2/5}t\right)^{-1{,}45}\right]H$

Smoke layer is constantly increasing its temperature until it arrives to a steady state value. Obviously, it is higher as larger is the heat source, while its value will decrease with an increment of heat losses to ambient. McCaffrey, Quintiere and Harkleroad [10] performed a non-dimensional study with more than 100 compartment fires, arriving to the deduction of equation (*2.16*), which is known as MQH in terms of fire science jargon.

$$\Delta T = 6{,}85\left[\frac{\dot{Q}^2}{(h_k A_T)\sum_{i=1}^{N}\left(A_{v,i}\sqrt{H_{v,i}}\right)}\right]^{1/3} \tag{2.16}$$

Where:

- ΔT is the difference between smoke layer temperature and ambient temperature, expressed in ºC or K.
- $\dot{Q}$ is the heat release rate, given in kW·m^{-2}.
- h_k is the heat loss coefficient, expressed in kW·m^{-2}K^{-1} (it is very important to keep these units).
- $A_{v,i}$ is the area of the ith ventilation opening, given in m^2.

- $H_{v,i}$ is the height of the i[th] ventilation opening, given in m.
- A_T is the compartment total exposed area (ceiling+floor+ walls–vents), given in m^2.

The heat loss coefficient value depends essentially thermal penetration time across the walls. This value, contemplating the fact that compartment peripheral surfaces might be different between them, can be calculated with equation (*2.17*) in the case of thermally thin walls, and with equation (*2.18*) in the case of thermally thick solids.

$$h_k = \sum_{i=1}^{N} \left(\frac{A_i}{A_T} \sqrt{\frac{k_i}{\delta_i}} \right) \tag{2.17}$$

$$h_k = \sum_{i=1}^{N} \left(\frac{A_i}{A_T} \sqrt{\frac{k_i \rho_i C_i}{t}} \right) \tag{2.18}$$

Where:

- k_i is the wall material thermal conductivity of i[th] compartment external surface, expressed in kW·m^{-1}·K^{-1}.
- δ_i is the wall thickness of i[th] compartment external surface, expressed in m.
- ρ_i is the wall material density of i[th] compartment external surface, expressed in kg·m^{-3}.
- C_i is the wall material specific heat of i[th] compartment external surface, expressed in kJ·kg^{-1}·K^{-1}.
- t is the time elapsed since ignition.

Notice that a certain solid surface can be considered as thermally thin if t is larger than its thermal penetration time, $t_{p,i}$, defined by equation (*2.19*) [4].

$$t_{p,i} = \left(\frac{\rho_i C_i}{k_i} \right) \left(\frac{\delta_i}{2} \right)^2 \tag{2.19}$$

Besides of BQH equation, Beyler [4] proposed another method, in which there is no apparent distinction between thin or thick compartment walls. However, a disadvantage of this method, especially in comparison with McCaffrey equation, is the necessity of estimating gas total mass within the compartment, which is not usually easy to do as it may vary according to fire stage.

$$\Delta T = \frac{2K_2}{K_1^2} \left(K_1 \sqrt{t} - 1 + e^{-k_1 \sqrt{t}} \right) \tag{2.20}$$

Where:

$$K_1 = \frac{0{,}8}{m C_p} \left(\sum_{i=1}^{N} \frac{A_i}{A_T} \sqrt{k_i \rho_i C_i} \right) \tag{2.21}$$

$$K_2 = \frac{\dot{Q}}{m C_p} \tag{2.22}$$

All symbols represent the same parameter as in McCaffrey model, while C_p stands for the gas specific heat capacity and m stands for the previously mentioned total gas mass within compartment.

Both MQH and Beyler methods are useful for the calculation of pre-flashover temperatures, whereas, other methods, such as the one proposed by Babrauskas [4] (see appendix A) should be applied in order to calculate post-flashover temperatures, although results obtained with this model were not apparently satisfactory.

3. FDS Simulator

3.1. Computational simulation of fire phenomena

Fires can be modelled through two types of widely used fire models [4]:

- Zone models divide the study domain into two regions: a hot region and a cold region, delimited precisely by smoke layer height. These models are based on empirical relationships between different fire parameters, as those defined previously, and are much simpler than field models. Their results are not as realistic as results given by field models, because many more simplifications are used, but computational time is enormously lower.

- Field models are based on Computational Fluid Dynamics (CFD), a branch of fluid mechanics that, due to the calculation complexity of the differential equations involved in the problems related to the flux of fluids, uses algorithms and numerical methods with the aid of a computer, which performs these operations faster. These models divide a control volume into different cells, where Navier Stokes equations of mass, species, momentum and energy conservation are solved. The large calculation capacity of modern computers to solve these operations make these models a suitable option for fire modelling nowadays.

CFD models are divided into three types, according to the strategy of resolution of the equations [11]:

- **Direct Numerical Simulation** is a CFD method that implies to solve the Navier Stokes transport equations directly, what requires a huge computational capacity and makes this method unpractical for most engineering applications, including fire simulations.

- **Reynolds Averaged Navier Stokes (RANS)** is a numerical method that uses as approach the decomposition of instantaneous values to a mean value with fluctuations. Softwares based on RANS method (for example, SOFIE) are recommended to be used for steady state simulations because this method executes Taylor expansion series with convergence for every time step [11]. This makes it independent of what has happened earlier (in time) in the simulation, which is appropriate for steady state fires. However, this strategy is not recommended to perform simulations with many time steps, due to lack of time efficiency.

- **Large-eddy simulation (LES)** is a numerical technique for integrating spatially filtered equations of motion that describe high-Reynolds number time-evolving, three-dimensional turbulence. Given this limitation, only a portion of the scale range can be explicitly resolved. LES solves just the most important scales of the flow of interest and approximates the other scales. As the grid resolution of LES becomes finer, a wider range of turbulent eddies is resolved, less are parameterized, so an excessive fine mesh would imply a Direct Numerical Simulation. LES is, then, a compromise between Direct Numerical Simulation (DNS, in which all turbulent fluctuations are resolved) and traditional RANS approach (in which all turbulent fluctuations are parameterized and only ensemble averaged statistics are calculated). In LES, every calculation is based on the calculation performed in the previous time step.

3.2. FDS Background

3.2.1. Overview

Fire Dynamics Simulator (FDS) is a CFD (Computational Fluid Dynamics) software, developed by the National Institute of Standards of Technology and released initially on February of year 2000 after several years of development. Since then, it has experienced continuous revisions and updates. Current version is 6.6.3.

This software applies large eddy simulation (LES) numerical method to solve low speed (low Mach numbers), heat-driven-flow Navier-Stokes equations for a single or multiple species fluid. These low-speed equations are obtained by filtering out pressure waves from Navier-Stokes equations [12], so they allow for large variations in density but not in pressure, fact that conditions its applications to simulation of stages with no significant sudden pressure changes. As FDS is developed to low-speed flows ($Ma \leq 0.3$), it cannot be used to model, for example, explosions [13].

FDS calculates directly all those eddies sized larger than the specified grid size and uses sub-grid models to calculate that which cannot be resolved in the largest eddy. In the model used in FDS for turbulence modelling, small eddies are filtered off and solved by the Smagorinsky turbulence model [11] in former versions and by the Deardorff turbulence model from the version 6 forth.

Supported features of FDS are [14]:

- Low speed transport of heat and combustion products from a fire.
- Radiative and convective heat transfer between the gas and solid surfaces.
- Pyrolysis.
- Flame spread and fire growth.
- Sprinkler, heat detector, and smoke detector activation.
- Sprinkler sprays and suppression by water or other agents.

Although FDS was designed specifically for fire simulations, it can be used for other low-speed fluid flow simulations that do not necessarily include fire or thermal effects.

3.2.2. Simulation file structure

FDS is written in Fortran Language [1], which imports input data from a text file and, after performing its calculations, returns, besides of simulation results that are always provided by default, the indicated output data, through .csv (comma separated values) files easy to convert to classic Microsoft Excel format through simple macros. Moreover, it is possible to see animated results within the three-dimensional scenario defined by input geometry, thanks to a complementary software, also designed by NIST, called *Smokeview*, which is included in FDS download pack and allows the user to view simulation results as an animation. Setting desired geometry through text lines is sometimes hard to do; this is the reason why alternative software as *Pyrosim* were developed, which provide a CAD interface that allows the user to build geometries graphically and then, convert them to FDS input format.

Usage of FDS is though. It needs to be called in the command prompt once the text file has been written, as does not own a user-friendly interface neither a direct executable icon.

FDS simulation text files are formed by a set of instructions or codelines, which must be started by the symbol “&” and ended by “/” in order to be read by the simulator. Every codeline consists indicates a parameter group, the pertinent parameter within that group and its attributes.

Common parameters found at all simulations are:

- Header, indicated with the parameter group HEAD including the simulation ID and title.
- The domain and mesh dimensions, that are set with the option IJK (found within MESH parameters group), that permits to set the number of cells in the i, j and k directions of the mesh, and the option XB defines the global dimensions of the simulation domain.

- The total time that the simulator will be running the file, indicated with the command T_END found within the TIME parameters group.
- TAIL, which indicates the end of the FDS code.

Moreover, an FDS code should include data about the geometry and properties of all involved materials, as well as eventual parameters for mathematical models or data required to be obtained in output. A sample FDS input file [1] is shown below:

```
&HEAD CHID='exemple', TITLE='exemple' /
Mesh
&MESH IJK= 51, 50, 25, XB= 0.0, 10.2, 0.0, 10.0, 0.0, 5.0/

Simulation time
&TIME T_END= 1500/

Combustion reaction parameters
&REAC ID='PYROLYZATE'
        HEAT_OF_COMBUSTION= 16300
        SOOT_YIELD=0.015
        CO_YIELD=0.004
        C=1
        H=1.7
        O=0.74
        N=0.002
        AUTO_IGNITION_TEMPERATURE=50/

Material properties & pyrolysis reaction
&MATL ID= 'WOOD'
        EMISSIVITY=0.95
        CONDUCTIVITY=0.15
        SPECIFIC_HEAT=2.5
        DENSITY=50.
        N_REACTIONS=1
        A= 5.72E10
        E=171880
        N_S=1
        SPEC_ID='PYROLYZATE'
        NU_SPEC=1
        HEAT_OF_REACTION=950
        N_O2=1
        GAS_DIFFUSION_DEPTH=0.05 /
&SURF ID='FUSTA', MATL_ID='WOOD', THICKNESS=0.2, COLOR='BROWN', EXTERNAL_FLUX=100 /

Geometric parameters
Materials-
&MATL ID='FORMIGO', CONDUCTIVITY=1.4, SPECIFIC_HEAT=0.837, DENSITY=2200./
&SURF ID='TERRA', MATL_ID='FORMIGO', THICKNESS=0.2, COLOR='GRAY' /
&MATL ID='MAO', CONDUCTIVITY=0.69, SPECIFIC_HEAT=0.840, DENSITY=1600./
&SURF ID='PARET', MATL_ID='MAO', THICKNESS=0.2, COLOR='BRICK' /
&MATL ID='SANDVITX', CONDUCTIVITY= 2.03, SPECIFIC_HEAT=0.82, DENSITY=472.4/
&SURF ID='COBERTA', MATL_ID='SANDVITX', THICKNESS=0.052, COLOR='BLACK' /
Obstacles-
&OBST XB= 0.0, 10.0, 0.0, 10.0, 0.0, 0.2, SURF_ID='TERRA'  /
&OBST XB= 0.0, 0.2, 0.0, 10.0, 0.2, 4.8,  SURF_ID='COBERTA'  /
&OBST XB= 9.8, 10.0, 0.0, 10.0, 0.2, 4.8, SURF_ID='COBERTA'  /
&OBST XB= 0.2, 9.8, 0.0, 0.2, 0.2, 4.8,   SURF_ID='COBERTA'  /
&OBST XB= 0.2, 9.8, 9.8, 10.0, 0.2, 4.8,  SURF_ID='COBERTA'  /
&OBST XB= 0.0, 10.0, 0.0, 10.0, 4.8, 5.0,   SURF_ID='COBERTA' /
Palet-
&OBST XB= 4.4, 5.4, 4.6, 5.6, 0.2, 1.2, SURF_IDS='FUSTA', 'FUSTA', 'INERT'/

Output parameters
&SLCF PBY=5.1, QUANTITY='TEMPERATURE' /
&SLCF PBY=5.1, QUANTITY='oxygen' /
&SLCF PBY=5.1, QUANTITY='VELOCITY', VECTOR=.TRUE. /
&BNDF QUANTITY='WALL_TEMPERATURE' /
&BNDF QUANTITY='BURNING_RATE' /

&TAIL /
```

Figure 3.1 Example of FDS input file by Illa [1]

3.3. Mathematical models

3.3.1. Hydrodynamic model

LES equations used by FDS are derived by applying a low-pass filter parameterized by a width δ to the transport equations for mass *(3.3)*, momentum *(3.4)*, species *(3.5)* and energy *(3.6)*. For example, the 1-Dimensional filtered fluid density (of lumped species) field for a cubical[1] cell of width $\Delta = \delta x$ is [15]:

$$\bar{\rho}(x,t) = \frac{1}{\Delta}\int_{x-\frac{\Delta}{2}}^{x+\frac{\Delta}{2}} \rho\,(x,t)\;\, d\rho \tag{3.1}$$

Filtering of pressure shows the same structure. However, velocity, species fractions, temperature and enthalpy, and any ϕ scalar quantity must be filtered through Favre-filters [16]. Favre-filtered quantities are denoted by a tilde and are defined as:

$$\tilde{\phi} = \frac{\overline{\rho\phi}}{\bar{\rho}} \tag{3.2}$$

The Navier Stokes filtered equations, which are governing flow motion in FDS are, for the i[th] component of velocity are [16]:

$$\frac{\partial \bar{\rho}}{\partial t} + \frac{\partial \bar{\rho}\tilde{u}_j}{\partial x_j} = 0 \tag{3.3}$$

$$\bar{\rho}\left(\frac{\partial \tilde{u}_i}{\partial t} + \frac{\partial \tilde{u}_i\tilde{u}_j}{\partial x_j}\right) = -\frac{\partial \bar{p}}{\partial x_i} + \bar{\rho}g + f_i + \frac{\partial \tau_{ij}}{\partial x_j} \tag{3.4}$$

$$\frac{\partial(\bar{\rho}\tilde{Y}_e)}{\partial t} + \frac{\partial(\bar{\rho}\tilde{u}_j\tilde{Y}_e)}{\partial x_j} = -\frac{\partial}{\partial x}\left(\overline{\rho u Y_e} - \bar{\rho}\tilde{u}\tilde{Y}_e\right) + \frac{\partial}{\partial x}\left(\overline{\rho D_e \frac{\partial \tilde{Y}_e}{\partial x_j}}\right) + \bar{\dot{m}}_e''' \tag{3.5}$$

$$\frac{\partial(\bar{\rho}\tilde{h})}{\partial t} + \frac{\partial(\bar{\rho}\tilde{u}_j\tilde{h})}{\partial x} = \frac{D\bar{p}}{Dt} - \frac{\partial \dot{q}_{r,j}''}{\partial x_j} + \frac{\partial}{\partial x_j}\left(k\frac{\partial \tilde{T}}{\partial x_j}\right) + \sum_e \frac{\partial}{\partial x_j}\left(\bar{\rho}D_e\tilde{h}_e\frac{\partial \tilde{Y}_e}{\partial x_j}\right) + \dot{q}''' \tag{3.6}$$

Where:

- g is the gravity.
- $\bar{p}$ is the total (fluid average) pressure.
- k is the gas mixture thermal conductivity.
- t is the time.
- ρ is the gas mixture density.
- u is the fluid velocity vector (in the i,j and k directions).
- x is the position (in the i,j and k directions).
- $\dot{q}_r''$ is the radiation heat release vector (in the i,j and k directions).
- D_e is the mass diffusivity.
- h_e is the specific enthalpy.
- Y_e is the fraction of an e species.
- f_i is the drag force due to unresolved lagrangian particles, which will not affect in the cases studied in this project, as there is not any lagrangian particle.
- τ_{ij} is the stress due to viscous forces, which can be found according to equation *(3.7)*.
- $\dot{m}_e'''$ is the source term of the species balance equation, determined through FDS combustion model [17].

[1] $\Delta = \sqrt[3]{\delta x \delta y \delta z}$, what supposes $\Delta = \delta x$ when cubical cells are used.

- $\dot{q}'''$ is the source term of the heat conservation, determined through FDS combustion model [17].

Both diffusivity and thermal conductivity are estimated from turbulent viscosity and turbulent Schmidt and Prandtl numbers respectively, which are constant values set to 0.5 by default. These numbers can be modified by FDS users, although its modification is not recommended. See FDS user's guide [18] for further information.

Stress due to viscous forces is determined according to following equation.

$$\tau_{ij} = 2(\mu + \mu_t)\left(\frac{1}{2}\left(\widetilde{\frac{\partial u_\iota}{\partial x_\jmath}} + \frac{\partial u_\jmath}{\partial x_\iota}\right) - \frac{1}{3}(\nabla \cdot \tilde{u})\delta_{ij}\right) \tag{3.7}$$

Mass and species transport is governed by equations *(3.3)* and *(3.5)* respectively, while momentum and thermal energy are governed by equations *(3.4)* and *(3.6)* respectively. In addition to these main governing equations, FDS uses an ideal gases equation *(3.8)*, which includes density and fluid average molar mass, in order to compute temperature at each time step [17].

$$\rho = \frac{\bar{p}M}{RT} \tag{3.8}$$

Where:

- ρ is the density of the gas mixture at current time step, expressed in kg·m^{-3}.
- $\bar{p}$ is mean pressure at current step, expressed in Pa.
- M is the mean molar mass of lumped species, expressed in kg·mol^{-1}.
- R is the constant of perfect gases, with value of 8,314 J·K^{-1}·mol^{-1}.
- T is the absolute temperature, expressed in K.

As can be seen in equation (3.7), viscous stress depends directly on velocity components, on fluid viscosity (computed by FDS from density, velocity and grid size) and on turbulent (or eddy) viscosity, which is modelled from FDS version 6 forth through a slight modification of Deardorff turbulence model (equation

(3.9)), which also depends on velocity components, density and grid size. δ_{ij} is Kronecker delta, which is 1 if $i = j$ or 0 if $i \neq j$ [17].

$$\mu_t = \rho C_v \Delta \sqrt{k_{sgs}} \tag{3.9}$$

$$k_{sgs} = \frac{1}{2}(\bar{u} - \hat{u})^2 + (\bar{v} - \hat{v})^2 + (\bar{w} - \hat{w})^2 \tag{3.10}$$

Where:

- k_{sgs} is the *subgrid scale kinetic energy* per unit mass.
- $\bar{u}$ is the average value of the u velocity component at the grid centre (the respective values for v and w components are determined exactly).
- $\hat{u}$ is the weighed value of u over the adjacent cells (the respective values for v and w components are determined exactly).
- C_v is a constant value (Smagorinsky constant), which is 0.1 by default and can be changed, although bibliography recommends this value [19].

Calculation of turbulent viscosity can be performed also through other models (Constant or dynamic Smagorinsky, Vreman, RNG or WALE) if the user indicates which model will be used. Vreman and Smagorinsky turbulent viscosities, however, also depend on velocity components, density and grid size. This is the reason why the most affective input variables seem to be fluid density (which depends on user-defined liquid fuel density), grid size and velocity (which can be modified as the environmental wind speed).

3.3.2. Combustion model

A source common of confusion in FDS and, generally, in fire science, is the distinction between gas phase *combustion* and *pyrolysis* (in case of solid phase) or liquid phase vaporization. While, pyrolysis refers to the reaction of formation of flammable fuel vapour and oxygen from a source fuel in solid phase, combustion refers to the chemical reaction between flammable fuel vapour and oxygen. Parameters such as formation of combustion products and heat produced due to the chemical reaction are modelled through a combustion model.

In order to model combustion, last FDS version uses a single-step, mixing controlled fast chemistry combustion model [20] and the reaction of fuel and oxygen is not necessarily complete. From version 5 forth FDS default fast chemistry model only considers three lumped species: air, products and fuel. All species are considered to have a certain mass fraction of each one of their components.

This model, based on mixture fraction model of previous FDS versions, considers an infinitely fast reaction and a non-premixed combustion [21] that, however, can be modified through changing the option INITIAL_UNMIXED_FRACTION (ζ_0), set to 1 by default in LES and to 0 in DNS [18]. Although FDS considers by default infinitely fast reactions and that fuel and oxygen cannot coexist, users are allowed to define Arrhenius-law parameters in order to model non-infinitely fast reactions.

The mixture fraction is computed according to:

$$Z = \frac{s\,Z_F - (Z_O - Z_O^0)}{s\,Z_F^0 + Z_O^0}$$

FDS models the combustion as a partially stirred batch reactor, and the used combustion turbulence model is based on the eddy dissipation concept (EDC) model for initially unmixed reactants, that considers that “all mixed is burnt"; it implies that fuel vapour disappearance is controlled by the limiting reactant at a rate set by a characteristic mixture time (McGrattan et al., 2014).

$$\dot{m}_F = -\rho \frac{\min(Z_F, {}^{Z_A}/_{s})}{t_{mix}} \tag{3.11}$$

Where:

- Z_F is the mass percent composition of fuel in lumped species.
- s is the mass stoichiometric coefficient of air.
- Z_O is the mass percent composition in oxygen.
- Z_O^0 is the initial mass percent composition in oxygen.
- Z_F^0 is the initial mass percent composition of fuel in lumped species.
- $\dot{m}_F$ is fuel mass loss rate.
- ρ is average fluid density.
- t_{mix} is the characteristic mixing time.
- Z_A is the mass percent composition of air.

The basic idea behind the model used by FDS in order to determine characteristic mixing time is to consider the three physical processes of diffusion, subgrid scale advection, and buoyant acceleration and to take the fastest of these processes (locally) as the controlling flow time scale. However, the mixing time must be larger (or at least equal) than time required for the chemical time, which is zero by default. Then, mixing time is given by equation *(3.12)*.

$$t_{mix} = \mathrm{Max}\left(t_{chem}, \min\left\{ \frac{\Delta^2}{D_{mix}}, \frac{0.4\,\Delta}{\sqrt{{}^{2}/_{3}\;k_{sgs}}}, \sqrt{\frac{2\Delta}{g}} \right\} \right) \tag{3.12}$$

Where:

- t_{chem} chemical time required for the chemical combustion reaction occur.
- k_{sgs} is the *subgrid scale kinetic energy* per unit mass, expressed in $m^2 \cdot s^{-2}$.
- Δ is the cell width, expressed in m.
- g is the acceleration of gravity, expressed in $m \cdot s^{-2}$.
- D_{mix} is the mixture mass diffusivity, expressed in $m^2 \cdot s$.

The unmixed fraction decreases with time, according to equation *(3.13)* and, once it is known, the composition of this point at any time step, may be determined according to equation *(3.14)*. The product of the time differential of the e species composition and the mixture density gives the chemical composition source term used in equation *(3.5)*.

$$\zeta(t) = \zeta_0 e^{-t/t_{mix}} \tag{3.13}$$

$$\widetilde{Y_e}(t) = \zeta(t)\widetilde{Y_e^0} + (1 - \zeta(t))\widehat{Y_e}(t) \tag{3.14}$$

$$\dot{m}_e''' = \rho \frac{d\widetilde{Y_e}(t)}{dt} \tag{3.15}$$

Known the composition of an e species in a given point, the variation of mean fuel mass concentration can be also determined according to equation *(3.19)* in the fast chemistry model that FDS uses by default [17].

$$\Delta\hat{Y}_F = -min\left(\hat{Y}_F, \hat{Y}_e \frac{\nu_F M_F}{\nu_e M_e}\right) \tag{3.16}$$

Where:

- $\zeta(t)$ is unmixed fraction calculated at time step t within a certain computational cell.
- ζ_0 is initial value of unmixed fraction, which is set to 1 by default (diffusion flame).
- $\widetilde{Y_e}(t)$ is the composition of the mixture on species e at time step t.
- $\widehat{Y_e}(t)$ is the mass fraction of species e in mixed zone of a computation cell.
- $\widehat{Y_F}(t)$ is the mass fraction of fuel in mixed zone of a computation cell.
- ν_F is the stoichiometric coefficient of fuel at combustion reaction.
- ν_e is the stoichiometric coefficient of species e at combustion reaction.
- M_F is the molecular mass of fuel.
- M_e is the molecular mass of species e.

Heat release rate per unit volume obtained from the gas phase chemical reaction (source term of equation *(3.6)*) can be found as the sum of products between species formation rate and enthalpy of formation for all species [17].

$$\dot{q}''' = -\sum_e \dot{m}_e''' \Delta h_{f,e} \tag{3.17}$$

Enthalpies of formation of combustion products and common fuels are by default stored in FDS library. However, in the case of non-common fuels or mixtures, the user is obliged to specify either the enthalpy of formation of the fuel or its heat of combustion, from which this former parameter is calculated. In addition, FDS could calculate heat release rate as the product of depleted oxygen mass flux and heat release per mass of oxygen consumed, using a default value of 13,1 kJ/kg O_2 consumed. See section 12.1.2 of FDS User's Guide [20] for further information.

According to Nielsen [13], FDS combustion model makes a good approximation for large-scale, well ventilated fires, but in under-ventilated fires, in FDS Technical Reference Guide Vol.1 [17] is it proposed to introduce a burn no burn criterion to make possible the mixing of fuel and oxygen without combustion.

3.3.3. Hot gases thermal radiation transport model

While heat transfer by convection is estimated by solving the filtered Navier-Stokes equations, FDS calculates the net contribution from thermal radiation to heat release as [17]:

$$\dot{q}_r''' = \kappa(x)\left[\int_{4\pi} I(x,\vec{s})d\vec{s} - 4\pi I_b(x)\right] \tag{3.18}$$

For a non-scattering gas, radiation intensity I emitted in $\vec{s}$ direction is obtained by solving the radiative transport equation:

$$\vec{s}\cdot\nabla I_\lambda\,(x,s) = \kappa(x,\lambda)[I_b(x) - I_\lambda\,(x,\vec{s})] \tag{3.19}$$

However, an exact solution of this equation may result very computationally expensive given the dependence on electromagnetic wavelength λ. This problem may be solved by considering the global radiation intensity as the sum of N different partial intensities corresponding to the N different bands in which the electromagnetic spectrum is divided. As each band has its own absorption coefficient $\kappa(x)$ (which depends on the cross sectional area of the radiation emitting particles and on optical parameters, and due to their complexity, further study of absorption coefficients is out of the scope of this project), radiation intensity of an n band is given by the expression *(3.20)* for n=1, 2, 3...N.

$$\vec{s}\cdot\nabla I_n\,(x,\vec{s}) = \kappa(x)[I_b(x) - I_n\,(x,\vec{s})] \tag{3.20}$$

Despite dividing the total spectrum into different single bands, calculation is computationally expensive and some simplifications must be done:

- In large scale pool fires, soot production is much higher than CO_2 and water steam production, and as radiation spectrum of soot is continuous, gas released by a fire can be considered as a grey medium [17] with a single band. This is the default mode of FDS.

- In optically thin fires, soot production is smaller and then, contributions of CO_2 and water steam are most relevant, and considering all gas as a grey medium would imply an over-prediction of the emitted radiation [17]. In most cases, dividing the spectrum into 6 bands provides good enough results.

In FDS, radiation intensity of the black body (source term) at a given x position is calculated from the temperature raised to the forth power in this position. However, temperatures inside the flame zone can be under estimated if grid size is not fine enough, what provokes a high error in the source term. This is the reason why FDS provides two options in order to determine the radiation source term, as equation *(3.21)* reflects, allowing to determine radiation inside flame through a product between total heat release rate and a radiative fraction that users can specify (0.35 by default) [17]. For regions outside flame, as temperatures are not under estimated, this source term is estimated through the expression at right of equation *(3.21)*.

$$\kappa(x)\cdot I_b(x) = Max\left(\frac{\chi\cdot\dot{q}'''}{4\pi}, \frac{\sigma T(x)^4}{\pi}\right) \tag{3.21}$$

Where:

- $\dot{q}_r'''$ is the radiative heat release rate per unit volume, expressed in kW·m^{-3}.
- $\kappa(x)$ is the radiation absorptivity.
- $I_n\,(x,\vec{s})$ is the solution of radiation transport equation for grey gases (*3.20*).
- $I_b(x)$ is the radiation intensity source term, expressed in kW·m^{-3}.
- χ is the radiative fraction, set to 0,35 by default.
- $\dot{q}'''$ is the total heat release rate per unit volume, expressed in kW·m^{-3}.
- σ is the Stefan-Boltzmann constant, equal to 5,67·10-8 W·m^{-2}·K^{-4}.

- ε is the emissivity factor of the surface, non-dimensional.

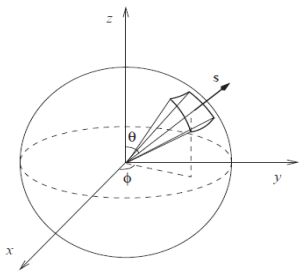

Figure 3.2 Circumference of all possible directions to which radiation is emitted. Source: [17]

For an emissive particle, radiation is emitted in all the directions (describing a circumference, as Figure 3.2 shows). However, as is dividing this circumference into infinite angles would require an infinite number of $\vec{s}$ vectors for equation *(3.20)*, FDS solves the radiations transport equations on a spherical mesh with a finite number of discrete angles, which can be modified by the user and are 100 by default [13].

3.3.4. Heat transfer in solids

FDS assumes that solid surfaces consist of multiple layers, with each layer composed of multiple material components that can undergo multiple thermal degradation reactions. However, before the definition of how pyrolysis works on FDS, a fast review of heat transfer models implemented for solids has been conducted.

Heat conduction in solids is modelled in FDS by the equation (*3.22*). Boundary conditions and solving strategy are all explained in FDS Technical Reference Guide, vol. 1 [17].

$$\rho_s C_s \frac{\partial T_s}{\partial t} = \frac{\partial}{\partial x}\left(k_s \frac{\partial T_s}{\partial x}\right) + \dot{q}'''_{s,c} + \dot{q}'''_{s,R} \tag{3.22}$$

Where:

- ρ_s is the solid density, expressed in kg·m^{-3}.
- C_s is the solid specific heat capacity, expressed in J·kg^{-1}K^{-1}.
- k_s is the solid thermal conductivity, expressed in W·m^{-1}K^{-1}.
- T_s is the solid temperature at the time step, expressed in K.
- $\dot{q}'''_{s,c}$ is the chemical source term due to pyrolysis reaction (W/m^3).
- $\dot{q}'''_{s,R}$ is the radiation source term due to heat absorbed as radiation (W/m^3).

Convective heat transfer to solids is modelled according to equation (*3.23*), Newton's law of cooling. The convection coefficient is calculated according to equation (*3.24*).

$$\dot{q}''_c = h(T_g - T_w) \tag{3.23}$$

$$h = Max\left\{C\left|T_g - T_w\right|^{\frac{1}{3}}, \frac{k}{L}Nu\right\} \tag{3.24}$$

Where:

- $\dot{q}''_c$ is the convective heat flux to the solid, expressed in W·m^{-2}.
- h is the convective heat transfer coefficient, expressed in W·m^{-2}K^{-1}.
- T_w is the solid surface temperature at the time step, expressed in K.
- T_g is the temperature of the hot gases at the time step, expressed in K.
- k is the thermal conductivity of the hot gases, in W·m^{-1}K^{-1}.
- L is a characteristic length related to the size of the physical obstruction, in m.
- Nu is the Nusselt number, which is function of Reynolds and Prandtl numbers.

Nusselt number depends on Reynolds and Prandtl numbers and therefore, on the transport properties of gases and geometry of solids. For further information, see FDS Technical Reference Guide, vol. 1 [17].

3.3.5. Pyrolysis model

In the case of solid or liquid fuels, these must be converted into gas in order to be susceptible to react with oxygen. This section focuses on the mathematical equations that lead to the determination of solid fuel mass loss rates when exposed to fire.

When the fire size is defined and HRR is known, often the desired information is a model for transport of smoke and heat. Then, solid mass loss rate can be obtained by equation (*3.25*) [17].

$$\dot{m}_f = \frac{f(t)\dot{q}''}{\Delta H_C} \tag{3.25}$$

Where:

- $\dot{m}_f$ is the mass loss rate of solid fuel (kg/s).
- $f(t)$ is an optional user-defined non-dimensional time ramp.
- $\dot{q}''$ is the user-specified HRR (kW).
- ΔH_C is the fuel heat of combustion (kJ/kg).

Nonetheless, in most of cases, fires are not defined and therefore, FDS must recur its pyrolysis mathematical model. This model departs from four simplificative assumptions [17]:

- Instantaneous release of gas species.
- Local thermal equilibrium between the solid and gaseous components.
- No condensation of gaseous products.
- No porosity effects.

Density of a given material component α is updated at every time step according to its species conservation equation (*3.26*) [17].

$$\frac{\partial}{\partial t}\left(\frac{\rho_{s,\alpha}}{\rho_s(0)}\right) = -\sum_{\beta=1}^{N,\alpha} r_{\alpha,\beta} + S_\alpha \tag{3.26}$$

Where:

- $\rho_{s,\alpha}$ is the density of component α at current time step.
- $\rho_s(0)$ is the initial density of component α in the previous step.
- $r_{\alpha,\beta}$ is the rate of reaction β, in which component α is consumed (s^{-1}).
- S_α is the production term of component α.

Reaction rate of a β reaction is composed the product of a reactant dependency term, an Arrhenius function, an oxidation function and a power function, set in order at equation (*3.27*) [17] and delimited by brackets.

$$r_{\alpha,\beta} = \left[\left(\frac{\rho_{s,\alpha}}{\rho_s(0)}\right)^{n_{s,\alpha\beta}}\right]\left[A_{\alpha\beta}\, e^{-\left(\frac{E_{\alpha\beta}}{RT_s}\right)}\right]\left[X_{O2,g} e^{-\left(\frac{x}{L_{g,\alpha\beta}}\right)}\right]\left[Max\{0, S_{thr,\alpha\beta}(T_s - T_{thr})\}^{n_t}\right] \tag{3.27}$$

Where:

- $n_{s,\alpha\beta}$ is the user-defined order of solid α component consumption reaction.
- $A_{\alpha\beta}$ is the user-defined preexponential factor of Arrhenius law on pyrolysis reaction.
- $E_{\alpha\beta}$ is the user-defined activation energy of Arrhenius law on pyrolysis reaction.
- R is the perfect gases constant.
- $X_{O2,g}$ is the local oxygen volume fraction in air.

- x is the depth inside the solid where oxygen concentration is evaluated.
- $L_{g,\alpha\beta}$ is the user-defined characteristic depth of oxygen diffusion. If this value is set to zero, the reaction only takes place at the surface of the solid.
- T_{thr} is a user-defined threshold temperature below or above of which the reaction does not take place. It is set to 0 K by default.
- $S_{thr,\alpha\beta}$ is a term that indicates if the reaction must not occur below (value of +1) or above (-1) the given threshold temperature. It is set to +1 by default.
- n_t is a user-defined power argument, disabled by default.

The production term of α component is the sum over all reactions where the solid residue is material α, as equation (*3.28*) shows [17].

$$S_\alpha = \sum_{\alpha'=1}^{N_m} \sum_{\beta=1}^{N_r} v_{\alpha,\alpha'\beta} r_{\alpha'\beta} \tag{3.28}$$

Where:

- $v_{\alpha,\alpha'\beta}$ is the yield of component α from reaction β of component α'.
- $r_{\alpha'\beta}$ is the rate of the reaction β that consumes component α' to form component α.
- N_m stands for the number of materials involved.
- N_r stands for the number of user-defined reactions.

Once solid mass loss and reaction rates are known, volumetric production rate of a gaseous product γ is given by equation *(3.29)* [17].

$$\dot{m}_\gamma''' = \rho_s(0) \sum_{\alpha=1}^{N_m} \sum_{\beta=1}^{N_r} v_{\gamma,\alpha\beta} r_{\alpha\beta} \tag{3.29}$$

Finally, under the assumption that gases are transported instantaneously to surface, gases mass flux generated from a solid layer of thickness L is found according to equation *(3.30)*, in cartesian coordinates.

$$\dot{m}_\gamma'' = \int_0^L \dot{m}_\gamma''' (x) dx \tag{3.30}$$

Determination of pyrolysis rate also permits to find the chemical source term present in equation *(3.22)* according to expression *(3.31)*.

$$\dot{q}_{s,c}''' = -\rho_s(0) \sum_{\alpha=1}^{N_m} \sum_{\beta=1}^{N_r} r_{\alpha\beta} H_{r,\alpha\beta} \tag{3.31}$$

Where $H_{r,\alpha\beta}$ is the enthalpy of reaction, specified by the user in the MATL parameter input group.

3.3.6. Extinction

Fire will extinguish when all the fuel has been consumed. If no further data is provided, fuel burnout time is computed according to equation *(3.32*) [20].

$$t_b = \frac{\rho_s \delta_s}{\dot{m}''} \tag{3.32}$$

Where:

- t_b is the time, measured from the fire initiation, when fire is estinguished, in seconds.

- ρ_s is the non-pyrolyzed fuel density, in kg·m^{-3}, a parameter found within MATL group.
- δ_s is the material thickness given in m, found within SURF parameter group.
- $\dot{m}''$ is the mass loss rate per unit area, which coincides with result of equation *(3.30)*.

Then time required in order to complete simulations, as well as computational requirements, will depend on pyrolysis model, fuel density and thickness parameter.

Yet, in many cases combustible materials contain non-combustible components which have a considerable volume. In order to represent this situation, FDS allows to define a parameter [20] known as BULK_DENSITY, defined in the OBST line and expressed in kg·m^{-3}, which stands for the total mass of flammable compound per unit volume of the burner. If this parameter is defined, the others are overridden and, as observed in section 6.4, total fuel mass is calculated as the product of the bulk density and the volume of the obstacle defined by coordinates (XB) in the OBST line, according to expression *(3.33*). Then, total time to fuel burnout is this total mass, divided by the product of the area of the XY-plane slice of the burner and the result of equation *(3.30)*.

$$m = \rho_b V \tag{3.33}$$

Where:

- m is the total consumed mass during the fire, given in kg.
- V is the obstacle volume, defined by its coordinates in OBST line, given in m^3.
- ρ_b is the bulk density parameter, given in kg·m^{-3}.

Nevertheless, FDS also contemplates mechanisms for which a fire could end although there is non-reacted fuel, mainly represented by two conditions [20]:

- If the mean temperature in a cell is under the autoignition temperature (AIT) of all the combustible chemical species present in that cell, there will be no combustion. By default, AIT is 0 °C for any fuel.

- If the heat released by the reaction is not high enough to keep the temperature over the known as critical flame temperature (TCFT), determined empirically, there is no combustion. This temperature corresponds to the adiabatic flame temperature in the lower flammability limit. The value that FDS uses by default is 1327 ˚C.

In the case of the use of fire suppressive agents, the knowledge of fire extinction mechanism that the simulator uses is important in order to judge their efficacy in a real case.

3.4. FDS limitations

3.4.1. Geometry

One of the most remarkable restrictions of FDS is that it only allows to define objects of rectangular geometry. The simulator only permits the resolution of conservation equations in non-cartesian coordinates if explicitly indicated in the case of for example, particles.

In most practical cases, rectilinear geometries will exist; the real behavior can be more approximate to reality decreasing the size of the cells. In order to achieve good results, meshes must be uniform and grid cells should be as much cubical as possible.

3.4.2. Number of cells

Total number of cells has no limit if there is enough computational capacity. However, due to the internal use of an algorithm to implement the fast Fourier transform, this number should be a multiple of $2^k3^l5^m$, if k, l and m are natural numbers.

3.4.3. Mesh alignment

The most important rule of mesh alignment is that adjoining meshes should have the same cross-sectional area. Figure 3.3 shows the basic rules governing mesh alignment.

According to FDS developers [20], the following rules of thumb should also be followed when setting up a multiple mesh calculation. These rules are applicable in both cases of using MPI or not.

- Putting mesh boundaries where critical action is expected, especially fire, should be avoided, since the exchange of information across mesh boundaries is not yet as accurate as cell to cell exchanges within one mesh.

- Overlapping meshes may bring certain advantage as information is only exchanged at exterior boundaries. However, if coarse grids overlap with finer grids, probably exchange of information between coarser and finer (more accurate) grids will not occur and detailed information will be lost. Then, meshes containing the fire or critical action should be constituted by fine-sized grids.
- In the case of a planar obstruction close to where two meshes converge, if the obstruction is even a millimetre outside of one of the meshes, that mesh does not account for it, in which case information is not transferred properly between meshes.

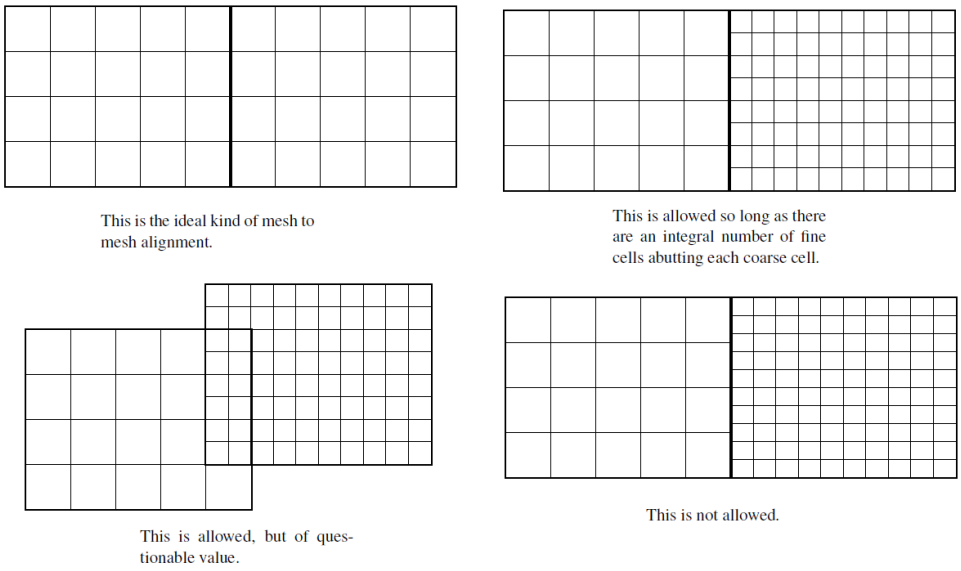

Figure 3.3 Rules governing mesh alignment [20]

3.4.4. Computational time

FDS is a field model based software that solves for every computational cell all conservation equations regarding to hydrodynamics, heat transfer and chemical reactions among many other calculations, which is considerably computationally expensive.

Better results will be obtained with meshes divided into smaller cells, but simulation time will be also higher. An interesting option is to divide the whole computational domain into different meshes, so that each mesh can be solved in parallel.

In order to solve different meshes in parallel, FDS simulations need to be launched through MPI (message passing interface) communication protocol. Intel® MPI library can be obtained for free and allows to run autonomously different instructions written in C, C++ or Fortran language, used by FDS if the processors of the computer used are compatible with the software.

The first step once MPI library has been installed is to divide the desired simulation scenarios into as many meshes as threads has the computer. Then, MPI batches including one or more FDS

files (automatically the second simulation is run when the first one is finished) must be created from a .txt file, indicating:

mpiexec.smpd -hosts #number_of_PCs #PCname #number_of_threads/meshes -env OMP_NUM_THREADS 1 -path "#FDS_Installation_Directory_name" -wdir "#File_location_directory_name" fds.exe #filename.fds >#filename\log.out 2>&1

Afterwards, the text file must be converted to format .cmd, which can be directly executed.
For example, in the case of a 8 threads computer in which FDS in installed at directory “D:\bin” running a 8 meshes simulation called “K2.fds” within folder “D:\bin\K2”, code of executable .cmd file would be, if FDS simulation is run at the same PC that executes the code:

mpiexec.smpd -hosts 1 localhost 8 -env OMP_NUM_THREADS 1 -path "D:\bin" -wdir "D:\bin\K2" fds.exe K2.fds >K2\log.out 2>&1

3.4.5. Constraints

FDS is subjected to the fulfilment of two basic constraints that avoid eventual mathematical instabilities [14]:

- The CFL (Courant, Friedrichs and Lewy) constraint ensures than a fluid particle does not travel to more than a grid cell per time step. The time differential per time step is automatically computed so that this constraint is accomplished and depends on the grid size.

- The Von Neumann constraint does not have a physical meaning as clear as former CFL constraint, but it could be understood as a similar restriction to CFL but for diffusive transport.

Each time step, density, mass fractions of lumped species, velocity vector, Bernouilli integral, pressure and temperature are computed for each cell following a predictor/corrector second order scheme [1].

In addition to these two constraints, FDS limits the maximum heat release rate per unit volume in order to prevent fictitiously high values of the reaction rate that could lead to numerical instabilities. Further explanation is available at 12.1.5 section of FDS User Guide [20].

4. Legal framework

4.1. Brief history of fire protection in Spain

Despite the existence of entities such as NFPA since ends of XX century, the first fire related normative in Spain did not enter into force until the year 1974, when the known as *Norma Tecnológica sobre Instalaciones de Protección contra el Fuego* (NTE-IPF) substituted traditional *rules of thumb* regarding the usage of fire extinction measures into a defined normative [22].

Since then, events as the fire declared in the hospital *Virgen del Rocío* of Sevilla the year 1977, and in the *Corona de Aragón* of Zaragoza on 12th July 1979, which took 79 fatalities, led to the issue of specific regulations for fire protection in hospitals and hotels.

However, the first wide regulation regarding fire protection did not come into force until the issue of RD 2059/81, that approved the national *Norma Básica de Protección Contra Incendios* (NBE-CPI-81), on April 10th of 1981, which was replaced the next year by another normative due to its difficulty to be applied as was too generalized. NBE-CPI-91 rule, approved by RD 279/91 of march 1st, was the first normative that suggested solutions for specific cases and at the same time, gave space to provide other solutions, valid if justified through technical methods.

Regarding to fire protection installations, on 5th November 1993, RD 1942/93 approved the regulation *Reglamento de Instalaciones de Protección Contra Incendios*, which was in force until the publication of the recent royal decree RD513/2017.

Fire protection in industrial establishments did not have an own regulation since 6th July of 2001 when RD 786/01 approved *Reglamento de Seguridad Contra Incendios en Establecimientos Industriales* (RSCIEI), whose last update was approved with RD 2267/04 on 3rd December of 2004. As well as in the case of RIPI, this regulation will be soon updated, although there is no official announcement yet. Requirements of materials about fire protection were not set up by normative until the year 2005, with RD 312/2005.

One of the last publications related to fire protection was released on March 17th, 2006. The new technical edification code (CTE) was approved, which included *DB-SI (Documento Básico de Seguridad contra incendios)* and DB-SU (Documento Básico de Seguridad de utilización) that currently constitute the main legal framework of fire protection in Spain.

In addition, it is important to point that Spanish National Institute of Safety and Hygiene on Work (*Instituto Nacional de Seguridad e Higiene en el Trabajo, INSHT*) also publishes good practices guides, known as *Notas Técnicas de Prevención* (NTPs), of non-compulsory nature, not on structural requirements, but on fire related topics. Sometimes, it is possible to find compulsory requirements in applicable legislation that refer to these NTPs, what makes them of obliged compliance.

Sometimes, regulations state precepts that are difficult to understand or may bring to misinterpretations. This is why Complementary Instructive Techniques (ITCs) are issued in order to clarify certain concepts. Since the establishment of Catalan Statute of Autonomy in 1979, the competence on civil protection belongs to *Generalitat de Catalunya*, who is reliable of the issue of ITCs.

4.2. Fire and constructive materials

4.2.1. Classification according to fire behavior

Constructive materials can be classified, according to RD 312/2005 of March 18th, into different categories regarding to their reactions with fire and their fire resistance [23].

Reaction in contact with fire can be understand as the easiness of the materials to its ignition, propagation and development of a fire according to parameters such as the heat of combustion.

European normative applied in Spain is UNE-EN-13501 (see Table 4.1). The normative sets up different *Euroclasses* according to the materials fire behavior, tested through different normalized ISO essay methods.

Table 4.1 Euroclasses set by UNE-EN-135

EUROCLASSES		
A1	Not combustible	No contribution to fire
A2		
B	Combustible	No flashover expected
C	Combustible	Limited contribution to fire; no flashover expected before 10 min
D		Medium contribution to fire; flashover expected between 2 and 10 min
E		High contribution; flashover expected before 2 min
F	Not classified	Fire behavior not determined

In addition to Euroclasses, different subcategories according to the tendency of releasing toxic fumes and flammable drops or particles are also set by UNE-EN-13501. This classification is shown in Table 4.2.

Table 4.2 Subcategories set by UNE-EN-135

Fumes opacity		Droplets or particles	
S1	Low	D0	Not produced
S2	Medium	D1	Limited production
S3	High	D2	Not classified

Fire resistance is understood as the capacity of a given material to keep during a time period its required bearing function, as well as the integrity and thermal isolation in the same terms as indicated in the corresponding normalized assay. Three different indicators are proposed by the technical edification code, RD 314/2006 of March 17th (see Table 4.3).

Table 4.3 Indicators according to technical edification code, RD 314/2006

Code	Description
R	Bearing capacity. Ability to support loads under fire exposition without structural stability loss.
E	Integrity. Capacity to support fire exposition in a face without pass of flames or hot gases that can spread the fire to the non-exposed face.
I	Insulation. Ability to support fire exposition in a face without propagation through heat transfer to the face which is not exposed (difference of at least 140 ˚C).

R, E and I codes are always followed by a number that might be 15, 20, 30, 45, 60, 90, 120, 180, 240 or 360. These numbers refer to the time that the material can keep their specified attributes while is exposed to a standard test. For example, a material or structural element labelled as R90 can keep its fire resistance during 90 minutes within a furnace whose temperature increases with time as defined by the standard temperature vs time curve it was designed with.

UNE-EN-13501 sets different normalized fire curves [24], representing different kinds of fires, such as standard fire, latent fire, door exposed to outside fire or semi-natural fire. The standard temperature vs time curve defined by this normative corresponds to ISO 834 cellulosic curve

equation (4.1) [25], the most extended design curve worldwide. It was developed in the 1930s according to data from fires in residential, office and commercial buildings, so that the curve should cover most of the potential courses of fires in common buildings.

$$T = 20 + 345\log(8t + 1) \tag{4.1}$$

Where t stands for the time elapsed since the fire is initiated, expressed in minutes .

As fire tests have shown, the maximum temperature of a natural fires can exceed the ISO-curve, but after the maximum it decreases again, whereas the ISO curve rises continuously [26]. Normally, the application of this curve results in a design on the safe side causing unsatisfactory costs for fire protection measures. However, in some cases the structural fire design with ISO 834 temperature–time curve can result in under-estimation of the thermal exposure [26], as Figure 4.1 shows.

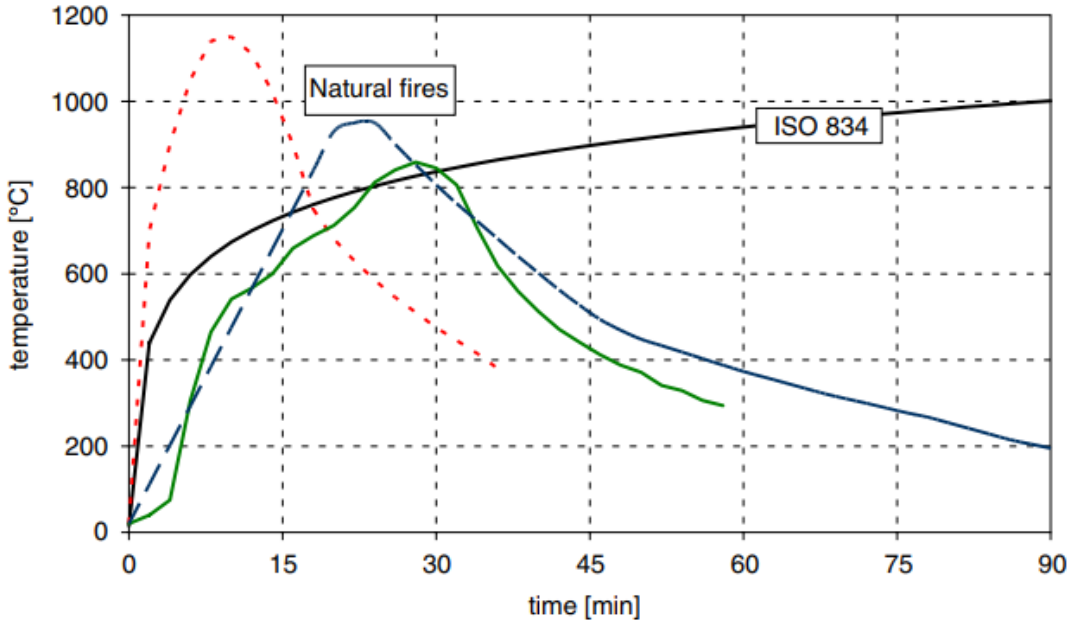

Figure 4.1 Comparison of temperature-time curves in natural fires with ISO 834 standard fire [26]

Annex B of DBSI established a proceeding in order to estimate the equivalent fire exposition time in the case of steel and reinforced concrete elements [24], according to:

$$t_{e,d} = k_b w_f k_c q_{f,d} \tag{4.2}$$

Where:

- $t_{e,d}$ is the equivalent time of fire exposition.
- k_b is a conversion coefficient, according to thermal properties of the environment. It can be taken as 0,07.
- w_f is a ventilation coefficient, according to the shape and size of the fire sector.
- k_c is a corrective factor depending on the nature of the material.
- $q_{f,d}$ is the corrected fire load within the sector, in MJ/m².

The ventilation factor is given by the expression:

$$w_f = \left(\frac{6}{H}\right)^{0.3} \left[0{,}62 + 90\frac{(0{,}4 - \alpha_v)^4}{\left(1 + \beta_v \alpha_h\right)}\right] \tag{4.3}$$

Where:

- H is the fire sector height, in m.
- α_v is the total area of the openings in the façade to total built floor surface ratio.
- α_h is the total area of the openings in the roof to total built floor surface ratio.
- β_v is a factor given by equation (4.4).

$$\beta_v = 12{,}5(1 + 10\alpha_v - {\alpha_v}^2) \quad (4.4)$$

The material corrective factor can be obtained from table:

Table 4.4 Material coefficient for the calculation of affordable fire exposition time [24]

Transversal section material	Material coefficient, kc
Reinforced concrete	1
Protected steel	1
Non-protected steel	$13{,}7\frac{A_v\sqrt{h}}{A_h}$

The corrected fire load within the sector can be found according to:

$$q_{f,d} = q_{f,k}\, m\, \delta_{q1}\delta_{q2}\delta_n\delta_c \quad (4.5)$$

Where:

- $q_{f,k}$ is the characteristic fire load per unit area, in MJ/m^2.
- m is the combustion coefficient, which is 0.8 for cellulosic fuels and 1 for others.
- δ_{q1} is the fire initiation risk factor due to sector size.
- δ_{q2} is the fire initiation risk factor due to use or activity of the sector.
- δ_n is the product of all coefficients due to voluntary safeguards adopted.
- δ_c is the corrective coefficient depending on fire consequences.

These values can be collected from the tables Table 4.5 to Table 4.8.

Table 4.5 Fire initiation risk factor due to sector size

Sector built surface (m^2)	δ_{q1}
<20	1,00
25	1,10
250	1,50
2500	1,90
5000	2,00
>10000	2,13

Table 4.6 Fire initiation risk factor due to sector activity

Activity	δ_{q2}
Residential, administrative, docent	1,00
Commercial, parking, sanitary, public	1,25
Low special risk buildings	1,25
Medium special risk buildings	1,40
High special risk buildings	1,60

Table 4.7 Corrective coefficients due to voluntary safeguards

Automatic detection δ_{n1}	Automatic alarm to firefighters δ_{n2}	Automatic fire extinction δ_{n3}
0,87	0,87	0,61

Table 4.8 Corrective coefficient depending on fire consequences

Evacuation height	δ_c
Buildings with an evacuation height descending more than 28 m or ascending more than a floor.	2,0
Buildings with an evacuation height descending between 15 and 28 m or ascending up to 2,8 m. Parking under other uses.	1,5
Buildings with an evacuation height descending less than 15 m. Exclusive use as parking.	1,0

In the case of fires that could disable buildings that cannot stop their activity or that could cause several deaths, the values of the previous table must be multiplied by 1,5.

4.2.2. Steel

Steel is a common constructive material, consisting on an alloy of iron and carbon, and in most of cases, some other elements, such as chromium (avoids corrosion, leading to the material known as stainless steel). It is not combustible, although steel varies its properties sensibly with temperature, so that mechanical properties are drastically reduced. The material has an important plastic face and deforms considerably before it breaks.

Steel structures, when exposed to fire, follow the collapse scheme shown below (Figure 4.2).

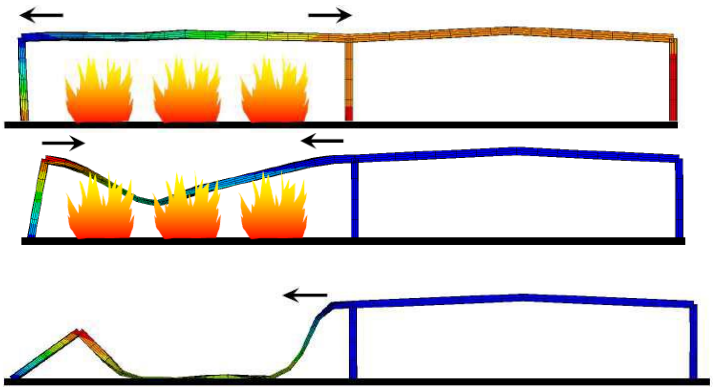

First phase: Expansion of the structure due to thermal dilatation.

Second phase: The heated region of the steel structure collapses due to the loss of mechanical properties.

Third phase: Final of collapse.

Figure 4.2 Scheme showing the different phases of a metal structure collapse. Source: [27]

As shown in previous figure, steel structures suffer a drastic loss of mechanical properties when heated. Indeed, this collapse is produced when a certain value is reached, known as critical temperature [28], at which the steel structure bearing capacity equals stress induced by the mechanical loads and represents the most important parameter to know regarding fire design of metal structures. This value is given by UNE-EN 1993-1-1 and frequently is up to 500 ˚C in the case of thick steel profiles, while in the case of slender profiles often arrives to 350 ˚C.

In addition to the steel critical temperature, another important factor to be considered is the known as shape factor which is defined as the area exposed to the action of fire divided by the volume of the steel element per unit length. According to the type of profile (shape) and the shape factor, the IPN nomenclature for the structural element can be found, and with this, the coat layer of

protective coating materials, if required in order to achieve a certain R(t) status, according to tables provided by tables of appendix C of DBSI (*Documento Básico de Seguridad contra Incendios*) [29].

In addition to R(t) category, the steel piece must be always under the known as critical temperature. The temperature that a steel piece can reach [25], depends on the fire load at the fire sector (see section 4.3), on the shape factor, on an emissivity factor (depends on how exposed is the steel piece to fire) and on a ventilation (or openings) factor, which is directly related to the study matter of this project.

4.2.3. Concrete

Concrete is a mineral material composed by a mixture of different mineral particles, which are bonded together by the action of a binder, usually Portland cement, based on limestone (calcium carbonate). However, calcium, silicon, aluminum, iron, manganese, magnesium, sodium or potassium oxides are also present frequently on cementitious materials, while lost-on-ignition compounds do not usually exceed a 2,1 % in mass [30]; which provokes this material not to be combustible since its constituents are molecules within their maximum possible oxidation state.

Despite its non-combustibility, concrete, under fire conditions, decreases its resistance as function of temperature: once 500 ˚C have been reached, it loses about a 50% of its resistant capacity (less than steel, which loses an 80% of its bearing capacity). At high temperatures, concrete suffers dilatation and water contained in pores vaporizes explosively in a process known as *spalling*, which causes damages to structure [28].

The main reason of reinforcement of concrete with steel is the bad resistance of the concrete in front of traction (reinforced concrete). Moreover, concrete is a good thermal isolator, which makes it a good choice in the case of protection of nude steel structures, but adherence between concrete and metal becomes a critical aspect.

Thermal exposition is more severe in ceiling joists, due to the tendency of hot gases to go up; then, steel bars placed at the outer face must absorb higher traction efforts and the reduction of bearing capacity may bring the structure to collapse. In the case of pillars, the heat effect is not as visible, as stresses are compressive, for which concrete grants a good resistance.

Anyway, in the case of reinforced concrete, the thickness of the concrete covering the bars is an important parameter (known as minimum equivalent distance to axis, a_m), that together with the minimum rib width, b_{min} , allows to find the time that the structure grants the REI stability [28] according to tables of appendix C of DBSI (*Documento Básico de Seguridad contra Incendios*).

4.2.4. Masonry

Common masonry articles such as bricks, stone blocks or glass are essentially inorganic, as concrete, previously presented and also often used in construction.

Probably, most used between masonry precast pieces are bricks, which are essentially made of clay, that, as other constructive ceramic materials, does not provide a high quantity of heat neither smokes under the effect of fire, as the most of their constituents are not combustible. In fact, unless these contain more than a 1% in mass or volume of organic materials shared homogeneously along the whole ceramic mass, are considered as A1 class regarding fire reaction, and do not need further essays (according to CE 96/603/CE).

Values regarding the fire resistance of bricks or ceramic precast units are directly provided by tables with reference values (applicable for RSCIEI and other regulations) , originally published in the Annex F of DBSI [24]. Only values for precast constructive pieces of at least 1,5 cm thickness are provided, which are not reinforced or covered by a coat of plaster or mortar. Anyway, composed material features could be estimated as the sum of the individual material constituents [24].

4.2.5. Coating materials

Most used protective coating materials include [28]:

- Intumescent and ablative paints: Applied as a fine layer over the constructive material. These are paints, or burnishes that in contact with fire, react yielding to the formation of a char protective layer much thicker than the original layer (about 80 to 100 times), able to act as an isolating agent since the thermal conductivity coefficient of carbon is much lower than in the case of for example, steel. In addition to the isolating effect, these char layers act as coolants, since could react again with fire in an endothermic reaction (absorb heat) to generate gases which are usually toxic. Ablative paints are applied as a fine layer over concrete. In contact with fire, are able to generate a high thermal isolation as these dehydrate and form a thick carbon layer that grows progressively while the temperature increases.

- Mortars: Mineral layers holding a base of perlite (volcanic rock) with various additives, such as vermiculite (lightener), hardeners or ingredients that make their application easier. This fireproof protection is finally applied in a mixture with gypsum plaster or cement leading to a final rugose appearance.

- Rockwool: Isolating material, composed by a framework of filaments of petrous materials that constitute a felt which keeps immobilized air inside it, offering a high fire resistance. These materials are completely non-combustibles, so that there is no heat formation neither fumes release. Its application can be through mortar or rigid panels.

- Gypsum and silicate rigid panels: This type of isolations is used mainly to the sectorization of fire areas in false ceilings or firewalls. These kinds of materials are also an interesting option in cases in which the final aspect of the installation matters, especially if an additional intumescent paint layer is required. Silicate panels are composed by calcium silicates, reinforced with fire resistant organic fibers while gypsum panels are formed by a base of gypsum covered by sheets of non-combustible glass fiber.

4.3. Establishment types according to RSCIEI

The concept of establishment is defined as the set of buildings, single building, zone, open area of industrial use or warehouse led to its usage under a differentiated ownership (different zones of the same building that have different owners are different establishments) and whose construction or reform projects, as well as the planned activity initiation, is concern of administrative control. The establishments can be classified into different categories according to their location and or configuration [31].

A type establishment: Those that are partially occupying a building that, has in addition, more establishments.

B type establishment: Those that occupy a whole premise that is townhouse to at least another building, or that are separated at a distance of three meters or less.

C type establishment: Those that occupy a whole building, or even a set of buildings, which are at least more than three meters away from the closest building that belong to other establishments. This distance must be free of combustible materials or intermediate products susceptible to spread the fire. It is important to notice that, in a closed perimeter set of facilities, the whole set of buildings will be considered a C type establishment even if the distance between the buildings that constitute the establishment is lower than three meters, always that the closest building with different ownership is more than three meters away.

D type establishment: Those that are constituted by an open area, which could be totally covered, but one of the façades of which lacks lateral cover.

E type establishment: Those that are constituted by an open area that may be partially covered (until a 50% of its surface), but there are façades of which that lacks lateral cover.
The different classification of establishments according to its configuration is illustrated in Figure 4.3.

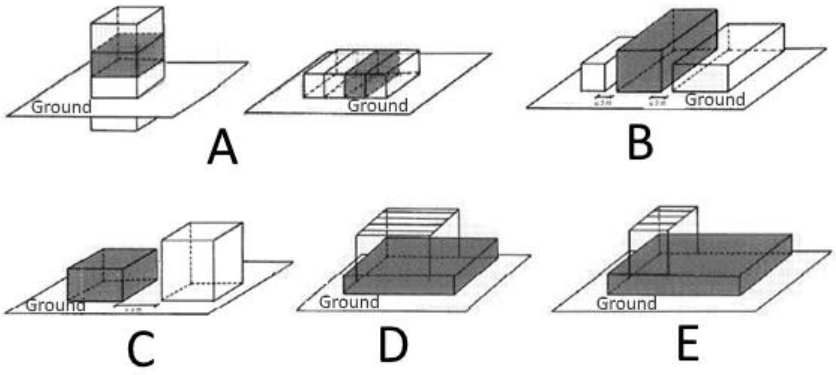

Figure 4.3 Establishments types according to their configuration. Source: [31]

In the case of horizontal buildings with no neighbors above or below the establishment, the difference between A and B type premises is slight and may lead to confusions. The key to assign establishment type in this case is clarified by an NTP issued by the Catalan government, according to the dependence or independence of structure, closing and cowling. See Figure 4.4 [32].

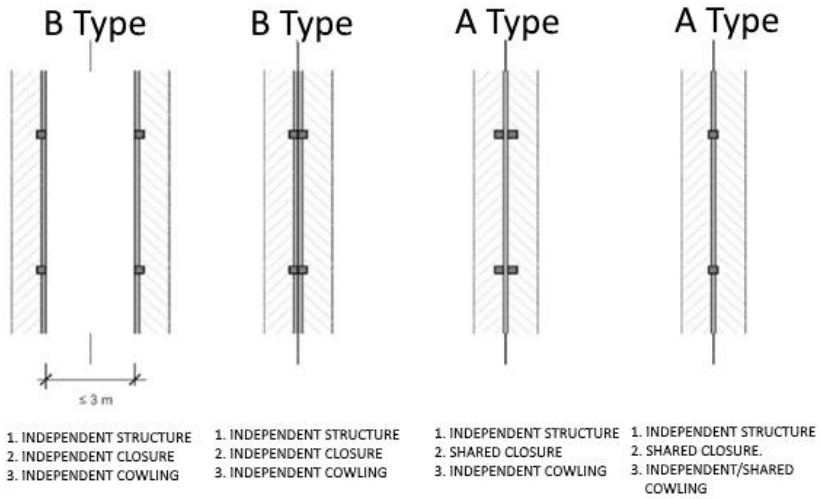

Figure 4.4 Difference between A and B establishment types [33]

In the case of horizontal industrial establishments that occupy a townhouse premise with a structure shared with the adjacent buildings (but independent cowling), it is admitted dealing with the exigencies that would correspond to a B-type establishment, but only if it is possible to justify through technical methods that the possible structure collapse would not affect the contiguous edifices.

This disposition is precisely one of the main motivations of this project, as B-type requirements are much less restrictive, but most industrial buildings are classified as A-type. Then, proving that the collapse of the cowling structure due to a possible fire does not affect its party wall neither the cover of the adjacent construction. The most critical element is the union point between the party wall and the cowling structure: a deformation or collapse provoked by a fire could blow away the neighbor cowling, despite the possible protection of the pillars that constitute the supporting structure [33].

The justification of no affection to neighboring cowling structures is traditionally performed with combination of structure calculations analytical methods with controls such as the heat dissipation achieved with automatic sprinklers installations. If the no-affection is justified through other techniques, the previous acceptance of prevention and fire extinguishment services will be needed.

4.4. Intrinsic risk level

Industrial establishments, which constitute one or more fire sectors or areas, may be classified into different categories (risk levels). Classification criteria given in the third section of the appendix of RSCIEI [31] stablishes the definitions of fire sectors and areas:

- In the case of A, B and C type establishments, a fire sector is any space of the building which is isolated from the rest by fire resistant elements.

- In the case of D and E type establishments, an open fire area is its whole surface, only delimited by its perimeter.

Classification of fire sectors into categories is performed according to their fire load, which is understood as the energy provided by the combustion of the materials stored in a certain fire sector per unit area of the sector:

$$Q_s = \frac{\sum_{i=1}^{N} G_i q_i C_i}{A} R_a \tag{4.6}$$

Where:

- Q_s is the fire load density, weighed and corrected, of the fire sector, in MJ/m2 or Mcal/m^2.
- G_i is the mass of each combustible material (even constructive materials) in the fire sector.
- q_i is the heating power (MJ/kg or Mcal/kg) of each one of the combustible materials in the sector.
- C_i is a non-dimensional hazard coefficient according to combustibility, which may have a value of 1.0, 1.3 or 1.6 according to the nature of the combustible material.
- R_a is a non-dimensional corrective coefficient associated to the hazard degree of the activity performed. It may have a value of 1.0, 1.5 or 2.0.
- A is the total built area of the fire sector given in m^2.

In addition, there is another definition of fire load according to the materials density. In this case, there is a distinction between production and storage activities [31]:

For production

$$Q_s = \frac{\sum_{i=1}^{N} q_{s,i} s_i C_i}{A} R_a \tag{4.7}$$

For storage

$$Q_s = \frac{\sum_{i=1}^{N} q_{v,i} s_i h_i C_i}{A} R_a \tag{4.8}$$

Where:
$q_{s,i}$ is the heating power density of each different zone inside the sector per m^2.
$q_{v,i}$ is the heating power density of each different zone inside the sector per m^3.
h_i is the storage height of each fuel, in meters.
s_i is the surface of each zone within the fire sector with different fire load density.

Once Q_s is known, intrinsic risk level can be found in table 1.3 of the I appendix of RSCIEI [31] (see Table 4.9).

Table 4.9 Intrinsic risk levels according to fire load. Source: [31]

	Intrinsic risk level	Fire load density weighed and corrected	
		Mcal/m^2	MJ/m^2
LOW	1	Q_s≤100	Q_s≤425
	2	100<Q_s≤200	425<Q_s≤850
MEDIUM	3	200<Q_s≤300	850<Q_s≤1275
	4	300<Q_s≤400	1275<Q_s≤1700
	5	400<Q_s≤800	1700<Q_s≤3400
HIGH	6	800<Q_s≤1600	3400<Q_s≤6800
	7	1600<Q_s≤3200	6800<Q_s≤13600
	8	Q_s>3200	Q_s>13600

Then, according to establishment configuration and intrinsic risk level, maximum permitted areas per fire sector as well as requirements of constructive materials can be found in Table 4.10 [31].

Table 4.10 Maximum permitted edified area according to intrinsic risk of fire sector. Source: [31]

Intrinsic risk of fire sector	Establishment type		
	A (m^2)	B (m^2)	C (m^2)
LOW	2000	6000	NO LIMIT
	1000	4000	6000
MEDIUM	500	3500	5000
	400	3000	4000
	300	2500	3500
HIGH	NOT PERMITTED	2000	3000
		1500	2500
		NOT PERMITTED	2000

The main interest of this project is to find a method to prove that an A type establishment can be dealt with the restrictions that would correspond to a B type establishment. Summary of the differences between the requirements of these two are shown from Table 4.11 to Table 4.13, when establishment activity is storage.

Notice that only intrinsic risk levels 2 to 4 have been studied, since no more could be studied with FDS simulations due to lack of time (see section 8).

Table 4.11 Differences between legal requirements of A and B establishment types for low risk (level 2) [27]

RISK LEVEL 2 (LOW)		
	A TYPE	B TYPE
Maximum sector surface	1000 m^2	4000 m^2
Supporting structure	R 90	R 60
Party wall	REI 120	REI 120
STCS[2]	No	No
Automatic detection system	Yes	No
Manual alarm system	Yes	Yes
Fire hose reel	Yes[3]	No

[2] Smoke and Temperature Control System.

[3] If the surface of the sector is at least 300 m^2 hoses of 25 mm diameter are needed.

Table 4.12 Differences between legal requirements of A and B establishment types for low risk (level 3) [27]

RISK LEVEL 3 (MEDIUM)		
	A TYPE	B TYPE
Maximum sector surface	500 m^2	3500 m^2
Supporting structure	R 120	R 90
Party wall	REI 180	REI 180
STCS	Yes (≥1000 m^2)	Yes (≥1000 m^2)
Automatic detection system	Yes (≥300 m^2)	Yes (≥2000 m^2)
Manual alarm system	Yes (≥800 m^2)	Yes (≥800 m^2)
Fire hose reel	Yes[4]	Yes[5]

Table 4.13 Differences between legal requirements of A and B establishment types for low risk (level 4) [27]

RISK LEVEL 4 (MEDIUM)		
	A TYPE	B TYPE
Maximum sector surface	400 m^2	3000 m^2
Supporting structure	R 120	R 90
Party wall	REI 180	REI 180
STCS	Yes (≥1000 m^2)	Yes (≥1000 m^2)
Automatic detection system	Yes (≥300 m^2)	Yes (≥2000 m^2)
Manual alarm system	Yes (≥800 m^2)	Yes (≥800 m^2)
Fire hose reel	Yes[4]	Yes[5]

4.5. Control of smoke and temperature

As seen in section 2.2, heat and smoke are accumulated in poorly or non-ventilated compartment fires. Deficient ventilation carries several drawbacks:

- Structural elements are exposed to high temperatures for longer, since heat is not evacuated. This causes a direct impact on structure resistance, which depends on exposition time. Under this condition, structure could collapse.

- Structures are also exposed to chemical agents- such as carbon and nitrogen oxides or even hydrogen chloride (gaseous hydrochloric acid)- that could cause corrosion on them, weakening their strength and easing collapse.

- Deficient heat evacuation contributes, if there is small presence of oxygen, to the feedback effect, in which heat released from combustion contributes to the pyrolysis of new unpyrolized solid fuel. This causes the fire to last longer and to have a wider spread, with the subsequent loss of the stored material.

- No ventilation may lead to situations of flashover or even backdraft if the fire is in latent phase and oxygen supply is suddenly re-activated.

- Potential damage for people that might be present at the compartment due to the emission of toxic fumes and extreme temperatures, which often makes evacuation impossible.

Industrial establishments ranked as medium or high risk will, as seen in previous tables, require the installation of devices that control the temperature of the room and the concentration of smoke in case of fire, at least to the point of permitting its safe evacuation.

In order to grant the elaboration of a safe evacuation plan, UNE-23585:2004, referenced in RSCIEI and CTE, establishes the guidelines for the calculation and design of a proper Smoke

[4] If the surface of the sector is at least 300 m^2 hoses of 45 mm diameter are needed.
[5] If the surface of the sector is at least 800 m^2 hoses of 45 mm diameter are needed.

and Temperature Control System and states that minimum height for the smoke layer must be at least between 2,5 and 3 m above the ground [34].

In order to prevent the arrival of smoke layer until heights below 2,5 m, as well as avoiding the other drawbacks, normative contemplates the installation of Smoke and Temperature Control Systems. Main types of components that can be used in order to implement STCS are:

- Smoke control barriers (or curtains), are physical barriers that guide the flow of smoke and force it to follow a certain trajectory, direct to vents or open gaps where it is expulsed out of the compartment, as can be seen at Figure 4.5. These barriers can be fix or mobile and rigid or flexible. Their specifications are given by norm UNE-EN 12101-1:2007.

- Natural extraction vents, set along the cowling or more commonly, walls. Consist on initially closed gaps that can be opened manually or automatically by the detection of a certain temperature or smoke concentration level. Natural extractors seize the buoyancy effect of hot gases as well as the overpressure generated at the smoke layer to evacuate them due to their natural tendency of leaving the compartment. Their specifications are given by norm UNE-EN 12101-2:2004, updated in 2013. According to normative [35] these elements must be able to open in presence of lateral winds of 10 $m \cdot s^{-1}$, and in presence of snow layers over them, and their size is limited to 2,5 meters per side.

- Mechanical smoke and heat extractors, which often are power-supplied electromechanical fans. Their specifications are given by norm UNE-EN 12101-3:2002, updated in 2006.

- Differential pressure systems, which can be divided into two main types:

    - Pressurization systems increase the pressure of protected areas, so that hot gases are pushed out of these zones.

    - Depressurization systems, that decrease the pressure at smoke region, so that hot gases in whole compartment are suctioned and forced to be kept adjacent to the roof.

  Specifications of both kinds of differential pressure systems are given by norm UNE-EN 12101-6:2006.

Power supply of smoke and temperature control systems, if required, must follow the specifications given by normative EN 12101-10:2007.

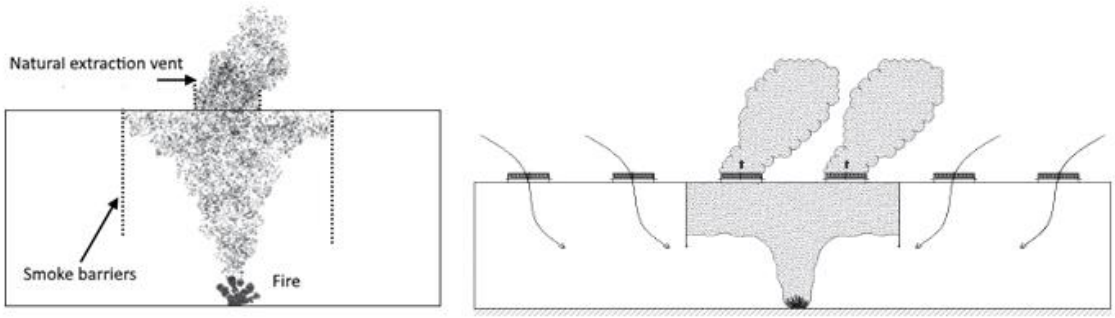

Figure 4.5 Operation scheme of operation barriers and natural extraction using single (left) or multiple (right) extractors. Source: [34]

The main scenario studied during this project will be provided of additional ventilation by adding natural extraction vents at the ceiling.

Mathematical model proposed by UNE-23585:2004 in order to estimate natural ventilation gaps total area is exposed in appendix B).

5. Previous work

5.1. Ozone simulations set by Generalitat de Catalunya fire service

Generalitat de Catalunya Fire Service [27] conducted a study to test the effect of ventilation and smoke extraction on the magnitude of temperatures reached at structure during compartment fires within A type establishments, discuss if damage to structures is possible and so that these results permit to sentence if the building can be dealt as a B type establishment or not. The study consisted on various simulations carried out in OZone, a two zones model-based software developed by University of Liège (Belgium).

5.1.1. Simulation scenario

Simulation scenario consisted on a 1000 m^2 closed rectangular compartment sized 50,0 x 20,0 x 6,5 whose longer sides (W2 and W4) are two equal party walls, as well as W1 and W3, two identical façades, corresponding to the shorter side, that are both provided with a door and a window. The building was full of 476 wooden pallets distributed uniformly along the floor, whose layout is shown at Figure 5.1.

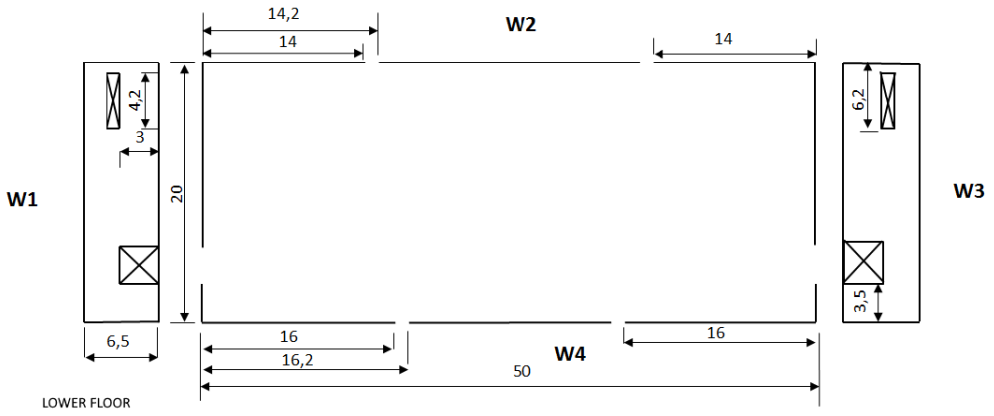

Figure 5.1 Lower floor layout of simulations scenario

Table 5.1 shows the list of solid obstacles and their attributes.

Table 5.1 Solid obstacles features at OZone simulations

Name	Thickness	Material
Party walls	20 cm	Precast brick
Façades	20 cm	Precast brick
Cowling	5,4 cm	Sandwich panel (5 cm of rockwool enveloped by steel layers of 0,2 cm)
Floor	20 cm	Concrete

Generalitat de Catalunya Fire Service, with the aim of studying the ventilation effect on the compartment fire, worked with two different scenarios: one of them had no ventilation at the ceiling, whereas the another one, according to UNE 23585, counted with five fire extraction openings, squares sized 2,08 m per side, arranged along the roof, considered as totally flat, as shown at Figure 5.2. These fire extraction gaps are initially closed (the air cannot cross them) but were set to open 120 seconds after the fire started, as smoke is supposed to be automatically detected by their sensors in approximately 60 seconds, and the necessary time expected to execute the action is also 60 seconds, as normative indicates. Table 5.2 lists the different ventilation gaps the two scenarios count with, indicates their size and activation time.

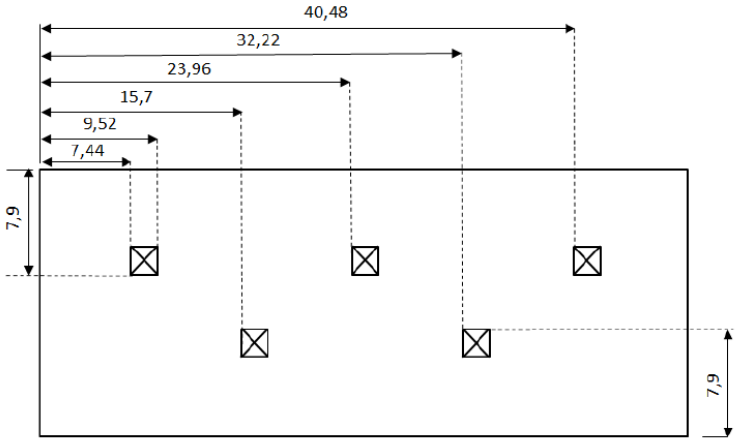

Figure 5.2 Cowling of original ventilated scenario

Table 5.2 Openings features at OZone simulations

			NON VENTILATED SCENARIO	VENTILATED SCENARIO
Name	Units (-)	Size (m)	Time to open (cause) (s)	Time to open (cause) (s)
Door	2	3x3	900 (firefighters arrival, only one door)	120s (automatic detection and actioning)
Window	2	4,2x1	300 (breakage due to thermal shock)	120s (automatic detection and actioning)
Extractors	5	2,08x2,08	Not present.	120s (automatic detection and actioning)

5.1.2. Input data

OZone uses an *alpha-square t* model [27] (see equation (2.2)) in order to represent fire growth until a steady state HRR value is reached, which is kept constant for a certain time until fire decays, so that users must specify both steady state heat release rate (RHRf) and fire growth rate (FGR, which stands for the time required to reach the final HRR value).

A total of 10 simulations were carried out, which included intrinsic risk levels 1 to 5 in both cases of ventilated and non-ventilated scenario. Input and design parameters for each simulation are shown at Table 5.3.

Table 5.3 OZone input data list for each simulation

Risk level	Ventilation	Fire load $MJ \cdot m^{-2}$	RHRf $kW \cdot m^{-2}$	FGR s
2 (low)	No	850	1250	300
2 (low)	Yes	850	1250	300
3 (medium)	No	1275	6000	300
3 (medium)	Yes	1275	6000	300
4 (medium)	No	1700	6000	150
4 (medium)	Yes	1700	6000	150
5 (medium)	No	3400	6000	150
5 (medium)	Yes	3400	6000	150

5.1.3. Simulation results

Results obtained by Generalitat de Catalunya Fire Service showed that there is an important difference regarding structural bearing capacity loss. Figures from 5.3 to 5.7 show that in the case of ventilated fires, temperature reaches higher peaks, to the point of beating ISO-834 curve; however, when ventilated, fires also speed up and the structure is not exposed so high amounts of time to the heat focus, which may prevent reaching structure critical temperature and, therefore,

structure collapse if this is protected with suitable fire resistant materials. Percentages present at the legend denote the percentage of total fuel that is burnt in the hypothetical fire.

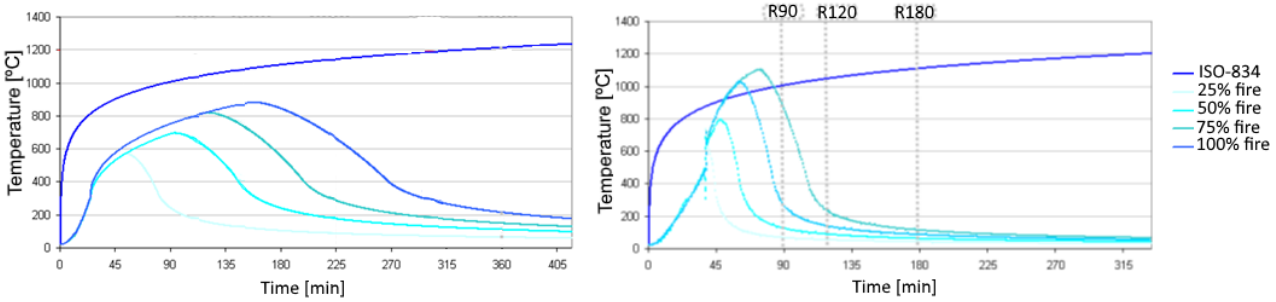

Figure 5.3 Temperatures of structure in the case of intrinsic risk level 1, with (right) and without ventilation (left). Source: [27]

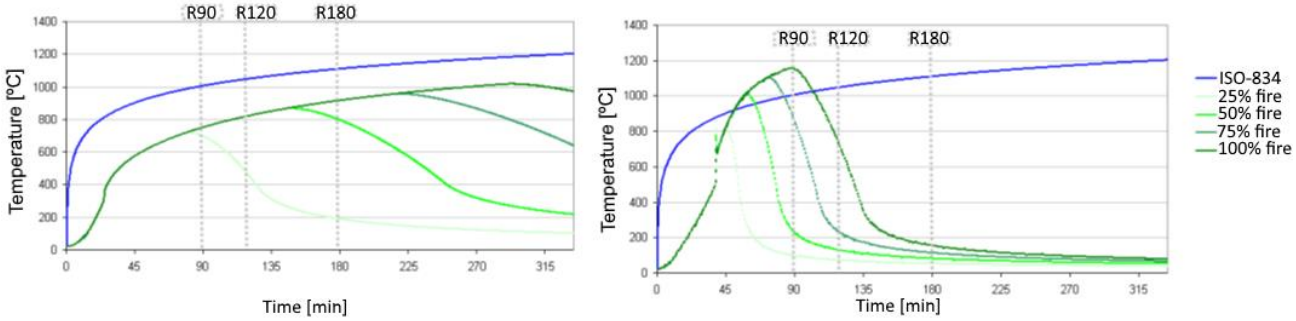

Figure 5.4 Temperatures of structure in the case of intrinsic risk level 2, with (right) and without ventilation (left) Source: [27]

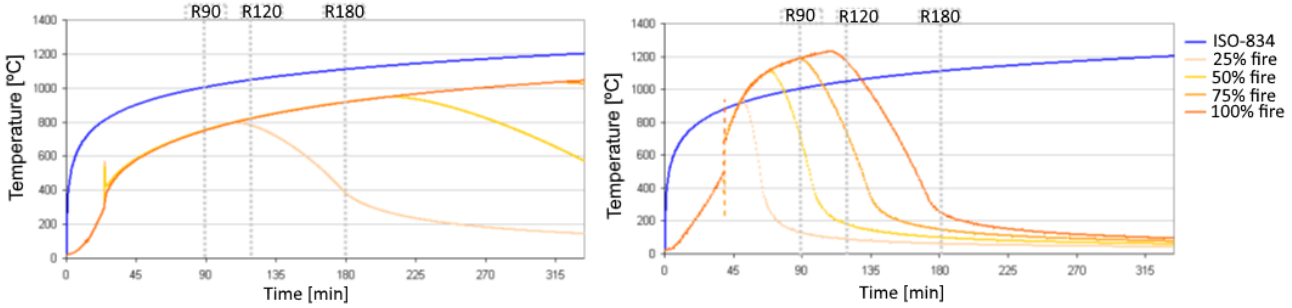

Figure 5.5 Temperatures of structure in the case of intrinsic risk level 3, with (right) and without ventilation (left) Source: [27]

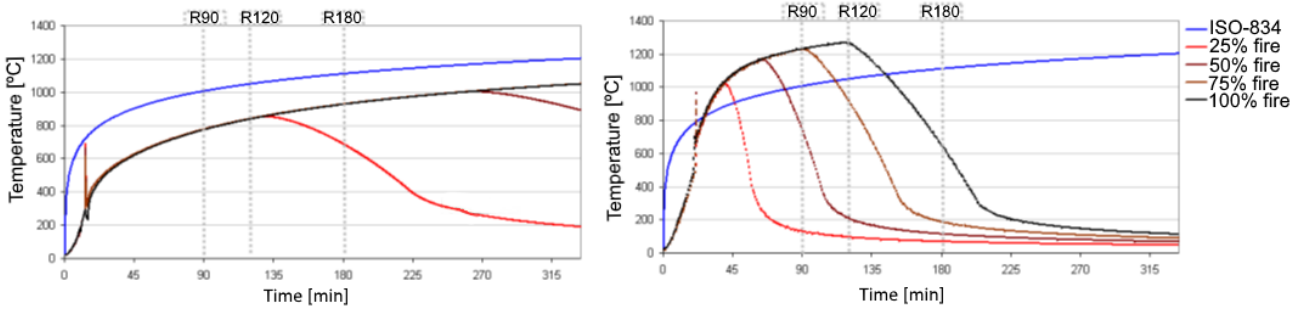

Figure 5.6 Temperatures of structure in the case of intrinsic risk level 4, with (right) and without ventilation (left) Source: [27]

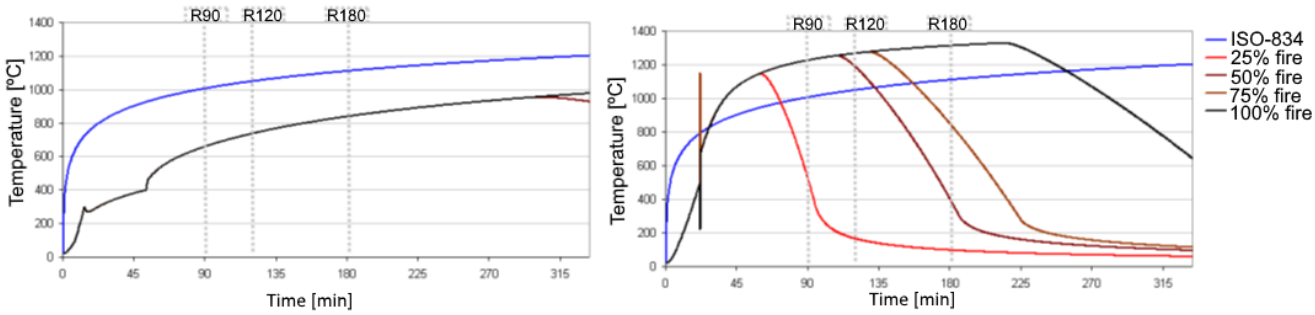

Figure 5.7 Temperatures of structure in the case of intrinsic risk level 5, with (right) and without ventilation (left) Source: [27]

Table 5.4 to Table 5.7 illustrate through an intuitive colour code if structures provided with certain fire resistance code would resist those conditions (green), would not (red) or it is not clear and should be discussed (orange).

Table 5.4 Summary of simulation results if structure was protected with R90 materials

R90									
Risk level		NON-VENTILATED				VENTILATED			
		25%	50%	75%	100%	25%	50%	75%	100%
Low	1								
	2								
Medium	3								
	4								
	5								

Table 5.5 Summary of simulation results if structure was protected with R120 materials

R120									
Risk level		NON-VENTILATED				VENTILATED			
		25%	50%	75%	100%	25%	50%	75%	100%
Low	1								
	2								
Medium	3								
	4								
	5								

Table 5.6 Summary of simulation results if structure was protected with R180 materials

R180									
Risk level		NON-VENTILATED				VENTILATED			
		25%	50%	75%	100%	25%	50%	75%	100%
Low	1								
	2								
Medium	3								
	4								
	5								

Table 5.7 Summary of simulation results if structure was protected with R240 materials

R240									
Risk level		NON-VENTILATED				VENTILATED			
		25%	50%	75%	100%	25%	50%	75%	100%
Low	1								
	2								
Medium	3								
	4								
	5								

5.2. Simulated scenario with FDS by Illa

Illa [1] tried to reproduce the same scenarios that Generalitat de Catalunya Fire Service had simulated but in FDS. This latter, however, is a field model simulator much more complex than OZone, which is two zones model-based, requiring huge amounts of computational time and requirements. This important drawback and the necessity to build a suitable scenario in order to be compared (definition of domain, mesh, setting of an appropriate pyrolysis model and ignition strategy and establishing a criterion in order to vary fire load) allowed him to perform just two simulations, including ventilated and non-ventilated cases for intrinsic risk level 2.

Simulation scenario consisted on the same as considered by Generalitat de Catalunya Fire Service, where all obstructions and openings are granted with the same features. Nevertheless, and due to computational restrictions, only a half of the building was considered, with the aim of saving computational time.

As this scenario, the design of which occupied the whole project by Illa [1], has been seized for the development of this project, it is further described in next section, especially dedicated to it.

6. Scenario and environment description

6.1. Domain

The main simulation scenario used during this project has been the same as Illa created during his final degree project, which at the same time was a representation in FDS of the model built by Generalitat de Catalunya Fire Service in their study with Ozone [27], who performed their work upon a building sized 50 x 20 x 6,5 m. However, due to FDS higher computational cost, a 25 x 20 x 6,5 m building was considered, setting an adiabatic wall at the inner face corresponding to X axis [1]. This wall does not let the energy neither mass exchange to the other side, so that outputs of the non-considered half would be, in fact, symmetric to results collected in actual scenario simulation. This simulation strategy permits to reduce computation time to almost a fourth part [1].

In order to simulate the effect of external air adjacent to outer face of walls entering by ventilations, additional 0,8 m in the x direction and 1,2 m in the y direction and 0,4 m in the z direction were added to the size of the domain. Therefore, the total dimensions of the domain were 25,8 x 21,2 x 7,0 m. As this domain was previously tested by Illa, no domain study was considered to be necessary.

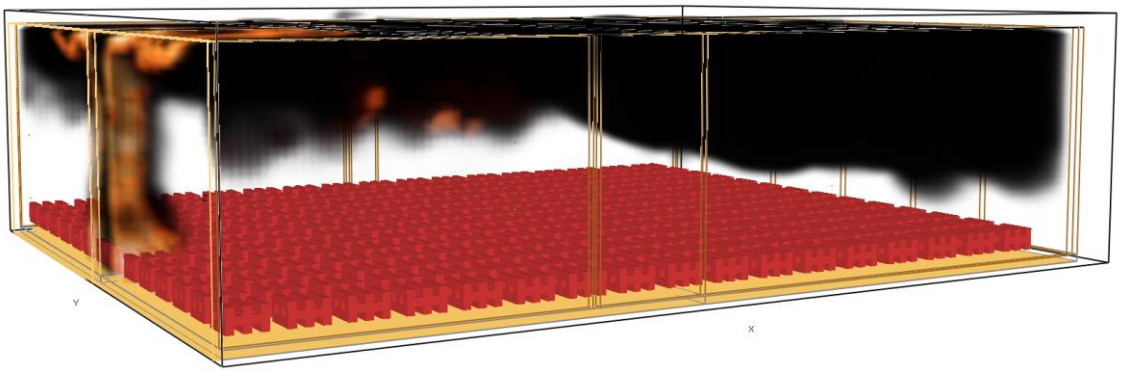

Figure 6.1 Base simulation scenario few seconds after the fire starts. Notice that building does not occupy whole domain. Image obtained as screenshot by the author.

6.2. Mesh study

One of the most remarkable problems that FDS simulator shows is the high amount of time required to perform the simulations. However, dividing the simulation domain into different meshes allows to run each mesh in parallel with different system cores, which speeds up the simulation time significantly. This is why the first active step in this project was trying to reproduce the simulations performed by Illa [1], who divided his base-case domains into four similar meshes (see Figure 6.2), but using eight meshes.

This study departs from the last simulations performed by Illa (H1 and H2, regarding to a non-ventilated case and a ventilated case, respectively, in which vents were opened at time=120 s), and generation of char is not contemplated. 8-core simulations, named HX1 and HX2 respectively, were identical but divided into the double of meshes.

Separation was performed through X or Y axis, so new mesh division does not separate burners, which may lead to communication errors between meshes; moreover, separation by the Z axis was discarded, as in that case there could be important errors since fire and hot smoke would be separated.

Cells in both divisions are cubes sized 0,2 per side, so that in the directions where number of cells was odd, domain had to be increased in some centimeters with the aim of making the total length

in that direction divisible by 0,2. Also, materials were set with the same properties as Illa did, so that the only difference between cases was number of meshes and the strict necessary modification of domain size.

Simulation times achieved by duplicating the number of computational meshes significantly shrinks: non-ventilated scenario simulations by Illa took 1,67 times these required to perform the analogue simulation in the 8 meshes scenario, while the ventilated scenario simulation multiplies the time needed by a factor of 1,7 if it is divided into 4 meshes instead of 8 (see Table 6.1).

Table 6.1 Summary of time parameters regarding mesh study-used simulations

	H1	H2	HX1	HX2
T_s- Simulated time [s]	2021,7	2231,5	2430,2	2666,8
T_c- Calculation time [h]	164,3	210,0	118,5	147,0
T_c/T_s [h/s]	0,081	0,094	0,049	0,055
$\theta=T_c/T_s$ [s/s]	292,55	338,78	175,54	198,44
$\theta_H/\ \theta_{XH}$	1,67	1,71		

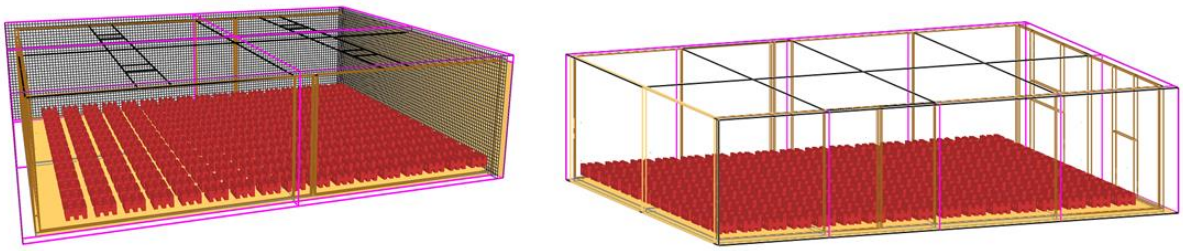

Figure 6.2 Simulation domain divided into four (left) and eight (right) meshes. Left image was taken from reference [1]*, while right image was obtained as screenshot by the author.*

Regarding to validity of results, steady state values of HRR and MLR (see from Figure 6.3 to Figure 6.6) do not seem to be significantly different from the simulations by Illa, which implies that splitting the domain into the double of meshes is a completely valid method. In both cases, ventilated scenario shows higher steady state values for HRR than non-ventilated case, due to the stimulation of the combustion reaction, which could feel choked in absence of oxygen.

However, one of the most characteristic features of Illa simulations were the apparently senseless peaks appeared in the instant of time 25 after the begin of the simulation, not when vents are set to open (120 seconds after simulations begin); these peaks do not appear in the simulations with domain divided into eight meshes, fact that reinforces the validity of the new simulations. This discrepancy could be due to the different versions of FDS in which each pair of simulations were performed (Illa used FDS v.6.1.0 version while the current release, which has been used in this project at the moment of the mesh study, is 6.5.3).

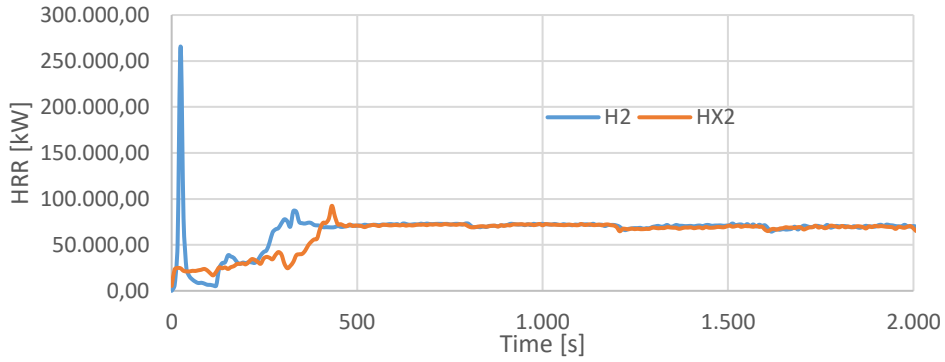

Figure 6.3 Mesh study ventilated scenario simulation results of HRR time curves

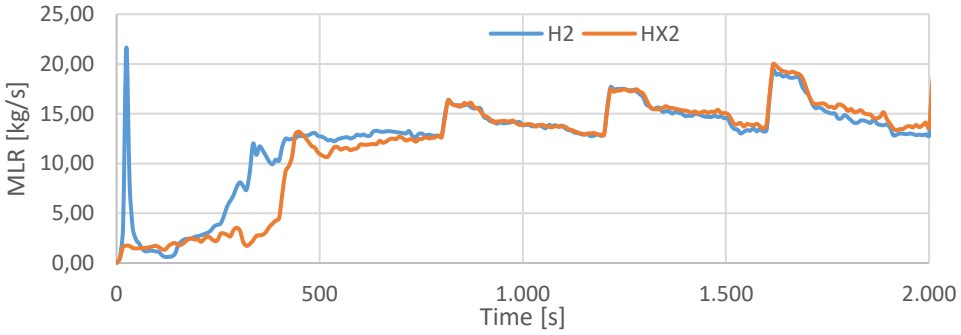

Figure 6.4 Mesh study ventilated scenario simulation results of MLR time curves

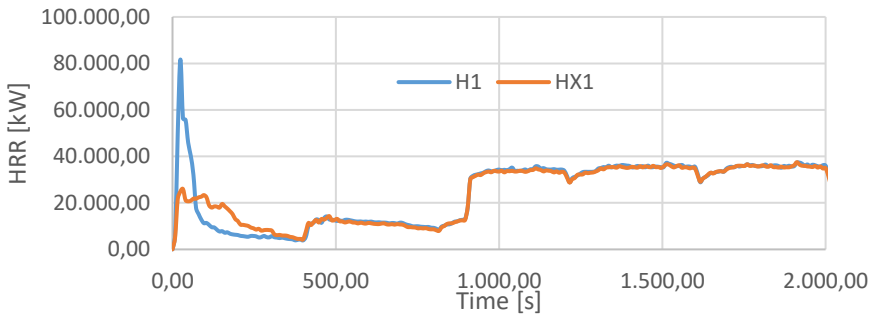

Figure 6.5 Mesh study non-ventilated scenario simulation results of HRR time curves

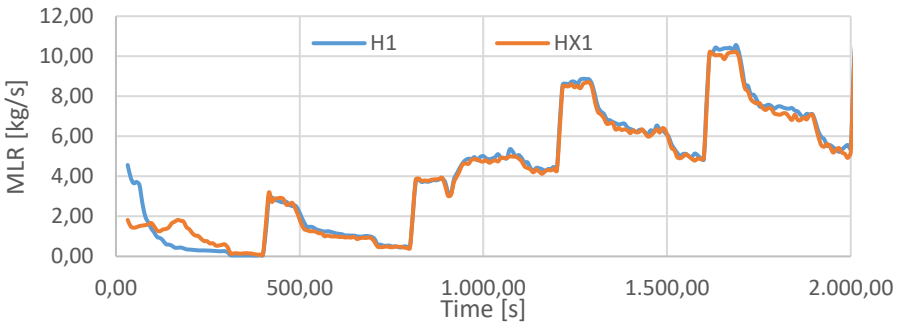

Figure 6.6 Mesh study non-ventilated scenario simulation results of MLR time curves

6.3. Inert obstacles modelling

6.3.1. Layout

The main scenario used for the simulations is a representation in FDS of that used by Generalitat de Catalunya Fire Service in their study with OZone. Layout of lower floor is shown at Figure 5.1.

Generalitat de Catalunya Fire Service, as well as Illa, with the aim of studying the ventilation effect on the compartment fire, worked with two different scenarios: one of them had no windows at the ceiling, whereas the another one counted with five openings arranged as shown at Figure 5.2. However, in the case of this project, more ventilation scenarios have been defined, which are described in next section. All vents are switch to open under the same conditions defined by Generalitat de Catalunya Fire Service, according to data in Table 5.2.

6.3.2. Constructive materials

As well as in the simulations by Generalitat de Catalunya Fire Service [27], building structure is made of:

- Standard clay bricks of 20 cm thickness for all four walls (W1, W2, W3 and W4).
- Standard concrete of 20 cm thickness for the ground.
- A sandwich panel composed of outer steel layers of 0,2 cm thickness filled by an inner content of rockwool with 5 cm thickness. Its properties have been calculated according to the weighed average contemplating steel as a 4% of the total volume, and that the rest is all occupied by rockwool.

Material properties input to FDS, as well as effective thermal penetration time according equation *(2.19)*, are indicated at Table 6.2.

Table 6.2 Inert surfaces constructive material properties

Material	Density ($kg \cdot m^{-3}$)	Thermal conductivity ($W\ m^{-1}K^{-1}$)	Specific heat ($J\ kg^{-1}K^{-1}$)	Thermal penetration time (s)
Brick	1600	0,69	840	19478
Concrete	2200	1,40	837	13153
Sandwich panel	472,4	2,03	820	129

According to thermal penetration times and to a previous study by Illa [1], the brick walls can be considered as thick solids, and therefore, the thermal effect on external air is not contemplated, exactly what FDS does by default.

6.4. Fuel modelling

6.4.1. Burners geometry

Fuel load is constituted exclusively of empty crib-shaped wooden pallets set along the whole compartment area. The whole compartment (50 x 20 x 7 m) is full of a total of 476 wooden pallets, which are separated between them by a distance of two cells (0,4 m).

The geometry of the pallets used for the simulations performed in this project was proven to be the most similar to a real case and takes the least time to be completely consumed, thus decreasing the simulation time, according to results obtained by Illa [1], who compared different geometries for burners. Graphical representation, together with specifications, are shown in Table 6.3.

Table 6.3 Wooden pallets (fuel) geometry. 3D image obtained from reference [1] *and 2D images prepared by the author.*

Graphical representation		Description	Exposed surface	Volume
3D 	XY Plane 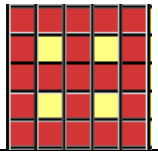	Crib composed by 9 parts of 1 x 0,2 x 0,2 meters as shown in figures aside.	5,88 m^2	0,36 m^3
XZ Plane 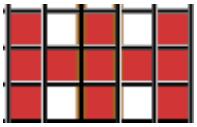	YZ Plane 			

6.4.2. Pre-defined fire curves

As well as OZone, FDS allows to define fire pre-defined curves, which are based on a hypothetical parabolic growth of fire until a maximum HRR value is reached; then, heat release rate becomes constant on time, according to equation (6.1).

$$HRR = \alpha\tau^2 \qquad (6.1)$$

FDS allows to specify the values of τ (TAU_Q) and HRR per unit area (HRRPUA) for a given surface, which are within the SURF group parameters. In these kind of fires, HRRPUA is a design value, while τ is calculated for a given α value (design parameter, tabulated in bibliography according to the fire growth speed). This option has not been used to model fires, but in order to validate BURN_AWAY FDS option, explained later.

6.4.3. Wood pyrolysis

Natural wood is a solid fuel, constituted mainly by cellulose (50%) and hemicellulose (25%) -both of them polyaromatic organic molecules containing alcohol functional groups- fibers and recovered by a layer of lignin (25%), also constituted by a set of different aromatic alcohol molecules similar to those previously mentioned [4]. These molecules are composed essentially of carbon, hydrogen and oxygen atoms, although some substances present in timber could contain nitrogen or trace elements such as sulfur, phosphor, halogens or metals and especially, a considerable water content.

Wood pyrolysis can occur through two different mechanisms [36], according to disarrangement of cellulose-formed structures (see Figure 6.7), which represents by far the controlling component of wood:

- At temperatures over 300 ºC, hydrogen bonds that keep cellulose molecules bounded together, as well as oxygen-carbon bonds between cycles are broken, so that original molecules are split, and free cycles are released in a quite endothermic reaction. Tar characteristic molecules, such as levoglucasan are formed according to this mechanism, which are easily decomposed into flammable volatiles in a exothermic reaction, which is which starts at temperature values even lower than those required for the initiation of pyrolysis. Finally, these volatiles are undergone to a very exothermic combustion reaction, leading to the formation of gaseous combustion products, such as water and carbon oxides.

- At temperatures nearby to 200 ºC, cellulose is chemically activated, forming an unstable intermediate, so that cycles are opened and volatiles are released (which are turned into gaseous combustion products), but part of the backbone of cellulose molecule, very rich in carbon atoms, does not get broken, which is translated into the apparition of solid char.

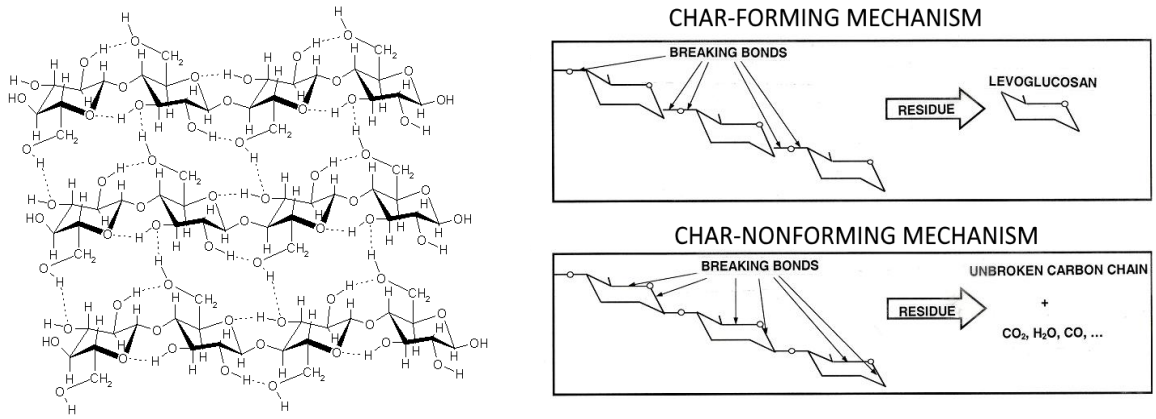

Figure 6.7 Cellulose chemical structure (left) and char-forming {upper} / nonforming {lower} pyrolysis mechanism (right). Source: [36].

Char formed according to second combustion mechanism provides wood of an isolating effect in front of temperature and air contact, so that charred wooden pieces will keep part of their mechanical properties, as there is intact wood behind char layer. In fact, many coating agents or additives try to boost this second mechanism in front of the non-charring one.

The pallets present in the simulations performed for this project are expected to be made of a treated wood composed essentially by cellulose fibers, with a content of about 48% carbon, 45 % oxygen, 7% hydrogen and 0,1% nitrogen in mass, what is considered by FDS as a single species of formula $C_{500}H_{850}O_{370}N$ in order to model combustion, according to example exposed at FDS user's guide [20].

However, before combustion, solid must pyrolyze. Pyrolysis parameters, as well as physical properties, are set through MATL code line. Temperature dependent physical properties such as specific heat have been set as constant values due to necessary higher time required to perform the simulations. Properties defined for the fuel are shown in Table 6.4.

In this case, no char is supposed to be generated, so that all wood mass becomes flammable vapors. Although Illa [1] initially considered a more realistic scenario contemplating that a 18% of the wood becomes char after combustion, finally, as a consequence of computational restrictions and deficient fire spread as fire was choked by protective non-flammable scorch layer, no char was decided to be set for the comparison of FDS results to those obtained by Generalitat de Catalunya Fire Service [1].

Due to a wide range of data regarding kinetic parameters for wood pyrolysis in pyrolysis, taken values correspond to the example illustrated in 8.5 section of FDS User Guide, as Illa [1] decided in order to use after an exhaustive study varying kinetic-related data in various simulations.

According to results observed by Illa [1], the use of the REAC line-defined parameter AUTO_IGNITION_TEMPERATURE (set to 0 by default) does not provide satisfactory results, and therefore will be omitted. A proper ignition condition has not been found, so that all pyrolysis gases that get in contact with oxygen will burn, which supposes a conservative approach and at the same time helps to reduce the computational time. However, the wood pallets at default ambient temperature set by FDS (20 ˚C) do not burn as there are no pyrolysis gases susceptible to react with oxygen, and these need a pyrolysis reaction to elapse, which needs a minimum amount of energy in order to beat the activation energy and lead to the formation of products. This is the reason why an ignition strategy had to be implemented.

Table 6.4 Properties defined for the fuel (same values as used by Illa [1] in H1 and H2 scenarios)

Description	FDS parameter	Value
Fuel chemical formula	C, H, O, N	$CH_{1,7}O_{0,74}N_{0,002}$
Heat of exothermic combustion reaction	HEAT_OF_COMBUSTION	14500 $kJ \cdot kg^{-1}$
Mass of CO formed per kg of fuel	CO_YIELD	0,004 $kg \cdot kg^{-1}$
Fraction of soot formed per kg of fuel	SOOT_YIELD	0,015 $kg \cdot kg^{-1}$
Heat of endothermic pyrolysis reaction	HEAT_OF_REACTION	430 $kJ \cdot kg^{-1}$
Arrhenius equation activation energy	E	151000 $kJ \cdot kmol^{-1}$
Arrhenius equation pre-exponential factor	A	$1,89 \cdot 10^{10}$ s^{-1}
Order of reaction	N_S	1
Thermal conductivity	CONDUCTIVITY	0,15 $W \cdot m^{-1}K^{-1}$
Specific heat capacity	SPECIFIC_HEAT	1,3
Emissivity	EMISSIVITY	0,95
Order of the heterogeneous reaction	N_O2	0 (default)
Oxygen diffusion depth along the solid	GAS_DIFFUSION_DEPTH	0,001 (default)

6.4.4. Energy provision for ignition

Illa, during his project, tested different ways to implement this energy provision that starts the combustion [1]: external flux and radiant panels.

- **External flux:** This technique needed the definition of a SURF_ID (VENT line group), see Figure 6.9, which was given a value of 110 kW/m^2 and a growth curve (RAMP). The surfaces, which need a "THICKNESS" value in order to be represented, were placed over the combustible obstacles and were set to disappear after 200 seconds. Despite its initial apparently satisfactory results, fire was not spread to other zones with no external flux, the explicitly defined SURF_IDs to include the external flux kept providing energy once disappeared and these were at the same time, combustible, so that there was fire if these surfaces were applied over an inert obstacle. Due to these unsatisfactory results, this method was discarded.

- **Radiant panels:** This technique consists on defining a surface at high temperature, separated from the pallet by 1 cell, as shown by Figure 6.8, which transfers energy to the desired combustible element through a radiation mechanism; in order not to cause direct effect on the ambient temperature of the enclosure, convection was set to zero (CONVECTIVE_HEAT_FLUX = 0), as can be seen at Figure 6.10.

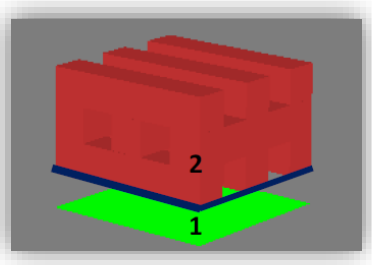

Figure 6.8 Burner (2) and panel (1)

The figure shows that the panels reach the temperature of 1780 ˚C according to a growth curve (RAMP).
In this case, the provision of energy disappears when the panels are switched off. However, Illa reported that the fire, once started was not able to feed back the solid fuel with the energy required to pyrolyze it and generate gaseous fuel. This is the reason why a specified fire growth strategy had to be implemented. However, radiant panels have showed to provide better results than external flux and therefore, will be implanted in the simulations of this project as "ignition source".

Neglecting the thermal power losses by the edges of the panel, and that exposed surfaces of obstacle and panel are equal, thermal power received by (2) from (1) (see Figure 6.8) can be found according to equation (6.2) [1].

$$q_2 = A_2 \frac{\sigma\,(T_1^4 - T_2^4)}{\frac{1}{\varepsilon_1} + \frac{1}{\varepsilon_2} - 1} \qquad (6.2)$$

Where:

- T_1 and T_2 are the temperatures of the panel and the obstacle, expressed in K.
- ε_1 and ε_2 are the emissivities of the panel (1) and the obstacle (0,95).
- A_2 is the area of the obstacle exposed to radiation, in m^2.
- σ is the Stefan-Boltzmann constant, equal to $5{,}67 \cdot 10^{-8}$ $W \cdot m^{-2} \cdot K^{-4}$.

```
&RAMP ID='inici', T=0 ,  F= 0.2/
&RAMP ID='inici', T=100,  F= 0.6/
&RAMP ID='inici', T=200,  F= 1 /
&SURF ID='FUSTA', MATL_ID='WOOD', THICKNESS=0.2, COLOR='BROWN'/
&SURF ID='ENERGIA', MATL_ID='WOOD', THICKNESS=0.2, COLOR='BROWN', EXTERNAL_FLUX=110, RAMP_EF='inici'/
&VENT SURF_ID='ENERGIA', XB=4.4, 4.4, 4.6, 5.6, 0.2, 1.2, DEVC_ID='TIMER_ENERGIA'/
&VENT SURF_ID='ENERGIA', XB=5.4, 5.4, 4.6, 5.6, 0.2, 1.2, DEVC_ID='TIMER_ENERGIA'/
&VENT SURF_ID='ENERGIA', XB=4.4, 5.4, 4.6, 4.6, 0.2, 1.2, DEVC_ID='TIMER_ENERGIA'/
&VENT SURF_ID='ENERGIA', XB=4.4, 5.4, 5.6, 5.6, 0.2, 1.2, DEVC_ID='TIMER_ENERGIA'/
&VENT SURF_ID='ENERGIA', XB=4.4, 5.4, 4.6, 5.6, 1.2, 1.2, DEVC_ID='TIMER_ENERGIA'/
&DEVC ID='TIMER_ENERGIA', QUANTITY='TIME', XYZ=0.00,0.00,0.00, SETPOINT=200.00, INITIAL_STATE=.TRUE./
```

Figure 6.9 Codelines for the setting of external flux

```
Panell radiant-
&RAMP ID='inici', T=0 ,  F= 0.2/
&RAMP ID='inici', T=100,  F= 0.6/
&RAMP ID='inici', T=200,  F= 1/

&SURF ID='CREMA', CONVECTIVE_HEAT_FLUX=0, TMP_FRONT=1780, EMISSIVITY=1, RAMP_T='inici'/
&VENT XB= 4.4, 5.4, 4.6, 5.6, 0.2, 0.2, SURF_ID='CREMA'/
```

Figure 6.10 Codelines for the setting of radiant panels

6.4.5. Fire growth

Although the method of radiant panels has proven to be good for provoking the ignition of certain combustible obstacles, the fire was not spread to the nearby obstacles that were not "ignited" by the action of panels and, therefore, fire at the compartment ended when the wood pallets that were provided with the ignition source were completely consumed.

In order to solve this problem and grant that all combustible obstacles will be subject to pyrolysis, Illa [1] developed a Matlab script able to generate the FDS code lines so that, through a complex system of groups of pallets and radiant panels, every obstacle would burn at the time required in order to achieve the reproduction of the desired time vs HRR growth curve.

A total of 8 groups of pallets were set (distribution shown at Figure 6.11), below of which there are radiant panels that are activated and deactivated using a RAMP function, at times indicated at Table 6.5.

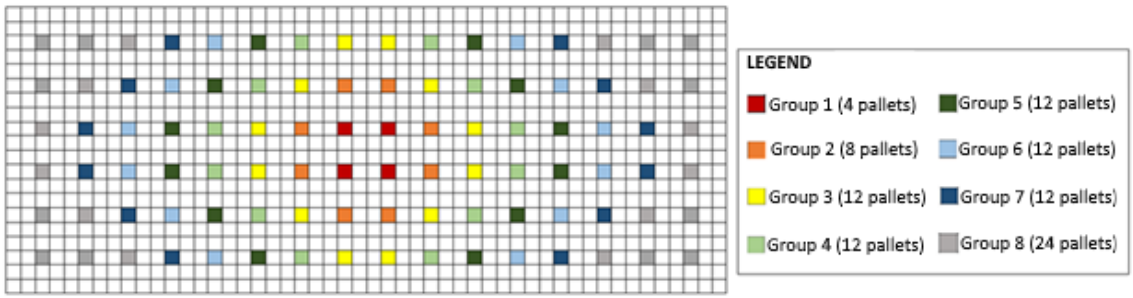

Figure 6.11 Distribution of different groups of panels along the original 50x20 m² scenario. Source: [1]

Table 6.5 Activation and deactivation times of the different pallet groups

Group	Activation time (s)	Deactivation time (s)
1	0	300
2	400	700
3	800	1100
4	1200	1500
5	1600	1900
6	2000	2300
7	2400	2700
8	2800	3100

6.4.6. Fuel burnout and consumed mass estimation

Another aspect to verify in order to judge the real discrepancy between ventilated and unventilated cases is if FDS is able to make fuel disappear following a real burning rate, as it directly conditions the duration of the fire.

FDS permits to simulate the disappearance of fuel thanks to a logical parameter (BURN AWAY) which must be specified in the *SURF* line. However, it was not clear that fire extinguished when total fuel mass specified in the FDS script is over, so a simple simulation was run in order to clarify how this option works. According to equation *(3.33*), if a bulk density is defined, the mass of fuel consumed will only depend on obstacle geometry and this first parameter, overriding data from MATL density and SURF thickness.

The simulation prepared for this proposal was a simple wood cube of 1x1x0.8 m as specified by OBST code line (geometry) with thickness 0.2 m, density ρ=200 kg/m3 and bulk density ρ_b=72.74 kg/m3. The fire, following a trial performed by Illa, used a specified growth rate by the TAU_Q option set to 300 and considered the formation of char. In parallel, another simulation identical but without a predefined growing rate (TAU_Q not defined) was also launched.

Simulations provided a given MLR for each instant of time, whose curves in front of time for both cases are shown in Figure 6.12 and Figure 6.13.

For both cases, total mass consumed when fire ends (theoretically the total fuel mass defined in the FDS code) was calculated as the area under the curve of these graphics using the trapezoidal rule, equation (6.3).

$$m_{\substack{Fuel \\ Consumed}} = \sum_{i=1}^{N} d_{x,i}\, d_{y,i} d_{z,i} \rho_{b,i} = \int_{ti}^{tf} \dot{m}(t)\, dt = \sum_{i=1}^{N} \left(\frac{\dot{m}_j + \dot{m}_{j-1}}{2} \right) (t_j - t_{j-1}) \qquad (6.3)$$

Where:

- $d_{x,i}$ is the length of a quadrangular obstacle i (defined in OBST line) along x axis.
- $d_{y,i}$ is the length of a quadrangular obstacle i (defined in OBST line) along y axis.
- $d_{y,i}$ is the length of a quadrangular obstacle i (defined in OBST line) along z axis.
- $\rho_{b,i}$ is the BULK_DENSITY parameter (defined in OBST line) of a quadrangular obstacle i.
- $\dot{m}(t)$ is the obstacle mass loss rate due to pyrolysis, which varies along time.
- $\dot{m}_j$ is mass loss rate value at time instant t_j (data provided by *HRR.csv* FDS output file).
- t_j is the time elapsed since fire initiation to instant at which $\dot{m}_j$ is evaluated.

This calculation lead to 58,192 kg in the first case and 58,228 kg in the second case, which is precisely the total mass defined in the FDS script if it is calculated as product of bulk density and the volume of material determined by geometry, so the wood cube height is defined by the OBST XB code line instead of by the SURF THICKNESS code line.

This study has proven that although growing rates of two simulations with the same burner specified (same OBST XB geometrical dimensions and density) are different, both of them will consume the same quantity of fuel and therefore, the total heat released will be the same.

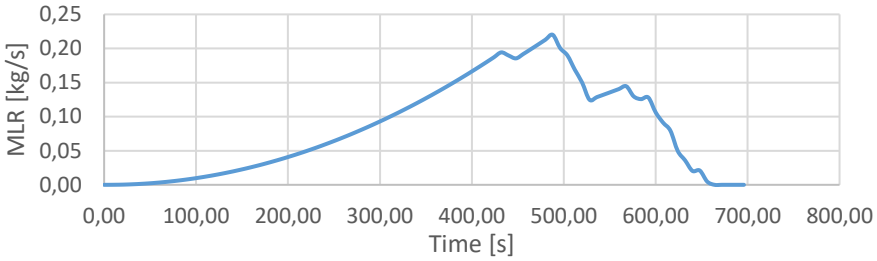

Figure 6.12 Time evolution of MLR curve when TAU_Q is specified

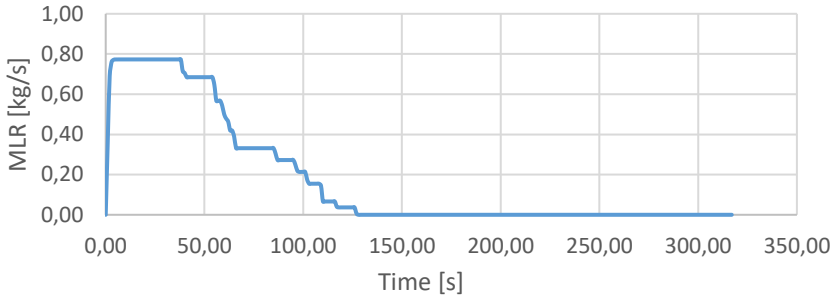

Figure 6.13 Time evolution of MLR curve when TAU_Q is not specified

Notice that area of XY-plain slice of wooden pallets, used as burners in the main simulation scenario, varies with height, so that time is supposed to be the sum of times for all obstacles constituting the crib-shaped pallet.

After this study, once validated the method for calculation of total consumed mass when the fire is over, this strategy has been used for the calculation of mass consumed in the main simulation scenario.

Total mass consumed in main simulation scenario (I2 simulation) is 17278,2 kg for a total of 238 wooden pallets, what leads to a mass of 72,6 kg per pallet after using the method of trapezoids to estimate the integral of mass loss rate with respect to time. In this case, bulk density has not been defined and MATL density is 200 $kg \cdot m^{-3}$. Each pallet has a volume of 0,36 m3, which leads to a mass of 72 kg if multiplied by density, which fits pretty well with value of 72,6 calculated using equation (6.3), which was already supposed to lead to a small error.

6.5. Simulation results and collected output data

FDS calculates several variables, related among them, in order to reach the results of HRR and MLRPUA data, provided within a .csv file, easily converted to Microsoft Excel® format called filename_hrr.csv, as well as another file that indicates computer CPU timing and efficiency and hydrodynamic behaviour of fire and gases visible at Smokeview animation.

However, in order to save time and memory, data such as temperatures, velocity, pressure or others are not directly provided if not required explicitly. Besides of the parameters required to model the fire behaviour, FDS also permits to request the explicit calculation of others, such as temperature values that would be registered from thermocouples.

FDS offers three possible formats in order to display simulation results:

- Through devices (DEVC), which require a sensor to be placed at a desired point where data will be collected from. Output data is exported to a .csv file.

- Through slices (SLCF), that show a plain within a Smokeview animation showing the time variation of the desired parameter. These animations can be rendered, converted into a set of images, which can be easily turned into graphics or tabulated data, with the help of a proper Matlab script.
- Output data on system boundaries (BNDF), also visible within a Smokeview animation.

Output data collected for this project is summarized at

Table 6.6.

Table 6.6 Collected output variables

Output variable	Output format	Variable name in FDS	Units
Temperature	DEVC, SLCF	TEMPERATURE	˚C
Adiabatic temperature	DEVC	ADIABATIC SURFACE TEMPERATURE	˚C
Pressure	SLCF	PRESSURE	Pa
Species mass concentration	SLCF	MASS FRACTION	kg kg^{-1}
Velocity	SLCF	VELOCITY	m s^{-1}
Boundary surface temperature	BNDF	WALL_TEMPERATURE	˚C
Burning rate	BNDF	BURNING_RATE	kg $m^{-2}s^{-1}$

The list of devices (DVCs) and slices (SLFCs) are summarized at Table 6.7 and Table 6.8.

Table 6.7 List of DVCs set along the simulation scenario

DVC	Description	Position coordinates
T11	Temperature at room center, ground	0,3; 10,1; 1,1
T12	Temperature at room center, medium	0,3; 10,1; 3,1
T13	Temperature at room center, ceiling	0,3; 10,1; 6,5
T21	Temperature at center of right half, ground	12,4; 10,1; 1,1
T22	Temperature at center of right half, medium	12,4; 10,1; 3,1
T23	Temperature at center of right half, ceiling	12,4; 10,1; 6,5
T31	Temperature at right wall, ground	24,5; 10,1; 1,1
T32	Temperature at right wall, medium	24,5; 10,1; 3,1
T33	Temperature at right wall, ceiling	24,5; 10,1; 6,5
T41	Temperature at back wall, ground	0,3; 19,8; 1,1
T42	Temperature at back wall, medium	0,3; 19,8; 3,1
T51	Temperature at the window	24,5; 15,1; 3,5
TAD1	Adiabatic surface temperature at room center, ceiling	0,3; 10,1; 6,5
TAD2	Adiabatic surface temperature at center of right half, ceiling	12,4; 10,1; 6,5
TAD3	Adiabatic surface temperature at right wall, ceiling	24,5; 10,1; 6,5

Table 6.8 List of slices possible to visualize within Smokeview animation

SLCF	Description	Plain coordinates
YT1	Temperature slice	Y=10,1
YV1	Velocity slice	Y=4,1
YV2	Velocity slice	Y=13,1
YV3	Velocity slice	Y=15,1
ZT1	Temperature slice	Z=3,1
ZT2	Temperature slice	Z=6,1

7. Study of ventilation effect

Ventilation effect on fire behavior and, probably, on the constructive materials of the compartment seems evident, since technical guides provided by legal framework suggest, that the time that a sctructure can keep its bearing capacity, when exposed to fire, is directly related to the total ventilation area of the compartment, which can be seen with expressions like equation (4.2).

This evidence has inspired the redaction of this section, in which the effect of increasing total openings area, as well as distribution of ventilation gaps along ceiling area, will be studied.

7.1. Effect of openings size

7.1.1. Analysis of .csv output files

This study departs from base cases, performed initially by Illa, but corrected in order to include the effect of fuel burnout. These two first simulations, which represents the base scenario (see layout at Figure 5.1) with and without smoke and fire exctacting gaps (see their size and distribution at Figure 5.2) already showed that the time that the fire lasts is considerably smaller when the compartment is provided with ventilation gaps at the cowling. Departing from the ventilated generic scenario, fire and smoke extractors area has been increased progressively in different simulations. Although gaps size increments were not regular, a clear dependence between ventilation area and fire duration could be found. Notice that this study is not based on reglamentary sizes for extractors, so that there are gaps which are non square or are wider than maximum established by normative (2,5 m^2 per side). Summary of simulation data is presented at Table 7.1.

Table 7.1 Summary of data regarding simulations carried out in order to study the effect of ventilation area.

Simulation	Openings total area	Maximum HRR peak	Fire duration	Simulation time (nº cores)
I1	-	39.826,01 kW	3000 s	189 h (8)[6]
I2	10,80 m^2	95.597,97 kW	2270 s	388 h (4)[7]
I3	21,62 m^2	148.970,36 kW	1500 s	272 h (4)[7]
I4	31,62 m^2	171.184,64 kW	1170 s	233 h (4)[7]
I5	414 m^2	102.809,57 kW	N/A	439 h (4)[7]

Last table shows a decreasing trend regarding relationship between total ventilation gaps area and the opposite behavior regarding to maximum HRR peak attained during the simulation (see Figure 7.1). This shows that fire is ventilation controlled, as variations in ventilation provoke higher HRR values. Besides, as reaction speeds up and the amount of fuel is not infinite, the reaction ends sooner, which is perfectly reflected in Table 7.1.

According to NTP-200 [25], in the case of compartment buildings, temperature at structural elements, and thus, power released, increases with ventilation until a certain value, when a certain equilibrium between oxygen provision and heat evacuation is reached: fire stops to be ventilation controlled, and up to then, increase on ventilation provokes higher cooling effect, which explains perfectly last results.

[6] Simulation carried out using 8 of a total of 44 cores with processor Intel® XEON® E5-2699V4
[7] Simulation carried out using 4 of a total of 4 cores with processor Intel® Core™i5 - 750

Heat release rate versus time curves that can be seen at figure Figure 7.2 show that when evacuation surface increases, maximum and steady heat release rates also increase, as a result of a better ventilation, and therefore, both enhanced mixture due to turbulency generated by entrying air speed and an extra provision of limiting reactant (air), which confirms that these scenario is completely ventilation controlled.

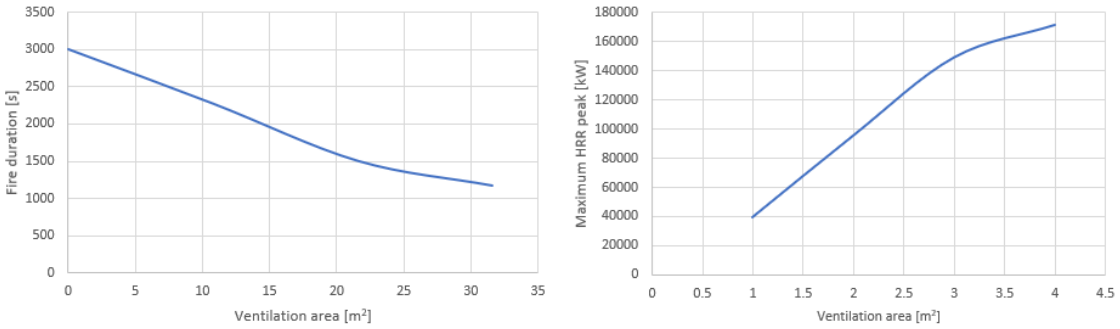

Figure 7.1 Fire duration and maximum achieved heat release rate peak as function of total ventilation area

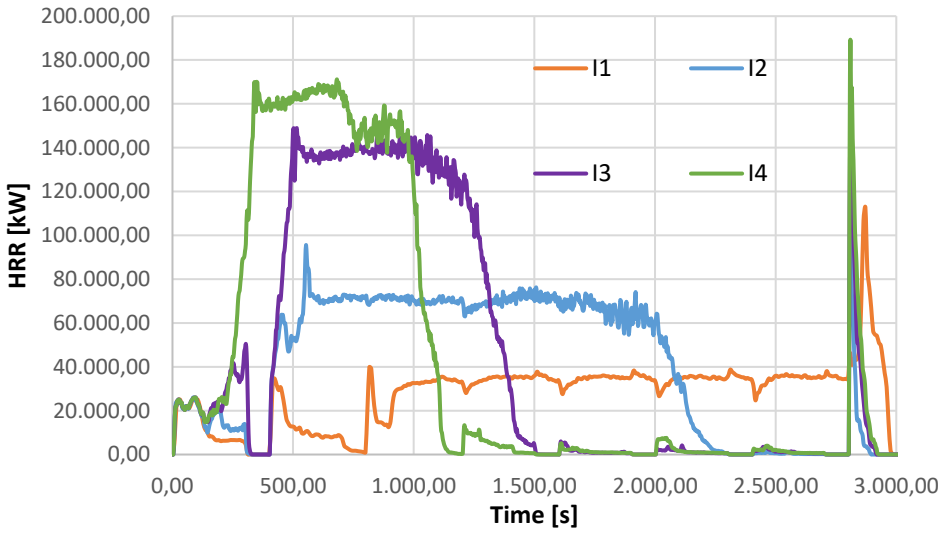

Figure 7.2 Fire time evolution curves variation according to ventilation area

FDS simulation results show a peak during the last seconds that the simulation lasts. This happens because of piloted ignition follows the model found using Matlab by Illa [1] when trying to represent the real behavior of a fire under these conditions. However, this supposes running different radiant pannels which provide the required energy to cause ignition once certain triggers have been activated (in this case, only time), so different ignition sources are activated in diferent regions in different time instants and then, small parts of fuel which were not burnt finally do - fire does not spread when a space between obstacles is found.

Since the appearance of that peak and the fact to study wether the whole fuel load is burnt or not, a proper new model for fuel pyrolysis should be implemented in FDS simulations in order to represent accurate fire time evolution curves variation with total ventilated area. This is well illustrated with Figure 7.3, that shows a open ceiling scenario, where the fire is only “alive” when radiant panels are on.

This confirms that, in order to study fires that are much shorter or longer than those the growth script was designed with, a proper pyrolysis must be set through direct FDS scripting, or through new piloted ignition instructions via radiant pannels in order to achieve a realistic fire growth and behavior.

It is also noticeable, according to Table 7.1 that computational time required to perform the simulation shows a decreasing trend when ventilated area is increased (with the exception of I1 simulation, which was performed by a high performance computer using 8 cores instead of 4, and that were provided with a better processor). This tendency is kept until open ceiling scenario, which shows higher necessary computational time than previous simulations, which could maybe be related to exceeding equilibrium ventilation rate, as suggested by NTP-200. One could suppose that time required to complete simulations has its minimum at the point of equilibrium between oxygen flow required by combustion stoichiometry and heat evacuation effect of ventilation. Nevertheless, should be confirmed and if convenient, this advantage could be seized in order to speed up simulations when not testing ventilation effect.

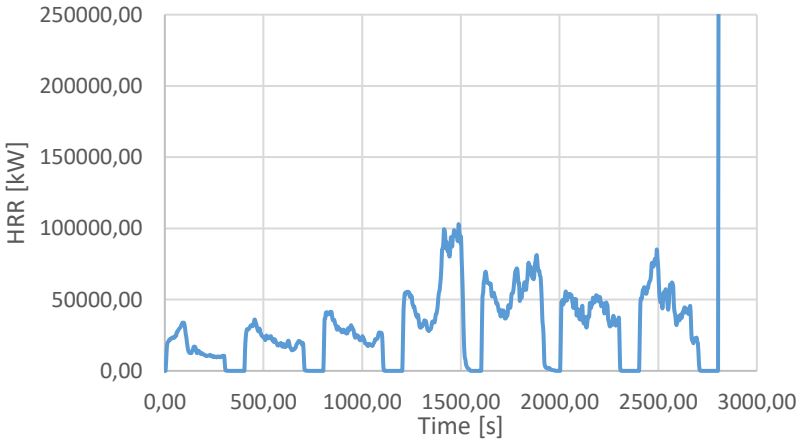

Figure 7.3 Fire time evolution curve in the case of open roof simulation (I5)

Temperatures registered at both right wall do not seem to be as sensitive to ventilation as heat release rate values (excepting the particular case of simulation representing open ceiling), but duration of exposition of structures to high temperatures, unlike maximum registered temperature values, seems to be drastically reduced when ventilation increases, especially at low axial positions of right wall (T31), as can be observed at Figure 7.4.

Predictions at back wall (T41 and T42) do not seem to show a so obvious relationship between maximum temperature values, exposition time to high temperatures and ventilation level; however, it is possible to see step-like shapes while radiant panels are on, which suggests that this effect will not be properly observed if no proper pyrolysis-ignition strategy is implemented.

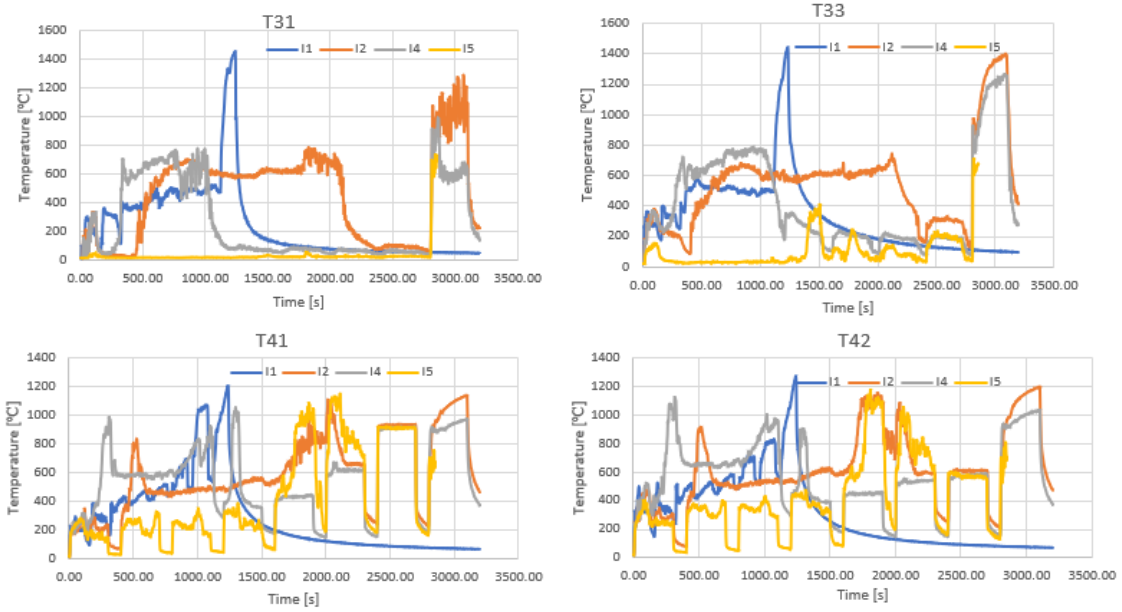

Figure 7.4 Time evolution of temperatures predicted at right (upper) and back (lower) walls for different simulations

7.1.2. Analysis of *Smokeview* animations

Besides of Excel-importable output files, FDS also provides Smokeview animations, showing how smoke, heat release rate and selected output variables (in this case, temperature and velocity) vary over time in three-dimensional simulated scenario.

An interesting feature that can be observed inspecting these simulations, and specifically, temperature slices, is the evolution of compartment fire stages (see section 2.4.2) within the room along time.

Taking as reference temperature at slice Y=10 m (just the centre of the room) and using the criterion proposed by McCaffrey, Quintiere and Harkleroad [10], by which temperatures over 500 ºC in whole room denote flashover (will be taken as maximum), different fire stages have been identified. Figure 7.5 shows different fire stages according to temperatures registered at each time instant. Notice that simulation I3 has not been included, as its data results were not significantly different from those observed with simulation I2.

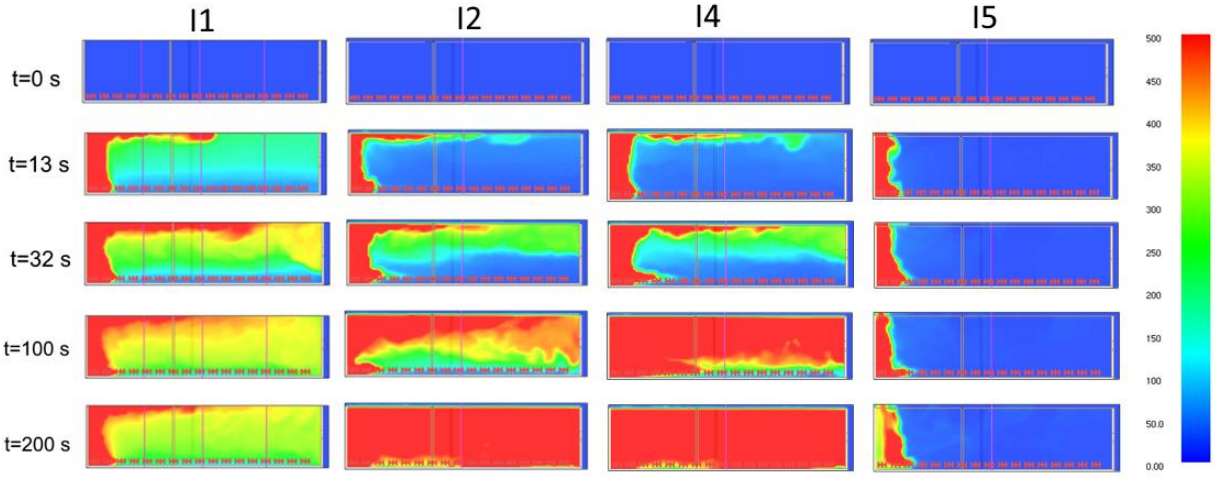

Figure 7.5 Temperature slice at Y=10 m in the case of different ventilation levels, showing different fire stages.

It is also important to consider that, although flashover would exist according to previously exposed criterion, it will not occur, as fire cannot burn by its own and requires ignition criterion set through the complex system of radiant panels, which will not grant the simultaneous burn of all fuel at the whole domain.

Results by I5 simulation denote that fire is well ventilated, as seems obvious, when ceiling is open and therefore, combustion gases seem to be properly evacuated and evacuation ways seem to be granted.

7.2. Effect of openings distribution on heat release rate curve

In addition to the size of the ventilation openings, another fact that could be related to the air entrance ratio, and then, to burning efficiency is the distribution of the smoke extraction vents along the roof or walls of the building. In order to find how this distribution could affect heat release rates, different simulations were carried out, keeping the same total fire extractors area as simulation I2 (10,816 m^2) run for the previous section. Tested ceiling vent distributions consisted on a single rectangular shape concentered at the center of the roof; and finally, four squares centered at each quarter, as Figure 7.6 shows.

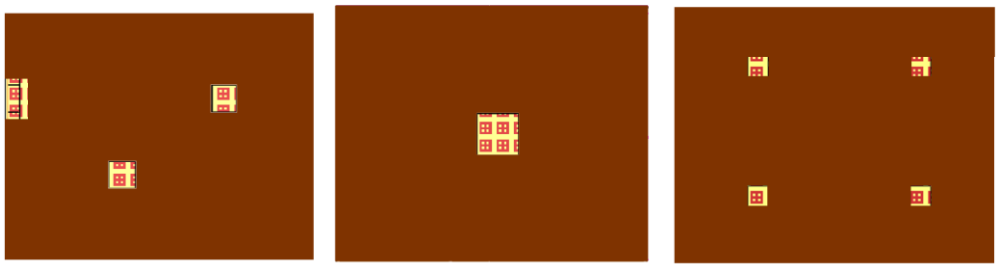

Figure 7.6 Plant view showing ceilings of different tested simulation scenarios; from left to right: I2, J2 and K2

Fire growth of all three cases, shown in the following HRR vs time curve (Figure 7.7), seem to follow the same pattern, characteristic for compartment fires: an initial small scale fire from 0 to 400 seconds (due to the timing of the radiant panels strategy used to force ignition), followed by a fast growth that lasts 50 seconds as much, a long steady state (plateau from approximately 500 seconds after the fire starts), a gradual extinction that starts approximately 2000 seconds after the fire is initiated and finally, a sharp peak that corresponds to the remaining fuel that the fire could not consume by its own but was forced to ignite by radiant panels activated at second 2800.

Yet, there is a main difference in these three cases: I2 and J2 simulations showed higher initial peak (t=500 s) and steady state HRR values than K2 case, whereas, according to mass conservation principle proven previously, K2 simulation fire is extinguished later.

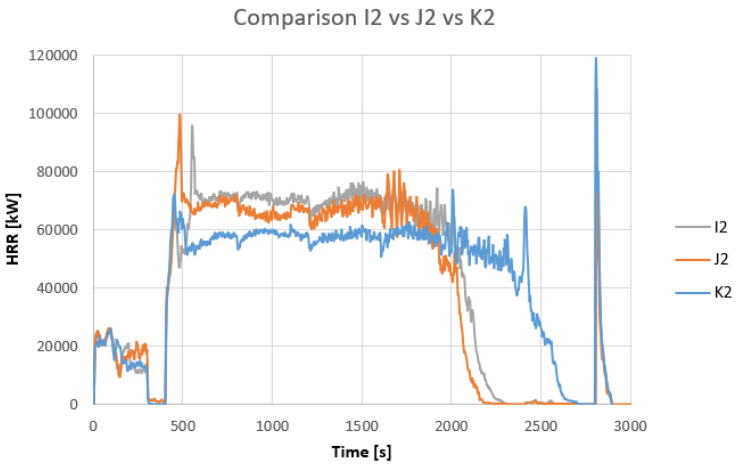

Figure 7.7 Time evolution curves of heat release rate for I2, J2 and K2 simulations

Temperatures show similar curve shapes and values, as well as the same growth tendency of HRR vs time curves: initial fast fire until t=400 s (see Figure 7.8 to 7.8), fast fire growth followed by a long steady state (showing values compressed between 600 and 800 ºC in the case of right and back walls) and a fire decay, which is the stage that varies most between I2 and K2 scenarios, showing these last a more abrupt decline, as the steady state mean temperature is still present 2400 seconds after the fire initiation, in contrast to the others, whose values are under 200 ºC by that time.

In all cases, temperature at room centre time evolution displays several fluctuations during the supposed steady state, where values over 1000 ºC are reached about 1700 s after the fire start, being this maximum larger in I2 and J2 simulations, whereas in the case of K2 does not even arrive to 1000 ºC. These fluctuations are due to the fire ignition strategy, implemented with the help of radiant panels, where temperature shows a peak when panels are activated to ignite. This shows up that central region is the more sensitive to ignition, where fire is supposed to start.

Differences, specially between I2 and J2 simulations, are scarce and basically gathered on temperature measures at the back wall. Yet, these differences do not seem to be statistically significant by visual inspection, but attributable to random flux fluctuations.

An important fact is that in all cases, peaks at room centre and back wall temperatures are over that defined by ISO-834 curve (see equation (4.1)). Fires last between 2000 and 2700 seconds (if final peaks is excluded) and less than 3000 seconds if the final sharp peak is included, which means that in this case, REI60 materials are good enough to build the compartment structures, considering that all peaks that are over the ISO curve, are below the critical temperature of the structure. Although temperatures reached at the center of the room might reach 1400 ºC, this region is not supposed to contain structural elements, and therefore, hypothetical overheat here would not affect as much as in walls if there are no pillars or beams there.

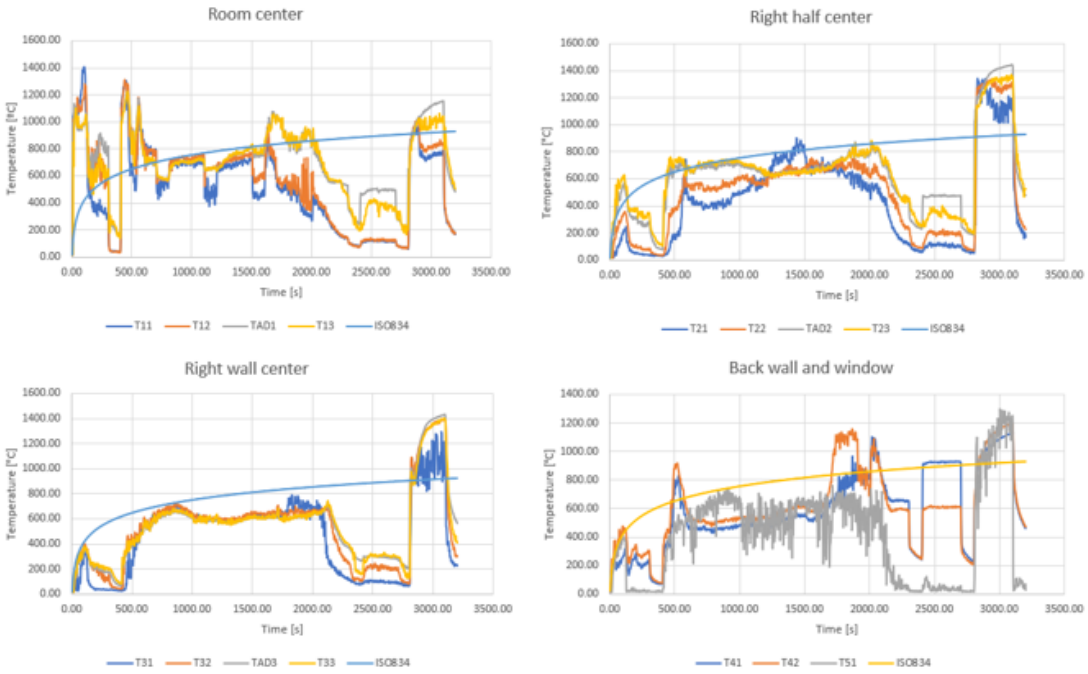

Figure 7.8 Comparative of results by different DEVCs and ISO-834 curve, simulation I2

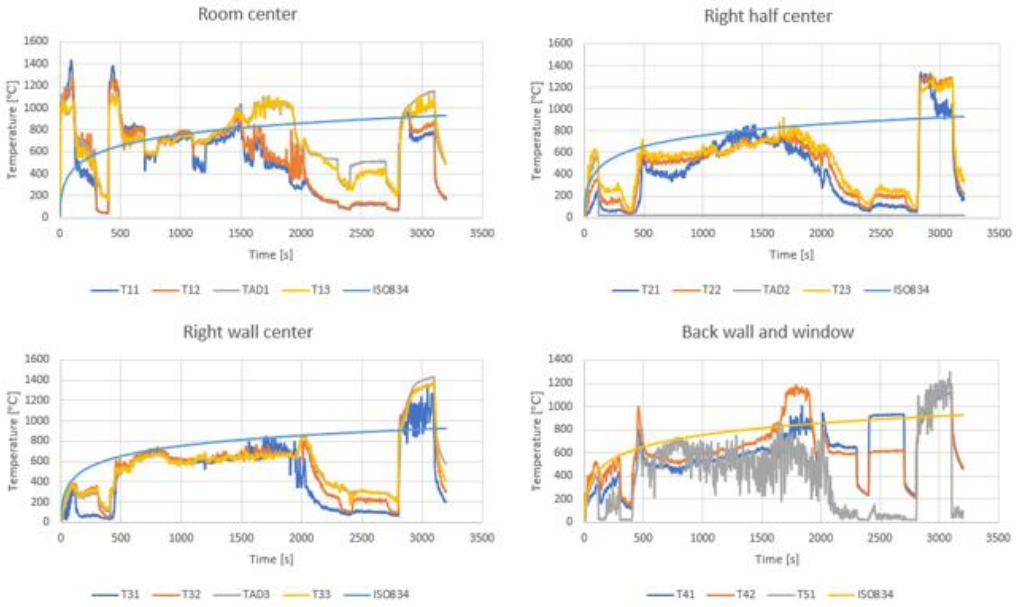

Figure 7.9 Comparative of results by different DEVCs and ISO-834 curve, simulation J2

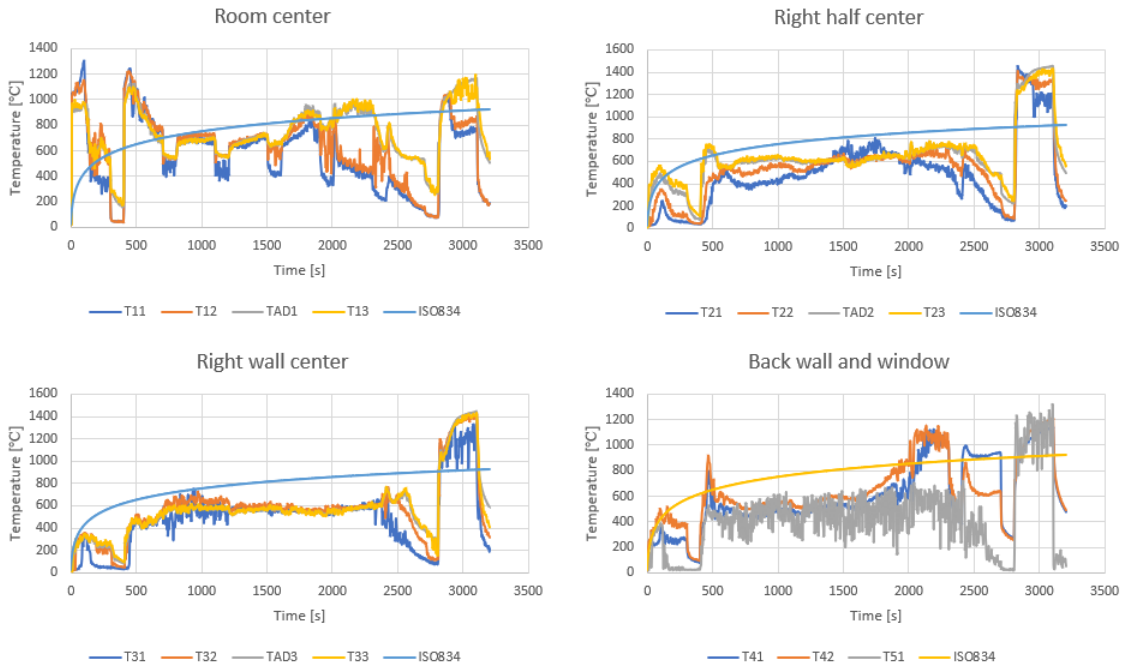

Figure 7.10 Comparative of results by different DEVCs and ISO-834 curve, simulation K2

7.2.1. KX simulation

K2 simulation provided lower heat release rate values than I2 and J2 simulations. The difference between those three was the way to distribute the total ventilation area, which was supposed to be the same for all three simulations, in three natural ceiling vents (I2), one (J2) or four (K2).

In order to confirm that distributing the total ventilation area among more and smaller gaps might lead to lower HRR values, another simulation named KX was launched. This counted on a total of eight smoke extraction gaps sized 1,35 m^2, setting a total of 10,816 m^2.

Since fires within this enclosure are ventilation controlled, HRR and, then, burning rate is proportional to air mass flow entering to the compartment. According to equation (*2.15*) this air mass flow, equal to mass flow leaving the compartment, depends on:

- **Discharge coefficient**, which gives an indication of pressure drop in flow while crossing narrow gaps. Shape of gaps has not varied; yet, the disposition of narrower vents, could lead to the loss of a larger amount of pressure and, therefore, velocity and flow. A possible cause of achieving lower HRR values, could be, then, higher pressure drops due to pass of air through narrower orifices.

- **Ventilation gaps area (width)**, which has varied between the different simulations. Nevertheless, air entrance flow is directly proportional to this factor but also to a sum involving its square, so that commutative principle is not expected to be fulfilled, and total mass is not thought to be equal if total ventilators open area is. Even though, no differences have been found between I2 and J2 simulation results.

- **Fresh air inlet gaps area (width)**, which could be supposed to be equal in all simulations, as same compartment is represented. Nevertheless, relative ubication of vents is not the same in different simulations, which implies that this factor could have certain influence.

- **Temperatures** of fresh air (is supposed to be the same for all simulations, 20 ºC, as FDS considers by default) and of the smoke layer, which will depend on total heat release rate.

- **Total compartment height**, which was equal for all three simulations.

- **Smoke layer height**, which will depend on total heat release rate and hence, is function of the air entrance mass flow itself. Smokeview animations related to all simulations performed for this study showed that stratified case is reached about 30 seconds after the fire starts, in which smoke layer temperature exceeds the value of 500 ºC, which leads to a flashover scenario. After 100 seconds from then, smoke layer within the compartment reaches floor level, yielding to a well-mixed scenario that lasts until the end of the fire, which implies that this height can be approximated to zero.

Simulation results shown in Figure 7.11 reveal that if total ventilation surface is maintained but divided into many different openings, results do not vary significantly from other scenarios in which openings are distributed following different patterns, which discards the possible hypothesis of significant quenching effect due to higher pressure loss if ventilation gaps are smaller.

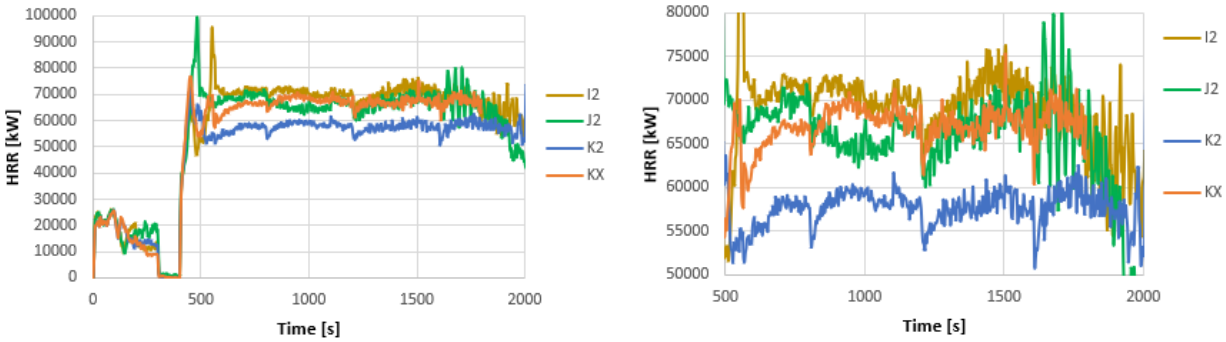

Figure 7.11 Comparison between HRR time evolution of I2, J2, K2 and KX simulations

Yet, K2 simulation results seem to be considerably different to other scenarios, fact that could be attributed, then, to a deficient mass exchange if smoke extractors are placed just at the center of the computational domain.

In order to study the possible effect of vents distribution, and considering a steady state fire within the simulations scenario (H=6 m), where air density is1,2 $kg \cdot m^{-3}$, ambient temperature is 20 ºC (293,15 K) and smoke layer is at ground level (H_D=0 m) and has a mean temperature of 500 ºC (773,15 K), a simple sensitivity study of input values of equation *(2.15)* has been carried out varying the values of parameters A_l and the couple A_c and number of natural ventilation gaps (so that total vent area is kept equal).

Results show a clear increment of entering air mass flux when total area of ventilation gaps is divided into more vents. However, this tendency decreases as the total area of cold air entrance gaps increases, so that there is no practical difference between dividing a certain ventilation area between 2 vents or more when A_l is considered to be 26,4 m^2 (the total area given by doors and windows in the considered simulation scenario) or between 8 vents or more then only a fourth part of this area is considered. Despite this initial difference, both cases seem to converge to the same final result when ventilation area is divided into many different gaps.

Under the assumption that, although windows and doors are not varied between simulations, the distribution of ceiling vents could change the efficient A_l value, these results could possibly explain why K2 heat release rate values are lower. While ceiling gaps are more nearby to the center of the meshes, these will be further to ventilation sources, placed at the room perimeter, which will make their relative A_l area smaller than if they were placed in a position where air currents in are more direct .

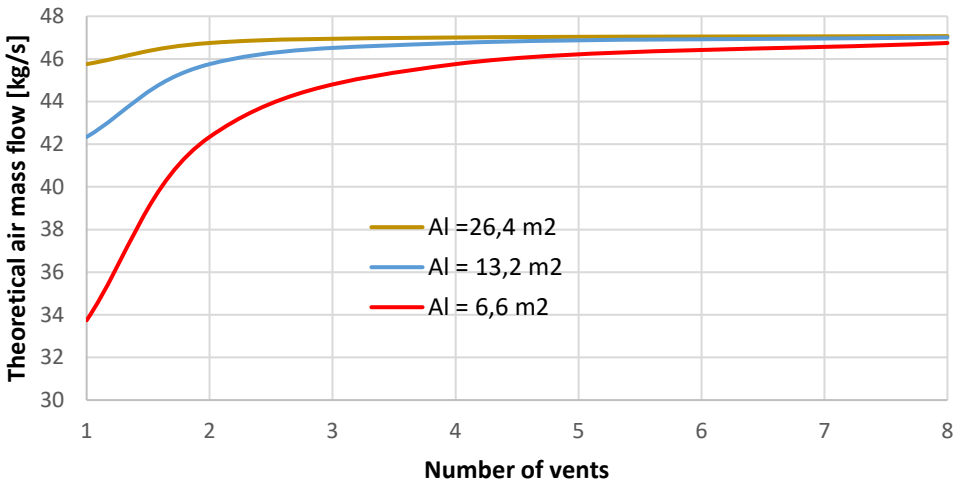

Figure 7.12 Theoretical air entrance mass flow according to number of vents for the same total vents area

8. Fire load and ventilation effect on structural resistance

8.1. Fire load calculation strategy

Fire resistance requirements of constructive materials as well as the other requirements that are established according to the intrinsic risk level, depend exclusively on fire load, once present fuel mass at area (see section 6.4.6) and built surface of fire sector are known. In FDS, if no *BULK DENSITY* is set, fire load can be calculated according to equation (8.1).

$$Q_s = \frac{1}{S}\sum_{i=1}^{N} d_{x,i} d_{y,i} \delta_i \rho_i \Delta H_{C,i} \tag{8.1}$$

Where:

- Q_s is the fire load of the simulation scenario, given in MJ·m^{-2}.
- $d_{x,i}$ is the length of a quadrangular burner obstacle i (defined in OBST line) along x axis.
- $d_{y,i}$ is the length of a quadrangular burner obstacle i (defined in OBST line) along y axis.
- δ_i is the THICKNESS of a quadrangular burner obstacle i (defined in SURF line).
- ρ_i is the DENSITY (defined in MATL line) of a quadrangular burner obstacle i.
- $\Delta H_{C,i}$ is the HEAT_OF_COMBUSTION parameter (defined in REAC line) of a quadrangular burner obstacle i.
- S is the total built surface of the fire sector where fire load will be evaluated.

According to this expression, fire load can be varied in FDS by changing combustible material density, burners thickness or burners surface, understand as product of lengths in x and y directions. Illa [1] performed an study in order to determine which effect could cause variations of these three factors on fire curve shape and computational time, besides that on theoretical fire load; the results showed that changing material density is the best way to vary fire load, as simulation time increment is much lower when density does than in the other two cases and unlike these latter, density changes do not imply significant changes in the shape of fire curves.

The particular case of the main scenario used in this project, the unique type of fuel available at the fire sector is wood (heat of combustion of 14,500 MJ·kg^{-1}), uniformly set along the whole surface (1000 m^2) as 476 crib-shaped pallets with a total volume of 0,36 m^3 per pallet, the last equation becomes:

$$Q_s = \frac{1}{1000} 476 \cdot 0{,}36 \cdot 14{,}500 \cdot \rho \approx 2{,}485\rho \tag{8.2}$$

Where:

- Q_s is the fire load of the simulation scenario, given in MJ·m^{-2}.
- ρ is the DENSITY (defined in MATL line) of wood, expressed in kg·m^{-3}.

8.2. Simulations plan design

This study tries to reproduce and hence, validate, the results obtained by Generalitat de Catalunya Fire Service (see section 5.1); as well as this institution did, two simulations are carried out for each type of risk level, considering both non ventilated and ventilated (extraction gaps placed according to scheme shown in Figure 5.2). Simulations plan is given in

Table 8.1.

Unfortunately, high computational requirements of FDS and lack of time lead to abandon the iniatial purpose of simulating 5-risk level scenarios, which required more than two months to be simulated if the domain was divided into 8 meshes.

Table 8.1 Summary of simulations plan

	Risk level	Ventilation	Density $Kg \cdot m^3$	Fire load $MJ \cdot m^{-2}$	Simulation Name
LOW	1	No	200	497	I1
	1	Yes	200	497	I2
MEDIUM	3	No	513,15	1275	LM3N
	3	Yes	513,15	1275	LM3V
	4	No	684,2	1700	LM4N
	4	Yes	684,2	1700	LM4V
	5	No	-	3400	LM5N
	5	Yes	-	3400	LM5V

However, excepting two high performance computers available at CERTEC, 8 cores of which were ceded for this project (see section 9.2), used computers had only 4 physical cores, so that simulations (excepting I1 and I2, performed during the beginning of this project) could not be ended. In order to reconduct this drawback, a fire-duration prediction strategy had to be implemented, which is described at next.

Table 8.2 List of simulations performed in order to compare with results obtained by firemen

	Simulation Name	Number of meshes	Simulated time
LOW	I1	8	8000 s[8]
	I2	4	3200 s[8]
MEDIUM	LM3N	4	1128 s[8]
	LM3V	4	714 s[8]
	LM4N	4	Steady state not achieved
	LM4V	8	1920 s[8]
	LM5N	4	Not launched
	LM5V	4	Not launched

8.3. Fire stages within compartment

Simulations representing low risk level scenarios (I1 and I2), which are the only ones that could be completely simulated with FDS, showed both all typical stages of compartment fires described in section 2.4.2 (see Figure 8.1). It is possible to see that when fire initiates, temperatures rise up faster during the first seconds if the room is not ventilated; if smoke is extracted, temperatures are still low enough to permit evacuation during the first half minute; whereas death by thermal burns seem to be assured if the same fire takes place at scenario defined for simulation I2.

However, although fire growth is not as fast during the first seconds when ventilation exists, it has been seen that well mixed scenario appears before if the room is ventilated. It was also observed in simulation I1 that fire revived when door was set to open at t=900 s (when firefighters were supposed to arrive).

Temperatures of smoke layer reach values over 500 ºC, which implies, according to the criterion established by McCaffrey, Quintiere and Harkleroad [10], reaching flashover (generalized combustion along all compartment volume). However, this assumption seems not to apply here, since fires need radiant pannels to spread pyrolysis according to used ignition strategy and therefore, no flashover is spected as not all fuel will burn at the same time.

[8] Simulations launched, but not finished due to lack of material time. As not all simulations could be launched, those were simulated until arriving to steady state.

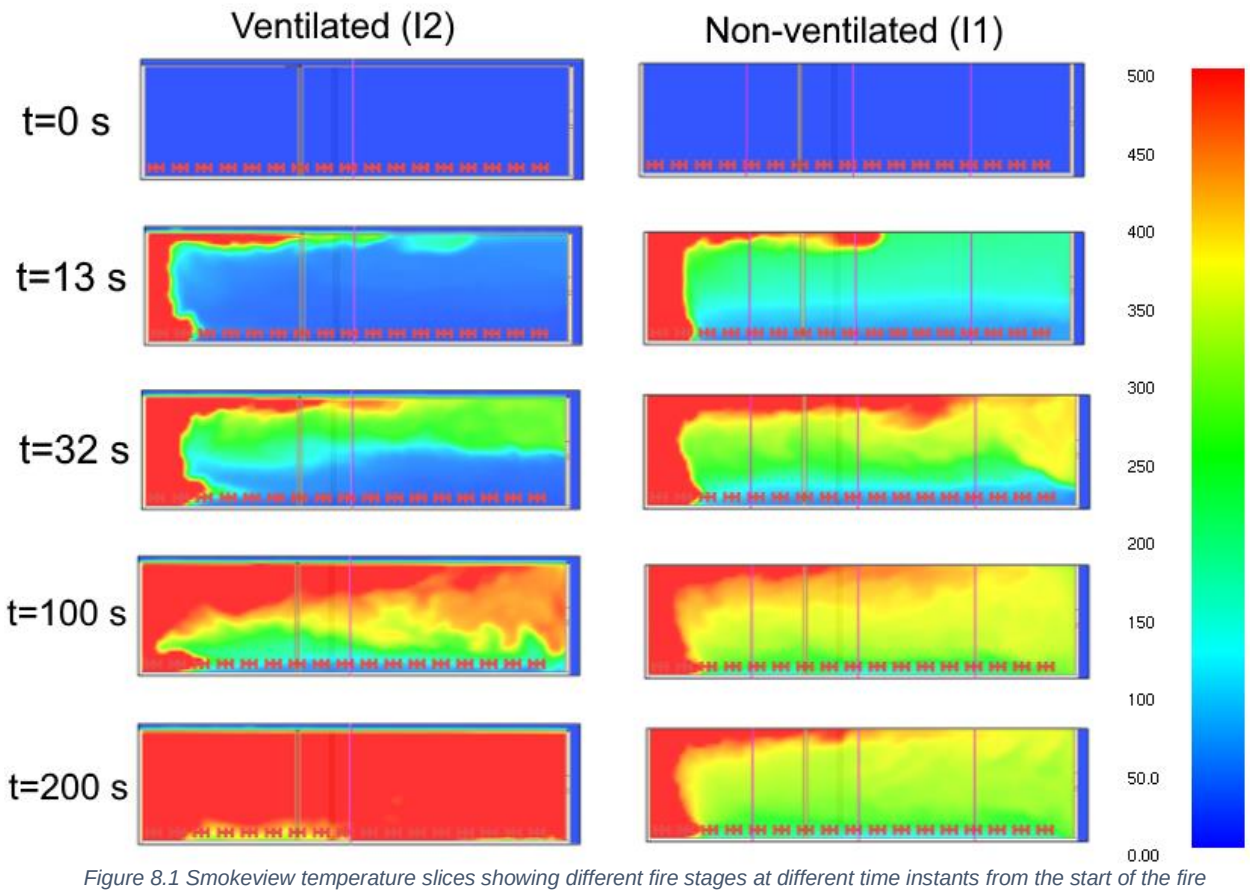

Figure 8.1 Smokeview temperature slices showing different fire stages at different time instants from the start of the fire

Comparison of low-risk scenario Smokeview animation with simulation representing ventilated scenario with risk level 4 (a total of 1920 seconds could be simulated, as a high performance computer was lent for this project during 3 weeks) showed that temperature increase is faster as higher is fire load, although ways of evacuation seem to last smoke free for approximately the same time. This behavior can be shown at Figure 8.2, in which color code is exactly the same as in previous figure.

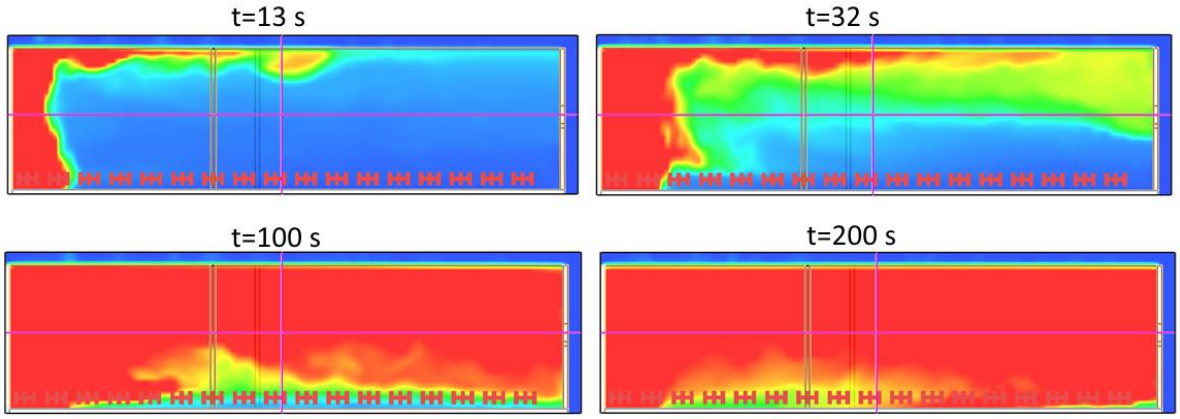

Figure 8.2 Smokeview temperature slices showing different fire stages at different time instants in simulation LM4V

8.4. Fire duration prediction strategy

As just explained, due to hard computational restrictions, simulations could not be completed. Nevertheless, one of the main purposes of this project was to predict the time that structures are exposed to certain temperatures, so that a fire duration prediction strategy had to be implemented.

As seen in figures of previous section, fires grow up until a certain HRR value -which depends only on ventilation and not on fire load, since fires are fuel controlled- and then, a certain steady-state plateau is attained until the fire has released about a 75% of its total energy, when it experiences a slow burnout. This constant scheme permits to establish the hypothesis that once fires achieve the steady state, their HRR and therefore, also the fuel mass loss rate values will be kept invariable with time until the decrease phase (75% of fuel is consumed) starts.

Simulations were launched until fire steady state was reached and had consolidated (about 1200 seconds), in which maximum HRR values (steady state) coincided with those of simulations I1 and I2, representing low risk level scenarios. Then, the data of MLR values obtained through FDS hrr.csv output file was ampliated with new data until the total fuel mass supposed to be consumed equals the integral of MLR vs time function. These new data points are the product of the immediately previous value and a random factor ranging from 0,98 to 1,02, implemented through the Excel function RANDBETWEEN.

This modification was also seized to delete the final peaks result of the ignition strategy implemented in these simulations, delivering the fuel mass corresponding to this peak among different time instants during the fire decreasing phase. The steps followed to eliminate these peaks are described below:

1) The first step is to identify the time instant at which the peak begins and when it ends.All the rows of the MLR column that correspond to the peak are isolated within an empty column.
2) A desired mean mass loss rate must be decided, so the former peak is replaced by it. Normally, it was decided to be the last reasonable MLR value before the peak appeared.
3) The duration time increment of the fire if the mass of the peak was burn together with the rest of the fuel, burnt previously, can be calculated by dividing the total mass of the peak by the desired mean mass loss rate.
4) Dividing the total additional time by the time variation per step will provide the total number of rows that must be added to the MLR column after the fire ended.
5) Each new row must contain the product between the desired mean MLR and a random factor, implemented to the previously mentioned Excel function RANDBETWEEN.
6) If possible, it is interesting to represent fire decay, considering that fire suppression is not immediate. So that, it has been found that a good strategy is to choose the proper time instant the decay period starts at and to multiply at the next step the MLR by a factor of 0,9, which will also be multiplied by this factor, up to the end (MLR=0 kg/s).

The next step to follow in order to get the desired temperature-time curves was to convert MLR values into HRR. Considering that the only varying parameter is fire load (through solid fuel density), and considering, as proven in section 7.1 and checked with the first values (until steady state is attained) of the uncomplete simulations, it was assumed that there were only two HRR vs MLR relationship, for both ventilated and unventilated scenarios. Then, heat release rate vs mass loss rate curves were plotted and regressed (see Figure 8.3).

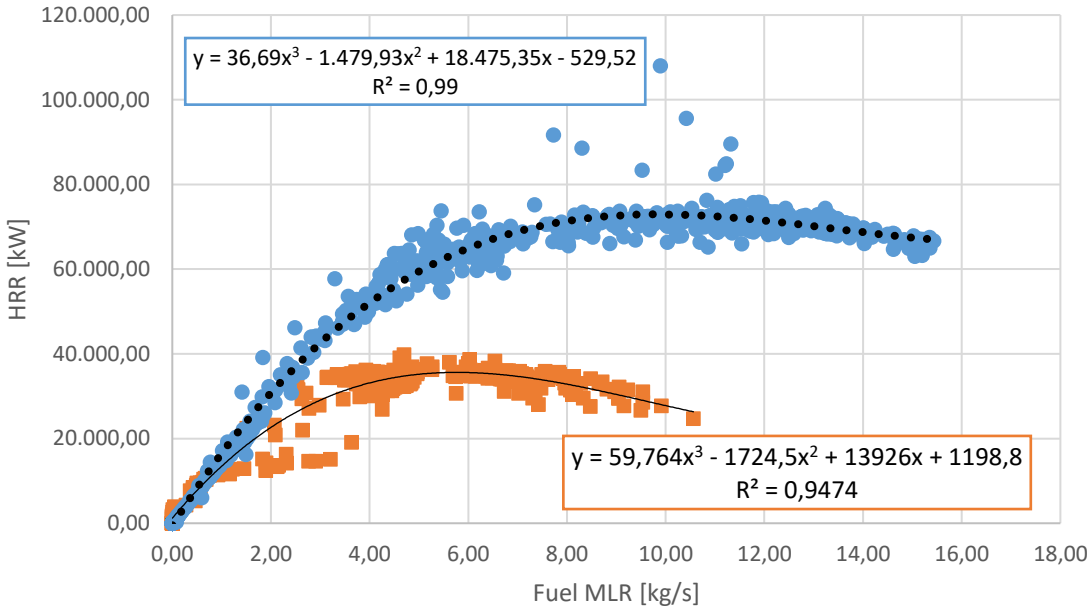

Figure 8.3 HRR vs MLR correlations for ventilated (I2, blue curve) and non-ventilated (I1, orange curve) scenarios

Corresponding heat release rate values are calculated through regression equations indicated in previous figure, obtaining results that fit quite correctly with original HRR curves provided directly by FDS, as can be seen at Figure 8.4 and Figure 8.5, which show, respectively, the direct comparison between I1 and I2 fire growth curves versus those predicted using this strategy directly from MLR data.

Once HRR is known, one can apply MQH correlation (see equation *(2.16)*) in order to obtain theoretical temperature difference between fresh air and smoke layer. Taking geometric parameters of walls and ventilation gaps from the scenario layouts (see Figure 5.1 and Figure 5.2) and Table 5.2, and material properties from Table 6.2, MQH correlation for this particular room.

$$T = 20 + a\dot{Q}^{2/3}t^{1/6} \tag{8.3}$$

Where:

- T is the smoke layer temperature, given in ºC.
- a is a constant whose value is 0,1210 in the case of the ventilated scenario or 0,1468 in the case of the non-ventilated scenario.
- $\dot{Q}$ is the heat release rate, expressed in kW.
- t is the time elapsed since ignition, expressed in seconds.

Assumptions taken in order to establish this particular MQH-based correlation for this specific compartment are that brick and concrete surfaces are thermally thick but sandwich panel is thermally thin, and that, in both ventilated and non-ventilated scenarios, vents are opened just when ignition occurs (t=0 s).

Although equation (8.3) makes a good prediction of steady state temperature values, it can be observed at Figure 8.6 and at results obtained by Generalitat de Catalunya Fire Service that, unlike HRR or MLR, temperature decrement when fire is completely extinguished is fast until a certain value, and from then, temperature decrement becomes slow, especially at low heights, as radiative heat loss (depends on fourth power of temperatures) shrinks considerably and convection is not as fast (see Figure 8.6).

This effect cannot be either better explained through the use of post-flashover smoke layer temperature correlations, since technically no flashover is produced (all fuel does not burn at the same time). Results of non-ventilation scenario suggest that considering fire time a 20% than what provided by calculations could give a good result.

Figure 8.7, however, shows that in the case of ventilated scenario, temperature steady state values predicted by MQH correlation are similar to those calculated by FDS. Nevertheless, as there was a certain amount of fuel that was not ignited until second 2800 (after the previous fire had been extinguished), temperature-time profiles show strange shapes in the case of FDS calculations. Here, it is also observed that temperatures remain high for few minutes after HRR is ceased, which can be explained by the fact that once fire is extinguished, evacuation of hot gases is not immediate. This effect cannot be explained by MQH correlation, since it accounts for the effect of air entrainment during fire steady state, but not for the effect of smoke gases evacuation. Anyway, increasing the time obtained by MQH correlation in 30% will be considered as an apt safety margin.

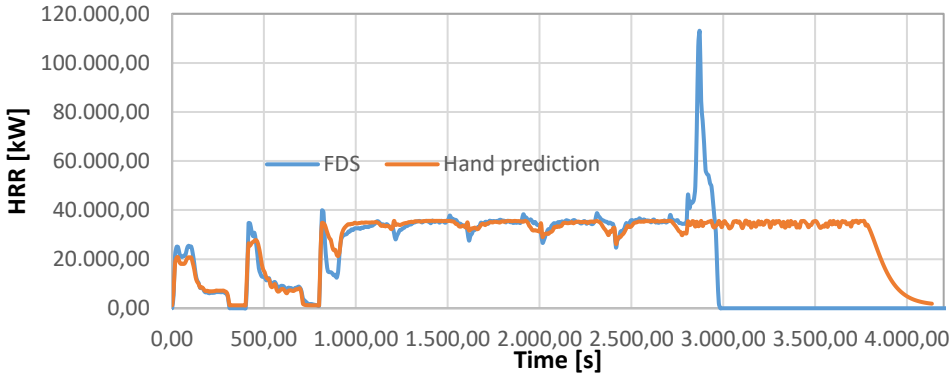

Figure 8.4 Comparison between HRR vs time non-ventilated curve predicted through FDS and through previous correlation

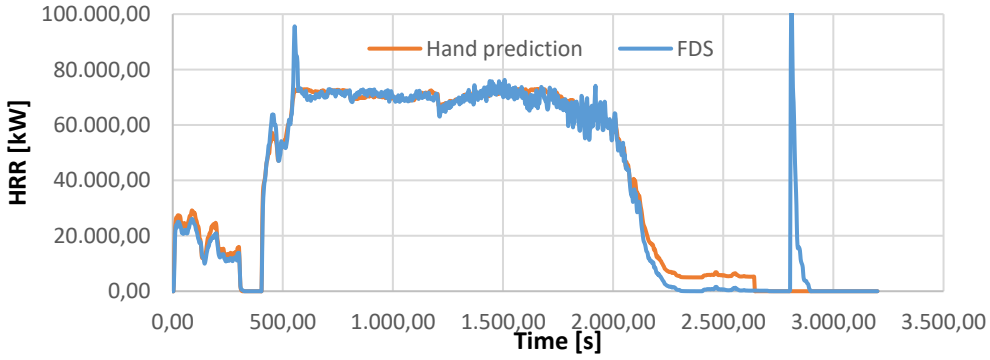

Figure 8.5 Comparison between HRR vs time ventilated curve predicted through FDS and through previous correlation

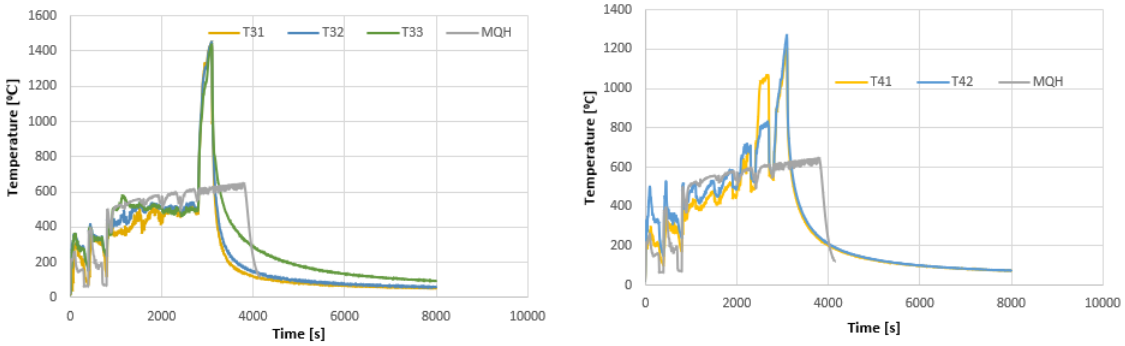

Figure 8.6 Comparison between temperature evolution at different positions FDS and MQH calculated – simulation I1

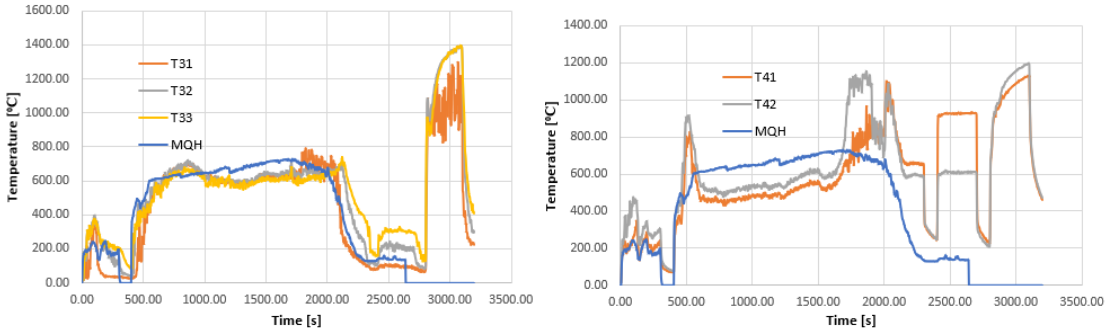

Figure 8.7 Comparison between temperature evolution at different positions FDS and MQH calculated – simulation I2

8.5. Simulations output data

Before proceeding to extrapolation of total fire duration, FDS simulations were carried out in medium risk level fires in order to know how would be fire overall fire behavior at steady state. Results of the incomplete simulations are compared with complete simulations in order to judge the possible effect that fire load variations might cause on FDS steady state predictions.

8.5.1. Intrinsic risk level 3, nonventilated

This simulation, which could be only kept until second 1128, did not show high differences with the case contemplating intrinsic risk level 1 regarding to start of steady state plateau. It is possible to appreciate at Figure 8.8 that the maximum mass loss rate peak values in the ascendant step-shaped curve, which, whereas, are wider in risk level 3 simulation, which agrees with the fact that there is more mass present at the fire scenario.

However, this additional consumption of mass does not seem to be translated into higher HRR values and in fact, it is possible to see that HRR peak at 500 s after ignition that initially appeared at I1 simulation does not occur in LM3N, and in return, HRR does not arrive to be zero when radiant panels are inactive, which seems to be more realistic.

Temperatures (see Figure 8.9) are slightly lower in intrinsic risk level 3 that were in intrinsic risk level 1, at least during first 1128 seconds, time that could be simulated. Anyway, according to results by firemen, it was expected that increasing fire load would increase time that exposition to fire lasts, but not temperature peak values.

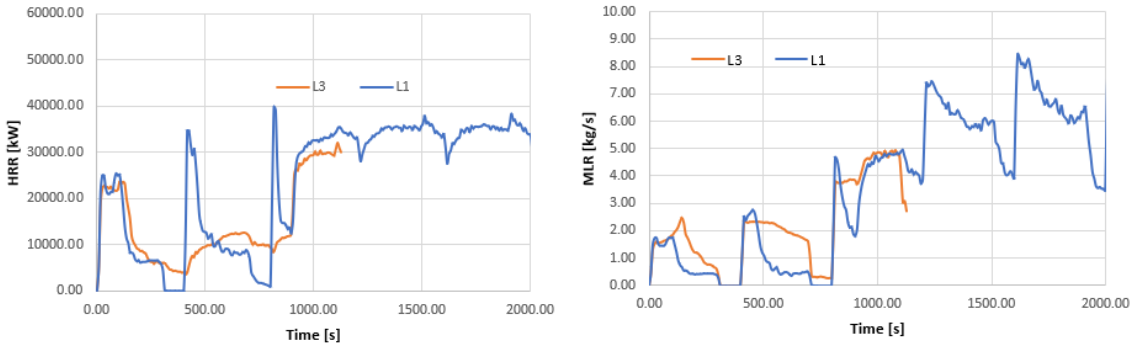

Figure 8.8 HRR time curve (left) and MLR time curve (right) showing LM3N simulation results

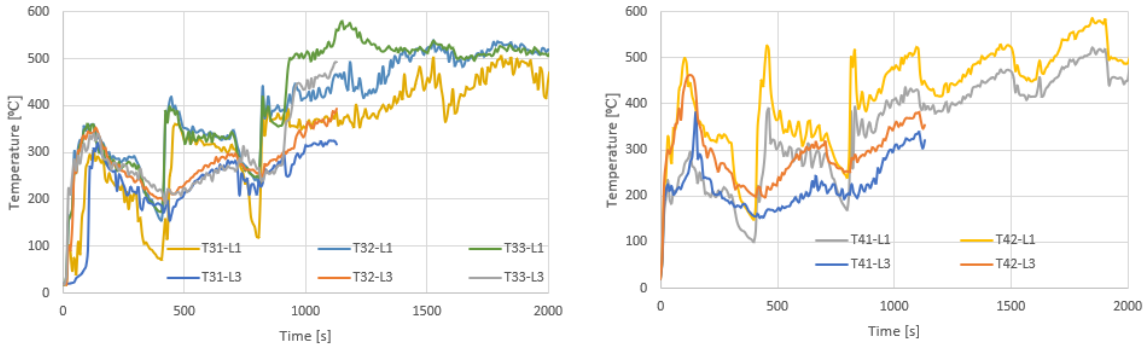

Figure 8.9 Temperatures calculated by FDS for different positions in the case of LM3N simulation

8.5.2. Intrinsic risk level 3, ventilated

This simulation, which could be kept until second 714, at which steady state was supposed to be reached. Although time simulated was too short, it can be seen that up to that time, heat release rate and mass loss rate values are not as large as they were when intrinsic risk level was lower (see Figure 8.10). As there is more fuel inside of the compartment and burning rate seems to be lower, fire duration could be supposed to be larger than expected with simple extrapolation of I2 simulation results. However, and analyzing integral of MLR curve, by second 714, a total of 3022 kg of wood have been burnt in LM3V simulation, while that amount was 2820 kg in the case of I2 simulation, which discards the initial hypothesis of larger duration than expected, and so that, a simple extrapolation as discussed at previous section will be performed.

On the other hand, Figure 8.11 does not show serious differences between 3 and 1 intrinsic risk levels, as both simulations show the same trend; whereas, LM3V simulation shows slightly lower values during the studied time period (0 to 714 seconds).

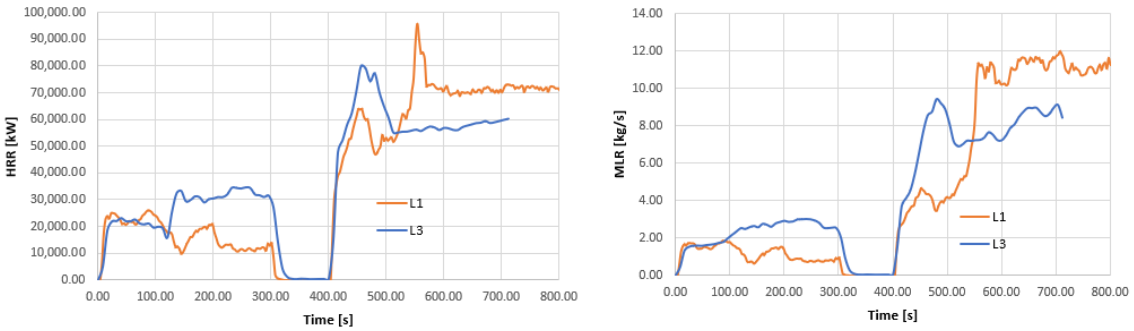

Figure 8.10 HRR time curve (left) and MLR time curve (right) showing LM3V simulation results

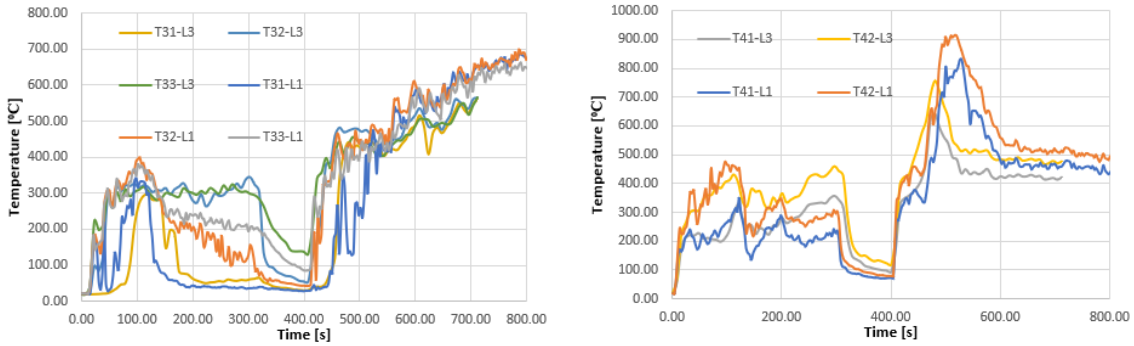

Figure 8.11 Temperatures calculated by FDS for different positions in the case of LM3V simulation

8.5.3. Intrinsic risk level 4, ventilated

In this simulation, while HRR curve (Figure 8.12, left) shows similar heat release values during steady state, MLR curve (Figure 8.12, right), shows a set of steps that correspond to mass peaks at time instants in which radiant panels are switched on, but, these do not seem to be translated into variations at HRR curve. Integrating MLR curve between time instants 0 and 1920 s, a total of 24.026,76 kg were consumed in LM4V simulation, while only 16.218,66 kg were consumed by that time in the case of I2 simulation, which leads to a ratio of 1,48 kg/kg, and then, this will be considered in concern to the prediction of new mass loss rate mean values and expected fire duration. Anyway, this factor is not proportional to fraction of densities (modified parameter in order to change fire load), which is 3,42.

Regarding to temperatures (see Figure 8.13), values predicted at right wall show similar values in both cases of 1 and 4 intrinsic risk levels; however, between seconds 800 and 1800, mean temperature estimation is nearby to 800 ºC in LM4V simulation, whereas it does not practically exceed 600 ºC in the case of I2 simulation. Temperature predictions at back wall do not seem to be significantly different between both simulations.

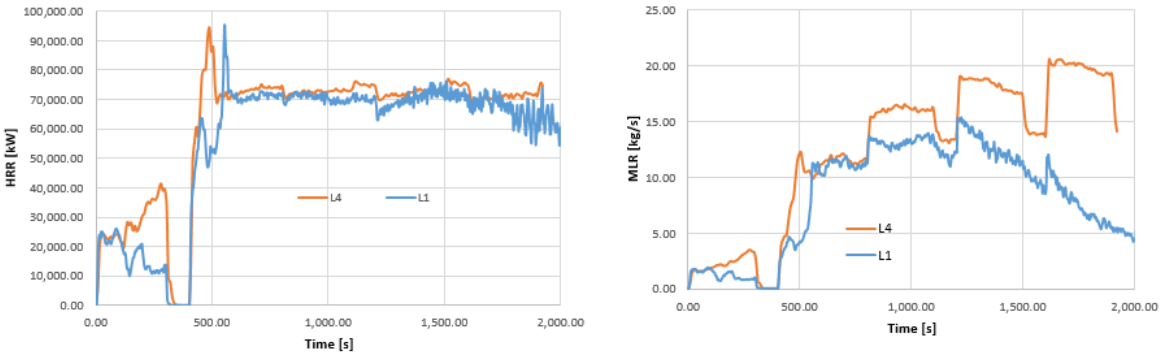

Figure 8.12 HRR time curve (left) and MLR time curve (right) showing LM4V simulation results

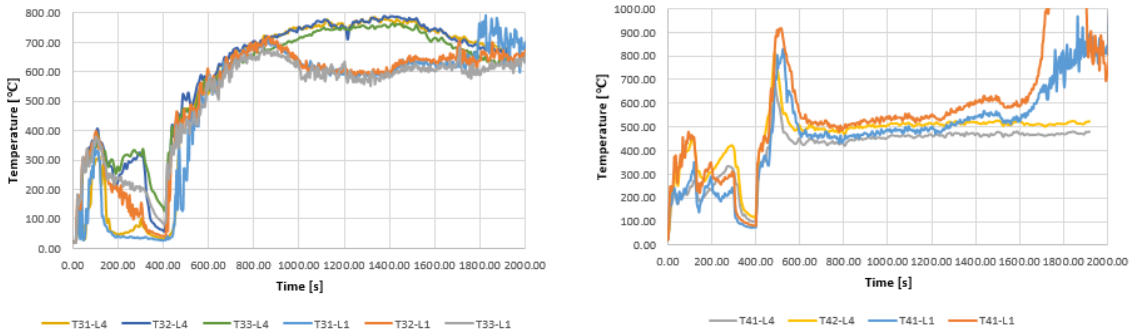

Figure 8.13 Temperatures calculated by FDS for different positions in the case of LM4V simulation

8.6. Results

8.6.1. Low risk level

FDS simulated temperature-time curves can be shown at Figure 8.14 for both non-ventilated and ventilated scenarios. Only temperatures adjacent to structural elements have been included. According to the figure, R90 structures could resist the whole fire in both cases, as temperatures at minute 90 after the fire initiation are practically ambient (under 200 ºC). In the case of ventilated scenario, simulated time is cut at minute 52, but it is supposed that temperatures at high regions will decrease to ambient temperature in less than 38 minutes.

Notice that fire load used in these simulations was 497 $MJ \cdot m^{-2}$, which is much below the upper threshold value for intrinsic risk level 2 (850 $MJ \cdot m^{-2}$), so that is not appropriate in order to assess validity of these results for all types of fire loads. Then, this value will be used in order to judge only intrinsic level 1 scenarios.

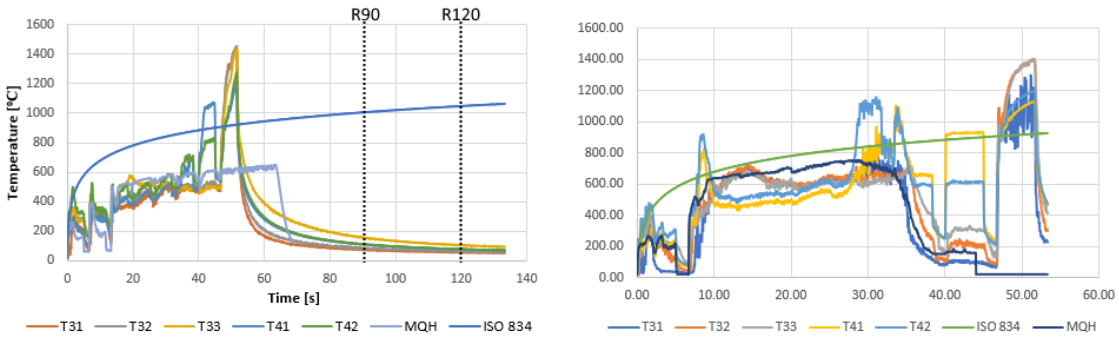

Figure 8.14 Temperature variations with time at different positions for I1 (left) and I2 (right) simulations

8.6.2. Medium risk level – FDS results

As no medium intrinsic level simulations could be finished by simulator, final values as well as simulation time have been predicted, through both MQH (pre-flashover) and Babrauskas (post-flashover) equations, as can be seen at Figure 8.15.

As can be seen, according to this data, setting ventilation would reduce drastically fire duration to the point of reducing it from about 160 min (R180) of duration to nearly 90 min (R90); however, a safety factor of 1,3 has to be applied in order to ensure safe conditions.

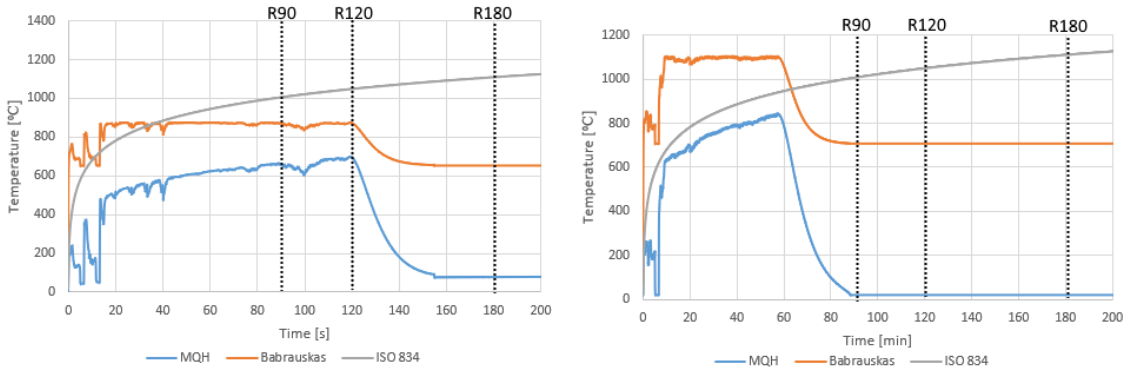

Figure 8.15 Temperature variations with time at different positions for LM3N (left) and LM3V (right) simulations

8.6.3. Summary of results and discussion

Minimum required resistance codes for structures of compartments according to ventilation conditions and intrinsic risk level are summarized at Table 8.3 and

Table 8.4.

Table 8.3 Summary of minimum required fire resistance codes according to intrinsic risk level for non-ventilated scenario

NON-VENTILATED SCENARIO				
	R90	R120	R180	R240
IRL1				
IRL3				
IRL4	Could not be simulated			

Table 8.4 Summary of minimum required fire resistance codes according to intrinsic risk level for ventilated scenario

VENTILATED SCENARIO				
	R90	R120	R180	R240
IRL1				
IRL3				
IRL4				

Results obtained at the study carried out for this project shows overall more permissive scenarios than study by Generalitat de Catalunya Fire Services did, this can be exemplified with the following cases:

- Table 5.4 and Table 5.5 identify, respectively, R90 and R120 structures as not valid in the case of intrinsic risk level 1 when scenario is non-ventilated, while both categories of fire resistant structures would be perfectly valid according to Table 8.3.

- Despite that both Table 8.3 and the pair Table 5.4 and Table 5.5 show R90 and R120 structures as not valid if the compartment is not ventilated, the first one considers R180 structures as a doubtful case while Table 5.6 clearly states that this kind of fire-resistant structure would not be valid for this purpose (if fire is fully developed). In addition, while Table 8.3 considers R240 category as clearly safe, its suitability would be questioned according to Table 5.7.

- In the case of a ventilated compartment, although, both studies consider that structures which can resist fire more than 90 minutes are perfectly appropriate, study by Generalitat de Catalunya Fire Services states that R90, R120 are directly not apt, R180 is doubtfully valid and R240 is wholly valid, while, according to Table 8.4, R90 and R120 structures would be doubtful, and the two others, perfectly valid.

- According to results obtained by Generalitat de Catalunya Fire Service with OZone, structures with fire resistance category R180 or worse would not resist an eventual fire scenario and the last case is unsure, whereas, according to this study, R90 would be the only non-valid type of structure, R120 is doubtful and the other two kinds of structures are perfectly valid.

As results obtained by Generalitat de Catalunya Fire Service are more conservative, these are recommended to be user rather than results obtained in this project in practical applications. Anyway, and despite safety margins taken to ensure more reliable results, the fact that fire duration could not be calculated directly by FDS could have induced serious errors regarding to time that structure is exposed to high temperatures.

Disparity between results obtained by these two studies cannot, validate results obtained by Fire Service, which, however, seem to be more reliable than results obtained by the methodology used here.

9. Project environment

9.1. CERTEC

This project has been performed in cooperation with CERTEC, (*Centre d'Estudis del Risc Tecnològic*) is an organization, founded in 1992, which has as objectives the research and formation of specialists in the field of industrial risk, dividing its activity into four main sections:

- Risk analysis in process industries
- Environmental impact evaluation
- Research on wild fires
- Research on indoor fires

This project can be understand as part of the research on indoor fires section, so that it could be performed at CERTEC facilities, located at 5th floor of I building of EEBE (*Escola d'Enginyeria de Barcelona Est*) which belongs to UPC University (*Universitat Politècnica de Catalunya*), which count on offices, different computational resources and a wide library including different books related to fire science, risk analysis, general science and other disciplines.

9.2. Equipment within CERTEC facilities

CERTEC disposes of two high performance computers specifically designed for running CFD simulations, as well as a large amount of general-purpose office computers that, however, can also be used to carry out simulations if necessary. Summary of CERTEC computational resources inventory is shown at Table 9.1.

Table 9.1 Inventory of computational resources available at CERTEC facilities

Name	Processor	N. Cores	Threads	Memory (GB)	Default OS
Ganimedes	Intel® XEON® E5-2699V4	44	44	256	Win 8 x64
Calisto	Intel® XEON® E5-2680V4	22	22	128	Win 8 x64
Xarxa	Intel® Core™i2 Duo	2	2	NV[9]	Vista x32
CERTEC 20	Intel® Core™i2 vPro™	2	2	NV	Vista x32
CERTEC 29	Intel® Core™i2 vPro™	2	2	NV	Vista x32
CERTEC 31	Intel® Core™i5 - 750	4	4	4	Win 7 x64
CERTEC 32	Intel® Core™i5 - 750	4	4	4	Win 7 x64
CERTEC 33	Intel® Core™i5 - 750	4	4	4	Win 7 x64
CERTEC 41	Intel® Core™i7 - 3770	4	8	16	Win 7 x64
CERTEC 42	Intel® Core™i7 - 3770	4	4	16	Win 7 x64
CERTEC 44	Intel® Core™i7 - 3770	4	4	16	Win 7 x64
CERTEC 45	Intel® Core™i7 - 3770	4	8	16	Win 7 x64
CERTEC 47	Intel® Core™i7 - 3770	4	4	16	Win 7 x64

In addition to these two high performance machines, there are 8 computers reliable to do simulations, as have 64 bits version of Windows 8, which is needed for using more than 4 GB of RAM memory. 5 of these computers have Intel Core i7 processors and the rest, Intel Core i5.

Most of simulations have been carried out with CERTEC 33. This computer, as all simulation-capable computers in CERTEC, counts on FDS v. 6.6.3 installed. From FDS 6 forth, computational time is significantly higher, so *OpenMP* (Multi Processing that allows paralleling internal tasks of FDS if the computer has multiple cores) and *MPI* (Multiple mesh running for a same simulation) strategies had to be followed, so that all cores in the computer were working at the same time. This caused an estimated mean consumption of 90 W.

[9] Not verified.

Unlike the two high performance computers, the rest of machines were not connected to a uninterruptible power supply (UPS), so that many simulations initially launched at CERTEC 33 where interrupted (and the progress was lost) in case of blackouts, which became frequent especially from autumn of year 2017 forth, due to the beginning of construction works for a future students housing next to building I of *EEBE*, where CERTEC facilities are located. This drawback provoked a certain delay in this project, to the point of using a home computer with slightly higher computational capacity that CERTEC 33 in order to launch the last simulations.

9.3. Equipment within home facilities

Despite CERTEC provided a general-purpose office computer with 4 cores and in the case of some simulations, 8 cores of high-performance computers were reserved for this project, frequent blackouts caused a serious delay in the development of this project, so that computational resources lacked to the point of the necessity of using home computer (Medion) to perform more simulations. This home desktop computer, as well to a laptop computer (Lenovo) were used for the redaction of this memory and the execution of minor simulations. Their specifications are summarized at Table 9.2.

Table 9.2 Features of own computers available at home facilities

Brand	Processor	Cores	Threads	Memory (GB)	OS
Medion	Intel® Core™i7 7700	4	8	16	Win 10 x64
Lenovo	Intel® Core™i5 3317U	4	4	8	Win 10 x64

Since simulations are stopped when the computer is shut down and process up to then is lost, the desktop computer performing simulations was connected to an uninterruptible power supply (UPS) unit to prevent progress loss in case of fast blackout. The specifications of this unit are shown at Table 9.3.

Table 9.3 Own UPS unit specifications

Item	Brand	Model	Power consumption
UPS unit	Conceptronic	ZEUS 1200 VA	720 W

Home computer, however, was heated significantly during the performance of simulations, as its internal fan was not powerful enough to beat heat generation. Since CPU cores temperatures reached values over 90 ºC soon, even using only 4 out of all 8 threads (50% CPU), a freeware called *CoreTemp (v. 1.11)* was installed [37]. This software displays on screen data from internal temperature sensors on cores (which are not shown otherwise out of BIOS) as well as mean power consumption on each core (in this case, 64 W at 50% load) and core percentage load; in addition, it allows to define a maximum temperature, that in case to be reached, the computer is shut down or put to sleep. Since FDS, unlike in the case of shutting the computer down, does not lose simulation progress if computer is suspended this option was selected to happen when any core reached 95 ºC (the maximum temperature permitted by cores manufacturer is 100 ºC).

10. Project sustainability study

The environmental impact of this project follows the guidelines indicated in article 7 of Spanish *Ley de Evalución de Impacto Ambiental de Proyectos* [38].

10.1. Project general description

The realization of this project consists on the study of effects caused by ventilation on the behavior of indoor fires, focusing on a certain building studied previously by Generalitat de Catalunya Fire Service and in validating via Fire Dynamics Simulator the results that this institution obtained with another simulator, called Ozone.

10.2. Alternatives study

As this project is completely theoretical, no alternative solutions are expected, excepting the usage of another simulator.

10.3. Work environment description

Most of the simulations performed during this project have been launched through CERTEC computers. However, due to lack of computational resources reserved explicitly for this project, few simulations had to be launched at home computer.

The realization of this project has not modified significantly the environmental quality levels, excepting the social impact related to usage of few CERTEC computational resources, which forced to the rest of PhD and master students performing their projects at CERTEC not to use them as these were dedicated to this project.

10.4. Identification of impacts on environment

10.4.1. Evaluation criteria

Environmental impacts that a project may cause on environment can be provoked by three reasons: due to the existence of the project, due to the usage of resources or due to the generation of waste.

The type of effect of impacts may be positive (the development of the project may provide benefits for the science, the society and the environment) or negative (the project may cause damage in environmental, social, economic and other terms).

According to the incidence degree of an impact, these can be divided into direct and indirect impacts.

Finally, in order to value the magnitude of the valuation of a potential environmental impact, according to its degree of environmental compatibility, these can be classified into the following categories:

- **Compatible EI:** Those for which the environment recuperation is immediate and does not require any protective measure.

- **Moderate EI:** Those for which the environment recuperation does not require any protective measure but recovering the initial environmental conditions may require certain time.

- **Severe EI:** Those for which the recuperation of environmental conditions requires to establish certain protective or corrective measures, in addition to a dilated time.

- **Critical EI:** Those impacts that present a magnitude over the acceptable limit, producing a permanent loss of the environmental conditions quality, without the possibility of recuperation not even with the adoption of protective or corrective measures.

In addition to evaluate the specific impacts of the different cause-effect relations, these are necessary to be valued regarding to project global impact. Global project magnitude will be considered as positive if the global valuation is compatible, moderate or severe, while it will be considered as negative if the global valuation is critical. Impacts caused by project realization are analysed below.

10.4.2. Impact due to project realization

The impact produced by the performance of this project is positive, as working with a simulation tool avoids experimentation with fire, which generates toxic gases product of combustion that are dangerous for health and cause damage to environment.

On the other hand, this study will help to complete the study performed previously by Generalitat de Catalunya Fire Service, in which type A buildings will be able to be dealt as type B establishments, which will suppose an economic save on unnecessary protective measures and in exhaustive technical studies.

10.4.3. Impact due to the usage of resources

There is a direct impact associated to the usage of different resources, especially office material, paper and printer ink. The management of the different wastes is performed according what the normative provided by *Agència Catalana de Residus* requires; then, paper wastes must be deposited into blue containers, printer ink must be taken to a specialized recycling plant and the office material must be thrown into the yellow container of separate collection.

10.4.4. Impact due to emissions

Although this project has not directly generated contaminating matter, there is an indirect impact related to the usage of electric energy, which is produced at thermoelectric centrals, generally using a combined cycle (including both Brayton and Rankine cycles), that consumes coal or other fossil fuel and, hence, emits combustion gases. The main contaminant product of the combustion of natural gas is carbon dioxide (CO_2), responsible of greenhouse effect.

Simulations scheduling, shown at Gantt diagram and summary of simulation times (see Table 12.1) manifested total number of hours that each computer dedicated to simulate; so that once powers were known, total consumptions were calculated. Summary of that data is shown at Table 10.1.

Table 10.1 Data regarding computational energy cost associated to the performance of this project.

Computer	Simulation hours	CPU load	Mean consumption [W]	Energy cost [Wh]

CERTEC 33	1690+960[10]	100%	184 [39]	487.600
Calisto	277	36,4%	140,74 [40]	38.985
Ganimedes	453	18,2%	98,73 [40]	44.725
Home computer	1262	50%	64[11]	80.768
TOTAL		**-**	**-**	**652.078**

Then, the total consumption of energy associated to this project (neglecting the amount consumed by laptop computer and small simulations) is 652,078 kWh.

Emission of CO_2 per produced kWh ratio that OCCC recommends to use at Iberian Peninsula for year 2017 (latest published data) is 0,392 kg CO_2/kWh [41]. As an approximation, is it possible to consider that all the produced energy is consumed (there are no loses in energy transport); then, the total mass of emitted CO_2 due to the performance of this project is 255,61 kg of CO_2.

10.4.5. Impacts valuation

All impacts derived from this project can be classified as compatible impacts and, therefore, the global impact associated to the whole project too, regarding the predicted corrective measures, which are detailed in next section.

10.4.6. Predicted measures

The predicted corrective measures in order to minimize the impact of this project on environment are centred basically in the management of the generated waste (paper notations, empty printer cartridges, etc.). Moreover, will it be tried to minimize the consumption of these resources by using documents in electronic format when it is possible and by printing documents by the both sides.

[10] Approximately, 960 hours were lost in simulations that could be not completed due to blackouts and that therefore, were not productive.
[11] Mean power consumption shown by CoreTemp software.

11. Project costs study

All the expenses produced during the realization of this project are classified into two categories: the cost associated to the consumption of material resources and the cost associated to human resources.

The total cost of the project is 7.556,55 €. Apportionment of costs is detailed below.

11.1. Human resources cost

This project has been performed by a master student with a graduate on chemical engineering, which, in addition, is working as a junior risk analyst in a chemical factory. The level of studies of a junior engineer fits within professional category nº 6, according to Chemical Industry General Agreement in Spain [42], which are granted with a minimum salary of 24814,26 € per year. Supposing 1691 hours of work per year [43], this makes 14,674 € per working hour, which can be rounded to 15 €. The average week active dedication to the project has been of 30 hours during a total of 14 weeks, which makes a total of 420 hours.

This project has been tutorized by a CERTEC ascribed professor which is PhD on engineering and has been supported by a PhD student at CERTEC. This professor, who has dedicated an average of half hour per week to this project (during approximately 14 weeks), is supposed to receive a wage of 60 € per hour, as a consulting agent.

In addition to the professor, this project has also been directed by a PhD student (researcher), who has lent assistance, especially regarding FDS-related questions, who has dedicated an average hour per week to this project and is supposed to receive a wage of 30 € per working hour.
Summary of personnel costs are detailed in Table 11.1.

Table 11.1 Summary of costs of human resources

Person	Cost per hour (€/h)	Dedicated hours	Total cost
Junior engineer	15	420	6.300 €
Doctor on engineering	60	7	420 €
Researcher	30	14	420 €
TOTAL COST	**-**	**-**	**7.140** €

11.2. Material resources cost

Material resources total cost is estimated to be 522,35 €. This cost can be divided into three different concepts:

- Computational resources: 354,50 €
- Office material: 87,00 €
- Electricity: 80,85 €

Each type of cost will be better explained in its corresponding section below. Notice that no rental cost has been considered, as this project has been developed with the help of computers present at CERTEC premises, the use of which was allowed by free, as well in personal home. No

transport cost has been considered either, as there were no visits to third companies or institutions related to the composition of this project.

11.2.1. Computational resources cost

No special computers or software licenses were bought explicitly for this project. However, amortization cost as a consequence of the use of different computers and the UPS unit must be considered. Amortization cost for all used equipment is 248,7 €, the apportionment of which is summarized at Table 11.2.

Table 11.2 Summary of all contributions to total amortization cost

Apparatus	Acquisition cost	Service life	Use during the project	Amortization
CERTEC 33	800 €	7 years / 84 months	10 months (11,9%)	95,2 €
Ganimedes	7.500 €	7 years / 84 months	2 months (2,4%)	180,0 €
Calisto	3.500 €	7 years / 84 months	1 month (1,2%)	42,0 €
Home computer	1.300 €	7 years / 84 months	2 months (2,4%)	31,2 €
Home UPS	110 €	3 years / 36 months	2 months (5,55%)	6,1 €
TOTAL	**-**	**-**	**-**	**354,5 €**

11.2.2. Office material cost

This cost is constituted by the expense derived of manual writing consumables (in the case of this project, a notebook the cost of which was 5 € and a pen which costed 2 €), but, cost associated to printing and binding this project is also inputted here, which is supposed to cost about 80 €. Then, the total cost due to office material would be of 87 €.

11.2.3. Electricity cost

A non-neglectable cost that must be considered in the elaboration of the budget is that associated to electrical consumption required for simulations, which was already estimated to be 652,08 kWh at section 10.4.4. Considering only the variable component on electric bill, which is supposed to be 0,123988 €/kWh [44], the total cost due to consumption of electricity in order to simulate would be of 80,85 €.

12. Project planning

The idea of performing a project in cooperation with CERTEC has been present since the development of a previous work with the help of this institution, which was finished in January 2015. Anyway, it is possible to consider the first day of project the day March 2nd 2017, when the first simulation was launched at CERTEC facilities.

First months of project were characterized by simulations launched through Ganimedes (high performance computer), while in parallel, small simulations were carried out using CERTEC 33 computer, and also a bibliographic research was conducted, in order to gather information about compartment fires, applicable legislation, FDS guides and especially, previous study by Illa.

However, the memory of the project was not begun to be written until a year later, at February 2018, when at least study of ventilation effect on fire features within compartment was finished.

12.1. Simulations scheduling

Simulations have been carried out through different computers since first simulation was launched in Ganimedes March 2nd 2017 until last simulation, finished at home computer at April 30th 2018. Simulation list is given at Table 12.1.

Table 12.1 List of large-scale simulations performed during this project

Simulation	Simulation began at	Simulation finished at	Discarded[12]	Computer
HX1	March 2, 2017 18:26:10	March 7, 2017 16:55:36	No	Ganimedes
HX2	March 7, 2017 17:03:28	March 13, 2017 19:10:35	No	Ganimedes
I1	March 31, 2017 15:28:41	April 8, 2017 12:30:02	No	Ganimedes
I2	May 11, 2017 19:22:34	May 27, 2017 23:07:20	No	CERTEC 33
I3	May 30, 2017 17:26:12	June 11, 2017 01:28:35	No	CERTEC 33
I4	July 19, 2017 10:02:40	July 29, 2017 02:58:14	No	CERTEC 33
I5	September 20, 2017 19:15:17	October 9, 2017 02:08:28	No	CERTEC 33
I6	November 15, 2017 19:17:55	December 3, 2017 09:19:34	Yes	CERTEC 33
J2*	December 3, 2017 09:20:09	December 13, 2017 04:19:07	Yes	CERTEC 33
J3*	January 8, 2018 18:51:54	January 18, 2018 09:48:40	Yes	CERTEC 33
J2	January 25, 2018 13:10:33	February 9, 2018 11:02:43	No	CERTEC 33
K2	March 2, 2018 19:21:19	March 11, 2018 05:56:10	No	Home
K3	March 3, 2018 19:17:55	March 4, 2018 08:14:44	Yes	CERTEC 33
KX	March 14, 2018 19:22:17	March 20, 2018 20:50:32	No	Home
LM3V	April 6, 2018 18:42:38	April 15, 2018 16:55:44	No	Home
LM3N	March 22, 2018 18:56:53	April 5, 2018 21:33:45	No	Home
LM4V	March 21, 2018 09:15:20	April 13, 2018 09:52:14	No	Calisto
LM4N	April 13, 2018 12:35:51	April 29, 2018 22:50:12	Yes	Home

[12] Some simulations had to be discarded due to different causes, such as insufficient simulated time or mistaken geometry.

In addition, work load of computers can be better visualized at Gantt diagrams, showed from Figure 12.1 to Figure 12.6.

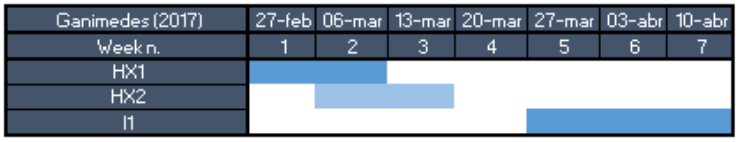

Figure 12.1 Gantt diagram showing simulations schedule at Ganimedes

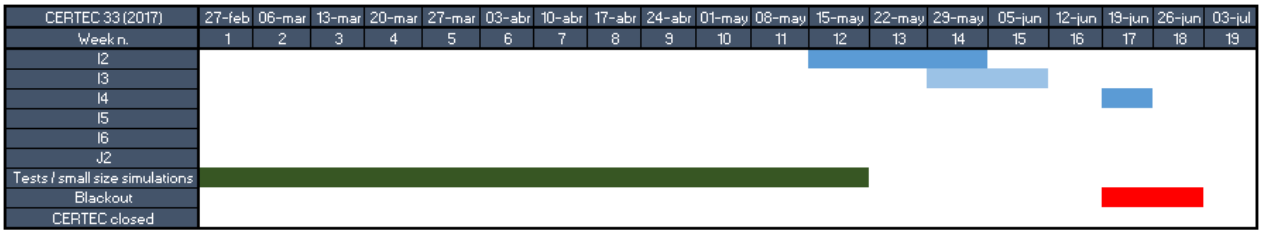

Figure 12.2 Gantt diagram showing simulations schedule at CERTEC 33 (1/4)

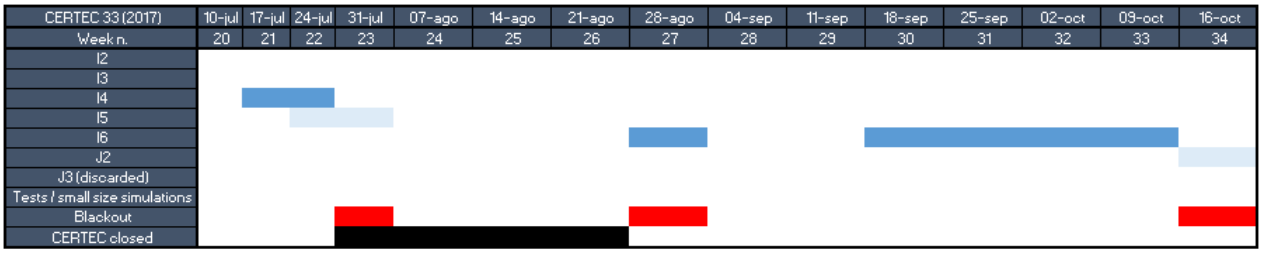

Figure 12.3 Gantt diagram showing simulations schedule at CERTEC 33 (2/4)

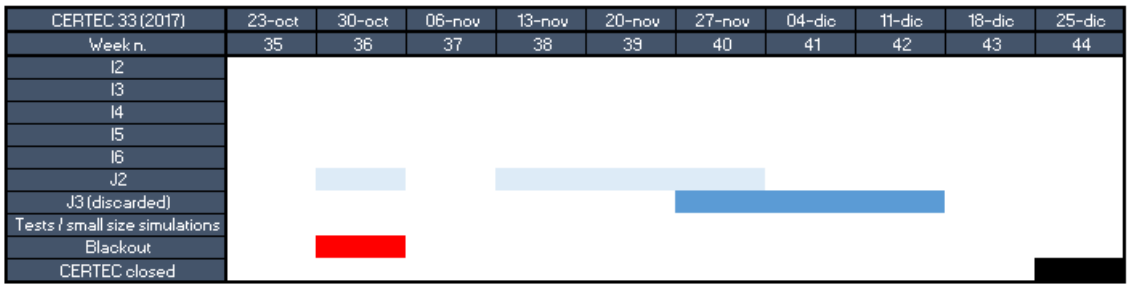

Figure 12.4 Gantt diagram showing simulations schedule at CERTEC 33 (3/4)

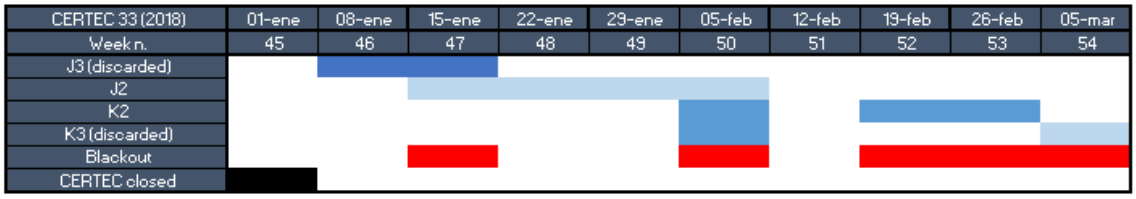

Figure 12.5 Gantt diagram showing simulations schedule at CERTEC 33 (4/4)

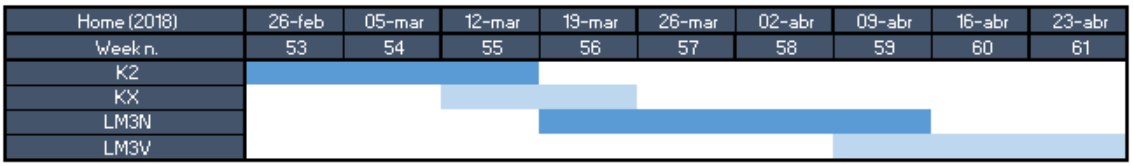

Figure 12.6 Gantt diagram showing simulations schedule at home computer

13. Conclusions

Various conclusions can be detached from the set of studies performed during this project.

- Compartment fires represented by simulations may be considered as ventilation controlled. While adding ventilation gaps with larger size or in a higher amount decreases significantly fire exposition time without increasing mean registered temperatures at structure in the same proportion, it has been observed that the spatial distribution of these extraction gaps does not seem to cause signification effect on fire effects on structure.

- In the case of ventilation controlled indoor fires, it is preferable regarding to structure integrity that, whenever possible the compartment are well ventilated. However, this could be in conflict with evacuation-related requirements, as higher heat release rate and, therefore, toxic species generation and radiative power will be reached, which is directly related to personal safety if evacuation is not immediate (providing compartment with ventilation helps to delay propagation of smoke layer to the floor for some seconds). In order to deal with this drawback, some additional measures, not studied during this project, are recommended to be set if ventilation level is planned to be increased.

- Besides of the effect of ventilation gaps size, it has been observed that if ventilation surface is maintained but divided into many different openings, results do not vary significantly from other scenarios in which openings are distributed following different patterns. Then, quenching effect due to higher pressure loss if ventilation gaps are smaller will not be expected.

- In order to evaluate the effects that increment on ventilation level has on fire features, a proper combined pyrolysis + ignition strategy should be implemented in FDS, which could not be achieved in this project despite of various attempts. It could not be checked if flashover could occur within this compartment at different ventilation levels or fire load; while different fire stages could be identified by analysing temperature slices of Smokeview animations and flashover temperature criterion was fulfilled at the centre of the domain, it did not actually occur if radiant panels were not on at regions which could be theoretically at flashover. However, ignition strategy developed by Illa with the help of radiant panels has allowed to see general steady state behaviour of fires and relative effects caused by varying other variables, despite not modelling properly mass loss rates, fire extinction and temperatures at façade.

- FDS performed good predictions at right wall (party wall), while not as much satisfactory results were obtained for façade wall. However, these first showed good agreement with results obtained by Generalitat de Catalunya Fire Service, and therefore, are recommended to be used as reference when fire effect on structural integrity is studied.

- It has been seen that strategy followed to extrapolate simulation points that could not be calculated by FDS, using MQH equation, could bring to underestimate the length of the fire. This can be explained remitting to the fact that MQH model considers a heat

generating factor, which depends on HRR and a heat evacuation factor, which depends on walls overall heat transfer coefficient; however, it does not account on time required for the complete evacuation of hot gases when the fire is extinguished, which are still hot enough to provoke damages to structures. This drawback has tried to be solved by multiplying time duration according to prediction by additional safety factors of 30%, although even multiplied by 1,3, fire durations seemed to be underestimated. As modelling the hot gases total mass change with time was difficult, agreement of results by Beyler equation could not be tested. Notice that Babrauskas model for post-flashover scenarios keeps temperatures after fire high at a constant value, which does not help to estimate time that structures are exposed to fire.

- FDS high computational requirements have not allowed to finish all desired simulations, so that results of non-simulated points had to be estimated through hand correlations, as zone models based software do. When simulating with FDS, powerful CPUs with large number of cores are obviously needed in order to launch simulations in parallel, but counting on good fans is also required, as this simulator occupies practically all the memory of the computer, causing it to be heated. All these requirements may lead to high prices for optimal simulation-dedicated computers but, in addition, it must be also considered that computer must be provided with an enough powerful UPS unit, as simulation progress is completely lost if computer is shut down. It must be mentioned that this project would not have been delayed by so much time if blackouts had not occurred.

- When simulating natural ventilation effect on compartment fires with the aim of evaluating affectation to structure it is more recommendable to use zone models, as FDS provides practically the same results with additional *Smokeview* animations that show hydrodynamic behaviour of smoke and gases, which, although could be interesting in the case of forced ventilation, is not worthy to be obtained at the cost of months of simulation in the present case.

- Discrepancy between results of study performed by Generalitat de Catalunya Fire Services and those obtained in this project cannot validate results obtained previously by the previously mentioned institution. However, since these first are more restrictive than results of this project, tables provided by Fire Services are preferred to be used rather than those provided in this project.

14. Bibliography

[1] A. Illa, "Validació d'un catàleg d'escenaris d'incendi en naus industrials mitjançant l'eina de simulació FDS," Barcelona, 2016.

[2] A. S. Hornby and S. Wehmeier, *Oxford advanced learner's dictionary*, Oxford Uni. Oxford: Oxford University Press, 1995.

[3] J. J. Quintiere, *Fundamentals of fire phenomena*, First edit. London: John Wiley & Sons, 2006.

[4] National Fire Protection Association, *SFPE Handbook of Fire Protection Engineering*, 3rd ed. Quincy, MA, 2002.

[5] B. Karlsson and J. Quintiere, *Enclosure fire dynamics*. Boca Raton, FL: CRC Press, 1999.

[6] C. Huggett, "Estimation of rate of heat release by means of oxygen consumption measurements," *Fire Mater.*, vol. 4, no. 2, pp. 61–65, Jun. 1980.

[7] B. G. Heskestad, "Dynamics of the fire plume," *Philos. Trans. R. Soc. A Math. Phys. Eng. Sci.*, vol. 356, pp. 2815–2833, 1998.

[8] G. Y. Wu and R. C. Chen, "The analysis of the natural smoke filling times in an atrium," *J. Combust.*, vol. 2010, 2010.

[9] R. J. Schaal, "A Users Guide for the CFI Calculator and Fire Dynamics Equations," CFITrainer.net Steering Committee, Crofton, MD.

[10] B. J. McCaffrey, J. G. Quintiere, and M. F. Harkleroad, "Estimating room temperature and the likelihood of flashover using fire test data correlations.pdf," *Fire Technol.*, vol. 17, no. 2, pp. 98–119, 1981.

[11] A. Björklund, "Risks in using CFD-codes for analytical fire-based design in buildings with a focus on FDS : s handling of under-ventilated fires," 2009.

[12] J. E. Floyd, K. B. McGrattan, S. Hostikka, and H. R. Baum, "CFD Fire Simulation Using Mixture Fraction Combustion and Finite Volume Radiative Heat Transfer," *J. Fire Prot. Eng.*, vol. 13, no. February 2003, pp. 11–36, 2003.

[13] J. G. Nielsen, "Validation Study of Fire Dynamics Simulator," Aalborg University, 2013.

[14] K. McGrattan, S. Hostikka, R. McDermott, J. Floyd, C. Weinschenk, and K. Overholt, "FDS Technical Reference Guide Volume 2 : Configuration Management," vol. 1, pp. 1–147, 2015.

[15] R. Mcdermott, K. Mcgrattan, and J. Floyd, "A Simple Reaction Time Scale for Under-Resolved Fire Dynamics," pp. 809–820, 2011.

[16] J. X. Wen, K. Kang, T. Donchev, and J. M. Karwatzki, "Validation of FDS for the prediction of medium-scale pool fires," *Fire Saf. J.*, vol. 42, no. 2, pp. 127–138, 2007.

[17] K. B. McGrattan, S. Hostikka, J. E. Floyd, and R. McDermott, "Fire Dynamics Simulator, Technical Reference Guide, Volume 1: Mathematical model," vol. 3, no. 1018, 2014.

[18] K. Mcgrattan and R. Mcdermott, "Sixth Edition Fire Dynamics Simulator User ' s Guide," 2015.

[19] J. W. Deardorff, "Stratocumulus-capped mixed layers derived from a three-dimensional

model," *Boundary-Layer Meteorol.*, vol. 18, no. 4, pp. 495–527, 1980.

[20] K. McGrattan, S. Hostikka, R. McDermott, J. Floyd, C. Weinschenk, and K. Overholt, "FDS User's Guide," 2004.

[21] J. W. Kwon, N. a. Dembsey, and C. W. Lautenberger, "Evaluation of FDS V.4: Upward flame spread," *Fire Technol.*, vol. 43, no. 4, pp. 255–284, 2007.

[22] R. Fernández Becerra, "Desarrollo de las normas contra incendios en españa," *Cercha*, pp. 56–62, 2009.

[23] Gobierno de España, "Real Decreto 312/2005, de 18 de marzo, por el que se aprueba la clasificación de los productos de construcción y de los elementos constructivos en función de sus propiedades de reacción y de resistencia frente al fuego," *Boe*, vol. 79, no. 5271, pp. 11318–11348, 2005.

[24] X. Cemeli Duran, "Resistencia al fuego, requerimientos normativos y sectorización fija," in *Protección*, First Edit., C. d'Enginyers G. i E. T. I. de Barcelona, Ed. Barcelona, 2016.

[25] S. González García, "NTP 200: Estructuras metálicas: comportamiento frente al fuego (I)," no. I. Instituto Nacional de Seguridad e Higiene en el Trabajo, Toledo.

[26] J. Zehfuss and D. Hosser, "A parametric natural fire model for the structural fire design of multi-storey buildings," *Fire Saf. J.*, vol. 42, no. 2, pp. 115–126, 2007.

[27] J. Gallart, A. Gonzàlez, and E. Caimel, "Anàlisi d'un incendi en una nau industrial a Gavà. Conclusions per a l'aplicació del RSCIEI en naus de tipus A en horitzontal.," Barcelona, 2012.

[28] L. M. Clavera, "Estabilidad al fuego. Protección estructural," in *Colección de Fichas de Seguridad Contra Incendios*, First edit., vol. Protección, Col·legi d'Enginyers Graduats i Enginyers Tècnics Industrials de Barcelona, Ed. Barcelona: Col·legi d'Enginyers Graduats i Enginyers Tècnics Industrials de Barcelona, 2016.

[29] Ministerio de Fomento, "Documento Básico de Seguridad en caso de Incendio Documento, con modificaciones del RD 173/2010 señaladas," *Cte*, vol. 2013, pp. 1–129, 2010.

[30] Q. Nie, C. Zhou, X. Shu, Q. He, and B. Huang, "Chemical, mechanical, and durability properties of concrete with local mineral admixtures under sulfate environment in Northwest China," *Materials (Basel).*, vol. 7, no. 5, pp. 3772–3785, 2014.

[31] Gobierno de España, *Reglamento de Seguridad Contra Incendios en los Establecimientos Industriales*. Spain, 2004, pp. 39355–39357.

[32] Direcció General de Prevenció Extinció d'Incendis i Salvaments. Departament d'Interior, *SP119: Determinació de la configuració dels establiments industrials*. Catalonia: Generalitat de Catalunya, 2009, pp. 2168–2176.

[33] M. Xampeny, *El Reglament de seguretat contra incendis en els establiments industrials (RSCIEI) Mòdul : Tècnic d'incendis Nivell Bàsic*. 2015.

[34] Á. Fernández de Castro Díaz, *Sistemas de control de temperaturas y evacuación de humos de incendio*. Madrid, Spain: Instituto Nacional de Seguridad e Higiene en el Trabajo, 2012, pp. 3–8.

[35] Tecnifuego AESPI and Asociación Española de Normalización y Certificación, "Fire safety. Smoke and heat control systems. Requirements, calculation and design methods for

temperature control systems and smoke exhaust systems projecting in case of fire.," Madrid, Spain, 2017.

[36] VTT Technical Research Centre of Finland Ltd, "Innovative eco-efficient high fire performance wood products for demanding applications." [Online]. Available: http://virtual.vtt.fi/virtual/innofirewood/stateoftheart/database/burning/burning.html. [Accessed: 22-Mar-2018].

[37] A. Liberman, "CoreTemp," 2017. [Online]. Available: http://www.alcpu.com/CoreTemp/. [Accessed: 01-Mar-2018].

[38] Ministerio de Agricultura Alimentación y Medio Ambiente, "Ley 21/2013, de 9 de diciembre, de evaluación ambiental," *Boe*, vol. 296, no. 12913, pp. 98151–98227, 2013.

[39] A. Lal Shimpi, "Intel's Core i7 870 & i5 750, Lynnfield: Harder, Better, Faster Stronger," 2009. [Online]. Available: https://www.anandtech.com/show/2832/17. [Accessed: 11-Apr-2018].

[40] P. Alcorn, "Power consumption - Intel Xeon E5-2600 v4 Broadwell-EP Review," 2016. [Online]. Available: http://www.tomshardware.com/reviews/intel-xeon-e5-2600-v4-broadwell-ep,4514-8.html. [Accessed: 11-Apr-2018].

[41] Oficina Catalana del Canvi Climàtic, "Guia pràctica per al càlcul d'emissions de gasos amb efecte d'hivernacle (GEH)." Generalitat de Catalunya, Barcelona, pp. 0–101, 2018.

[42] Ministerio de Empleo y Seguridad Social, *Boletín oficial del estado*. Spain, 2015, pp. 60502–60511.

[43] J. M. Abad Liñán, "¿Cuántas horas se trabaja en España? Estos son los países que dedican más tiempo al trabajo," *El País*, Madrid, 13-Dec-2016.

[44] Iberdrola, "Condiciones particulares. Plan estable," 2018. [Online]. Available: https://www.iberdrola.es/webclipb/gc/prod/es_ES/planes/docs/plan_estable.pdf. [Accessed: 13-Apr-2018].

A) Post-flashover method to predict smoke layer temperature

As mentioned in different occasions during the body of the project, Babrauskas suggested a method for the prediction of temperatures at smoke layer after the declaration of flashover [4].

This author considered that after a flashover, temperature at room would depend on five parameters:

- Burning rate stoichiometry, represented with factor θ_1.
- Wall steady-state losses, represented with factor θ_2.
- Wall transient losses, represented with factor θ_3.
- Opening height effect, represented with factor θ_4.
- Combustion efficiency, represented with factor θ_5.

Once all these efficiency parameters have been computed, smoke layer temperature can be found according to equation (A.1).

$$T_g = T_o + (1725 - T_o)\theta_1\theta_2\theta_3\theta_4\theta_5 \quad \text{(A.1)}$$

Where T_g stands for smoke layer temperature and T_o for ambient temperature, which must be expressed in K.

A1. Burning rate stoichiometry

Burning rate stoichiometry can be well defined according to dimensionless stoichiometric coefficient, which can be understand as the fraction between fuel mass pyrolysis rate and the stoichiometric mass burning rate. However, this ratio can be equivalently defined according to equation (A.2).

$$\phi = \frac{\dot{Q}}{1500 \sum_{i=1}^{N} A_{v,i}\sqrt{H_{v,i}}} \quad \text{(A.2)}$$

Where:

- $\dot{Q}$ is total heat release rate, expressed in kW.
- $A_{v,i}$ is total ventilation area, expressed in m.
- $H_{v,i}$ is height of ventilation gaps, expressed in m.

According to the value of this ratio, burning rate stoichiometry factor is calculated as shown by equation (A.3).

$$\theta_1 = \begin{cases} 1 + 0{,}51\phi, & \phi < 1 \\ 1 - 0{,}05 \ln \phi\,, & \phi \geq 1 \end{cases} \quad \text{(A.3)}$$

A2. Wall steady-state losses

Wall steady-state losses are represented by a factor the value of which, as expected, does not vary over simulation time. It is defined according to equation (A.4).

$$\theta_2 = 1 - 0{,}94exp\left[-54\left(\frac{1}{A_T}\sum_{i=1}^{N} A_{v,i}\sqrt{H_{v,i}}\right)^{2/3}\left(\sum_{i=1}^{N}\frac{A_i}{A_T}\frac{\delta_i}{k_i}\right)^{1/3}\right] \quad \text{(A.4)}$$

Where:

- k_i is the wall material thermal conductivity of i[th] compartment external surface, expressed in kW·m^{-1}·K^{-1}.
- δ_i is the wall thickness of i[th] compartment external surface, expressed in m.

A3. Wall transient losses

Unlike steady-state losses, transient losses are represented by a factor the value of which depends on time instant at which it is evaluated, according to equation (A.5).

$$\theta_3 = 1 - 0{,}92exp\left[-150\left(\frac{1}{A_T}\sum_{i=1}^{N} A_{v,i}\sqrt{H_{v,i}}\right)^{0.6}\left(t\sum_{i=1}^{N}\frac{A_i}{A_T}\frac{1}{k_i\rho_i C_i}\right)^{1/3}\right] \quad (A.5)$$

Where:

- ρ_i is the wall material density of i[th] compartment external surface, expressed in kg·m^{-3}.
- C_i is the wall material specific heat of i[th] compartment external surface, expressed in kJ·kg^{-1}·K^{-1}.
- t is the time elapsed since ignition, expressed in seconds.

A4. Opening height effect

This factor accounts for the fact that a same $A_{v,i}\sqrt{H_{v,i}}$ value could represent a tall and narrow or short and squat opening, which could lead to false results, as radiation losses depend only on opening area. This factor can be expressed according to equation (A.6).

$$\theta_4 = 1 - 0{,}205\left(\sum_{i=1}^{N}\frac{A_{v,i}H_{v,i}}{\sum A_{v,i}}\right)^{-0.3} \quad (A.6)$$

A5. Combustion efficiency

Although compartment is considered as a batch stirred reactor, this assumption is not completely correct. Since there is a certain amount of unmixed fraction, this factor will try to represent it, and can be calculated according to equation (A.7).

$$\theta_5 = 1 + 0{,}5\ln b_p \quad (A.7)$$

Where b_p stands for combustion maximum efficiency and is a value compressed generally between 0,5 and 0,9.

B) Calculation of natural venting according to UNE-23585:2004

UNE-23585 norm establishes a standard method to calculate the whole area that natural ventilation must assure, according to basically heat release rate of fire and compartment geometry [35].

The first step is to determine the total heat release fraction that contributes to heating, that is, once radiation losses as light emission are subtracted. This is done according to shown by equation (B.1).

$$\dot{Q}_c = 0{,}8\dot{Q} \tag{B.1}$$

Mass flow of air merging into smoke plume may be determined according to equation (B.2).

$$M_f = C_e P\sqrt{Y^3} \tag{B.2}$$

Where:

- M_f is the fresh air mass flow merging into smoke plume, expressed in kg·s^{-1}.
- C_e is a constant referring to entrance effect of air flow into smoke plume. Its value is supposed to be 0,190 in this case, according to norm.
- P is the fire perimeter, expressed in meters, which depends exclusively on fire HRR (see equation (2.9).
- Y is the smoke free height, which can be understood as the difference between total compartment height and smoke layer height. According to equations given at section 2.4.4, it depends basically on heat release rate.

After the parameters given by two first equations are known, temperature difference between ambient and smoke layer may be calculated according to equation (B.3).

$$\Theta_1 = \frac{\dot{Q}_c}{cM_f} \tag{B.3}$$

Where c stands for gas mixture specific heat capacity, equal to 1 kJ·kg^{-1}K^{-1} as suggested by norm.

And then, absolute temperature at smoke layer can be calculated by adding this recently calculated factor to ambient temperature, T_o, as shown by equation (B.4).

$$T_1 = \Theta_1 + T_o \tag{B.4}$$

Minimum depth of smoke layer that is conducted to extraction gaps can be determined according to equation (B.5).

$$d_1 = \left(\frac{M_f T_1}{\gamma\sqrt{\Theta_1} W_1}\right) \tag{B.5}$$

Where:

- d_1 is the minimum depth of the smoke deposit that is entrained to extraction gaps.
- T_1 is the smoke layer absolute temperature, expressed in K.
- γ is a factor which can have the value of 36 or 78 according to obstacles layout.
- Θ_1 is the difference between smoke layer and ambient temperatures, expressed in K.
- W_1 is the length of the channel the gases are conducted through.

Finally, total necessary ventilation area is given according to equation (0.1).

$$A_{v,TOT}C_V = \frac{M_f T_1}{\sqrt{2\rho_{amb}^2\ g\ d_1 \Theta_1 T_o - \frac{{M_f}^2 T_1 T_o}{(A_i C_i)^2}}} \quad (0.1)$$

Where:

- $A_{v,TOT}C_V$ stands for the total ventilation area, expressed in m^2.
- g stands for the acceleration of gravity.
- A_iC_i is the hydrodynamic surface of i^{th} vent, expressed in m^2.

Bibliography

[4] National Fire Protection Association, *SFPE Handbook of Fire Protection Engineering*, 3rd ed. Quincy, MA, 2002.

[35] Tecnifuego AESPI and Asociación Española de Normalización y Certificación, “Fire safety. Smoke and heat control systems. Requirements, calculation and design methods for temperature control systems and smoke exhaust systems projecting in case of fire.,” Madrid, Spain, 2017.